No. 493 is missing

UNIVERSITY OF ILLINOIS
COLLEGE OF ENGINEERING

ENGINEERING EXPERIMENT STATION
BULLETIN 494

STRESS CONCENTRATION AT EXTERNAL NOTCHES IN MEMBERS SUBJECTED TO AXIAL LOADINGS

by

A. T. Derecho
Portland Cement Association

W. H. Munse
Professor of Civil Engineering
University of Illinois

ENGINEERING EXPERIMENT STATION

BULLETIN 494

STRESS CONCENTRATION AT EXTERNAL NOTCHES IN MEMBERS SUBJECTED TO AXIAL LOADINGS

by

A. T. Derecho

W. H. Munse

Price: $3.00

Prepared as part of an investigation
conducted by
The Engineering Experiment Station
University of Illinois
in cooperation with
The State of Illinois
Division of Highways
and
The U.S. Department of Transportation
Federal Highway Administration
Bureau of Public Roads
Project IHR-64
Behavior of Welded Highway Structures
Illinois Cooperative Highway Research Program
Series No. 74

Edited by
Elisabeth Schillinger

REQUESTS FOR THIS PUBLICATION should be addressed to Engineering Publications Office, 112 Engineering Hall, University of Illinois, Urbana 61801. On your order refer to the Bulletin number on the front cover.

UNIVERSITY OF ILLINOIS BULLETIN

Volume 65, Number 62; January 5, 1968. Published twelve times each month by the University of Illinois. Entered as second-class matter December 11, 1912, at the post office at Urbana, Illinois, under the Act of August 24, 1912. Office of Publication, 114 Altgeld Hall, Urbana, Illinois 61801.

ABSTRACT

THE PRINCIPAL OBJECT OF THE STUDY REPORTED HERE WAS TO ANALYZE THE EFFECTS OF THE VARIOUS PARAMETERS THAT DEFINE THE EXTERNAL GEOMETRY OF PROJECTING NOTCHES ON THE ASSOCIATED STRESS CONCENTRATION FACTOR. THE STUDY DEALS PARTICULARLY WITH NOTCHES OCCURRING SYMMETRICALLY IN RECTANGULAR BARS SUBJECTED TO AXIAL LOADING.

THE METHOD OF ANALYSIS USED ACCOMPLISHED THE ABOVE OBJECTIVE INDIRECTLY BY CONSIDERING THE EFFECTS OF VARIOUS GEOMETRICAL PARAMETERS ON THE MAGNITUDE AND DISTRIBUTION OF THE SHEARING STRESSES ALONG THE BASE SECTION OF A PROJECTING NOTCH. AS A PRELIMINARY STEP, THE STRESSES ALONG SELECTED SECTIONS IN A PROJECTING NOTCH IN A HALF-PLANE WERE OBTAINED USING A SOLUTION GIVEN BY H. NEUBER. USING THESE DATA AND A SOLUTION BY L. N. G. FILON FOR THE STRESSES IN A RECTANGULAR BAR RESULTING FROM SURFACE STRESS LOADS IT WAS SHOWN THAT THE MAXIMUM LONGITUDINAL STRESS ALONG THE BASE SECTION OF A PROJECTING NOTCH IS PRODUCED PRIMARILY BY THE SHEARING STRESS COMPONENT ALONG THE BASE SECTION. THE EFFECT OF THE NORMAL STRESS COMPONENT ALONG THE SAME SECTION WAS SHOWN TO BE NEGLIGIBLE. THIS HAS LED TO THE OBSERVATION THAT THE MAXIMUM STRESS IN A PROJECTING NOTCH MAY BE APPROXIMATED REASONABLY BY THE LONGITUDINAL STRESS IN A PLAIN RECTANGULAR BAR SUBJECTED TO AN AXIAL LOAD AND A SURFACE-SHEAR LOADING OF THE PROPER MAGNITUDE AND DISTRIBUTION.

THE ABOVE OBSERVATION SERVED AS THE BASIS FOR EMPLOYING AN EQUIVALENT SURFACE-SHEAR LOADING TO APPROXIMATE THE STRESS-RAISING ACTION OF A PROJECTING NOTCH. THE RESULTS OF THE SURFACE SHEAR-LOAD METHOD WERE USED TO DEVELOP A PROCEDURE FOR ESTABLISHING A CORRELATION BETWEEN THE STRESS CONCENTRATION FACTOR AND THE GEOMETRICAL PARAMETERS CHARACTERIZING THE PROFILE OF PROJECTING NOTCHES.

This page is intentionally blank.

ACKNOWLEDGMENTS

The studies described herein were conducted as a part of the research under the Illinois Cooperative Highway Research Program Project IHR-64, "Behavior of Welded Highway Structures." The research was conducted by the Department of Civil Engineering of the University of Illinois in cooperation with the State of Illinois, Division of Highways, and the U.S. Department of Transportation, Federal Highway Administration, Bureau of Public Roads.

On the part of the University of Illinois, the work covered by this report was carried out under the general administrative supervision of W. L. Everitt, Dean of the College of Engineering; Ross J. Martin, Director of the Engineering Experiment Station; N. M. Newmark, Head of the Department of Civil Engineering; and Ellis Danner, Director of the Illinois Cooperative Highway Research Program.

On the part of the Division of Highways of the State of Illinois, the work was under the administrative direction of Virden E. Staff, Chief Highway Engineer; Theodore F. Morf, Deputy Chief Highway Engineer; and John E. Burke, Engineer of Research and Development.

The program was planned in cooperation with a Project Advisory Committee consisting of the following members:

Representing the Illinois Division of Highways:
James Branton, Field Engineer, Bureau of Construction
John E. Burke, Engineer of Research and Development
George T. Fischer, Engineer of Shop Plans and Inspection
Representing the Bureau of Public Roads:
J. L. Hirsch, Bridge Engineer
Representing the University of Illinois:
William J. Hall, Professor of Civil Engineering
John D. Haltiwanger, Professor of Civil Engineering

The direct supervision of this study was provided by W. H. Munse, Project Supervisor, and W. W. Sanders, Jr., and John Cannon, formerly Project Investigators. This report is based on a doctoral dissertation written by Arnaldo T. Derecho under the direction of Professor W. H. Munse. The authors are grateful to Professors S. Fenves, A. R. Robinson, and F. S. Shaw for their kind assistance and suggestions in connection with various phases of the program.

Acknowledgment is also extended to the reviewers of this Bulletin: G. T. Fischer of the Illinois Division of Highways and J. D. Haltiwanger of the University of Illinois.

This page is intentionally blank.

CONTENTS

FIGURES

TABLES

NOTATION

The following notation used in the text and the appendices are listed below for convenient reference:

In connection with H. Neuber's solution:

x, y, z = rectangular coordinate

α, β, γ = orthogonal curvilinear coordinates

β_o = the β = constant curvilinear coordinate line denoting the profile of a notch

$h_\alpha, h_\beta, h_\gamma$ = scale factors along α, β, and γ directions

η = a constant

E = Young's modulus

ν = Poisson's ratio

λ, G = Lame's constants

F = stress function

$\phi_0, \phi_1, \phi_2, \phi_3$ = harmonic functions

u, v, w = displacement components along the x, y, and z directions, respectively

U, V, W = displacement components along the α, β, and γ directions, respectively

e = dilatation

$\bar{e}$ = dilatation in generalized plane stress

$\varepsilon_\alpha, \varepsilon_\beta, \varepsilon_\gamma$ = strain components along the α, β, and γ directions, respectively

$\gamma_{\alpha\beta}$ = shearing strain in the α β plane

$\sigma_\alpha, \sigma_\beta, \sigma_\gamma$ = normal stresses acting in the direction of the α, β, and γ coordinate axes, respectively

$\tau_{\alpha\beta}$ = shearing stress in the α β plane

$(\sigma_\alpha)_{max}$ = maximum stress in the direction of the α coordinate line (occurring at the surface of the notch)

$\sigma_x, \sigma_y, \sigma_z$ = normal stresses acting in the direction of the x, y, and z coordinate axes, respectively

τ_{xy} = shearing stress in the x-y plane

X, Y = x and y components, respectively, of the external stresses acting on the boundary

s = arc length along boundary

x_o, y_o = coordinates of the point of maximum stress

R_{min} = minimum radius of curvature of the notch profile

$\alpha_{R_{min}}$ = α coordinate of the point of maximum stress (along profile $\beta = \beta_o$)

k, d = constants

x_t, y_t = coordinates of point on notch profile denoting arbitrarily defined 'toe' of notch

w = one-half the width of the notch, measured from centerline to toe

h = height of notch, measured from the base section $y = y_t$ to the highest point on the notch profile

ϕ = the angle which the tangent to the notch profile at any point (α, β) makes with the x axis

θ = flank angle -- the angle which the tangent to the notch profile makes with the x axis at the point of inflection

p = intensity of uniform tensile stress acting across a section x = constant sufficiently removed from the notch

F_σ = total force due to the stress σ_x acting across the centerline section of the notch -- for that part of the section above $y = y_t$

F_τ = ($= F_\sigma$) total force due to the shearing stress τ_{xy} acting along the base of the notch, from centerline to toe

c = distance from the point of maximum shearing stress along the base to the toe of the notch

In connection with the surface-shear load method:

a = one-half the total length of the bar considered

b = one-half the depth of the bar

t = one-half the thickness of the bar

w = one-half the loaded length, i.e., one-half the total length acted on by the surface-stress loading (corresponding to the half-width of the notch)

$\alpha = \frac{2\pi n}{a}$

A_n = Fourier coefficient for the surface-shear stress intensity curve

C_n = Fourier coefficient for the surface-normal stress intensity curve

F = Airy's stress function

Parameters defining the surface-shear stress intensity curve:

F_τ/p = total area of stress intensity triangle

τ_o/p = height of stress intensity triangle

c = distance from the apex of the stress intensity triangle to the end of the loaded length

Parameters defining the surface-normal stress intensity curve:

s = distance from the center of the loaded length to the point of zero stress

g = distance from the apex of the positive stress triangle to the end of the loaded length

$r = s - \sqrt{s^2 - (w - s - g)(w - s)}$

$\sigma_n^{(+)}/p$ = height of positive stress triangle

$\sigma_n^{(-)}/p$ = constant height of negative stress trapezoid

F_{σ_n}/p = total area of positive stress triangle

Most of the above quantities are illustrated in Figures B-1 and B-2.

$\sigma_x^{\rightarrow}, \sigma_y^{\rightarrow}, \tau_{xy}^{\rightarrow}$ = stress components due to surface-shear stress loading on rectangular bar

$\sigma_x^{\downarrow}, \sigma_y^{\downarrow}, \tau_{xy}^{\downarrow}$ = stress components due to surface-normal stress loading

$(\sigma_x)_{max}$ = maximum stress on surface of bar due to combined action of surface stress loading and the uniform tensile stress p acting at the ends of the bar

In connection with the finite difference solutions:

F = Airy's stress function

X, Y = x and y components, respectively, of the external stresses acting on the boundary

s = arc length along boundary

n = normal to boundary

p = uniform tensile stress acting at ends of bar

Δ = mesh interval

α = ratio of the distance from first interior point to boundary point, to Δ

F_i, F_e, F_b, F_a = values of stress function **F** at points i, e, b, and a, respectively, adjacent to boundary

This page is intentionally blank.

I. INTRODUCTION

A. GENERAL REMARKS

The localized increase in stress produced by a discontinuity in the shape or geometry of a load-carrying member has long been recognized. Such stress-raising discontinuities are broadly referred to as notches, whether they be geometrical, metallurgical, or other, in nature.

In the design of statically-loaded members, the increase in stress occurring in the immediate vicinity of a discontinuity is generally neglected. Here, reliance is placed on the beneficial effect of the redistribution of stresses that occurs when the stresses in the critical portions of the material reach the yield point. However, in members subjected to repeated loadings, in which failure, if it occurs, is generally nonductile, the localized stress concentrations produced by notches become significant. This is particularly true in the case of members subjected to relatively low (compared to the yield point of the material) stresses which result in failure, but at long lives.[1,2,3]*

A common type of discontinuity in welded members is represented by the weld reinforcement in a transverse butt-welded joint. Other members which are butt-welded into a main member, with the axes perpendicular to each other, provide the same general type of discontinuity. Experimental studies on butt-welded joints subjected to axial fatigue loading[1,2,3,4,5,6] have shown definite and often significant reductions in the fatigue lives of the members as a result of the weld reinforcement. Reductions in fatigue strength of as-welded specimens have been found to be as high as 45 per cent (relative to the fatigue resistance of the corresponding plain plate specimens).

Experiments by Newman and Gurney,[5] J. E. Tomlinson and J. L. Wood,[6] and W. O. Dinsdale[7] verify results of tests conducted at the University of Illinois[3] aimed at isolating and studying the effects of the external geometry of butt-welded joints**. They indicate that a reduction in fatigue strength increases with the severity of the notch geometry up to a certain point, beyond which the effect of the notch appears to remain more or less constant. This observation has led to the conclusion that for a given material and loading condition, particularly for long-life fatigue, the fatigue behavior of a member is, phenomenologically, at least, a direct function of the local stress and strain condition in the critical portions of the member, and hence of its geometry. However, the relationship between stress and/or strain and fatigue life may be far from simple.

---

*Numbers in parentheses refer to entries in References Chapter VII.

**Using specimens with the notch simulating the weld reinforcement machined from base metal.

This study is an outgrowth of the above-mentioned investigation on the effects of external geometry on the fatigue behavior of butt-welded joints under axial loading. Because of the dominant influence of high, localized stresses on the fatigue behavior of butt-welded and other similar joints, it was felt necessary to study in detail the effects of the various parameters determining the external notch geometry on the stress concentration factor.

B. OBJECTIVES OF STUDY

The primary objective of this study is to analyze the effects of the various geometrical parameters that characterize the profile of a projecting notch* on the associated stress concentration factor. The study deals particularly with rectangular bars which have symmetrically disposed projecting notches and which are subject to axial loading. The ultimate aim of the analysis is the development of a method of predicting the elastic stress concentration factors for projecting notches of varying characteristic dimensions.

The term projecting notch is used here to denote the geometrical discontinuity characterized by the projection of a part of a body above an otherwise plane surface. As mentioned previously, the weld reinforcement in a butt-welded plate as well as attachments or other members butt-welded into a main member fall under this category.

• • •

*Used here in its broader sense, i.e., any stress raiser.

II. THE PROBLEM AND THE METHOD OF ANALYSIS

A. THE IDEALIZED PROJECTING NOTCH; PARAMETERS CONSIDERED

The idealized projecting notch for which this study seeks to develop quantitative relationships between the elastic stress concentration factor and the significant geometrical parameters is shown in Figure 1a. This represents a two-dimensional problem with the projecting notches disposed symmetrically about the axis of a rectangular bar subjected to axial loading. The following geometrical parameters describe the notch adequately:

- R = the radius of the circular transition curve
- h = height of notch, measured from the base of the notch to the highest point on the notch profile
- w = one-half the total width of the notch, measured from centerline to toe or point of tangency with the base
- θ = the "flank angle", i.e., the angle which the tangent to the notch profile, taken at the point of tangency of the circular arc and the straight flank of the notch, makes with the surface of the bar or base of the notch.

A bar of unit thickness will be assumed throughout the following discussion.

B. PREVIOUS STUDIES

To the author's knowledge, little has been done to develop a relationship between the elastic stress concentration factor and the geometrical parameters that determine the profiles of projecting notches in bars subjected to axial loading.

H. Neuber[8] presents a solution for a projecting notch with a variable transition radius in a half-plane and gives a plot of the variation of the stress concentration factor with the minimum radius of curvature of the notch profile. However, no mention is made of the effects of the other parameters that determine the notch profile.

Values of the stress concentration factor for projecting notches in flat bars subjected to bending, based on photoelastic studies by M. M. Leven and A. J. Hartmann,[9] are given by R. E. Peterson.[10] Peterson,[10] as well as R. B. Heywood,[11] indicate that no similar data are available for the case of projecting notches in bars subjected to axial loading.

C. GENERAL DESCRIPTION OF METHOD OF ANALYSIS

An approximate method of analysis has been used since it is difficult to find a coordinate system or a set of transformation relationships in closed form* which gives a profile having the general shape of the notched bar under consideration and which allows a controlled variation of the geometrical parameters that characterize the notch.

As a preliminary step, Neuber's solution[8] for a projecting notch in a half-plane was considered (see Figure 2). The distributions

---

* T. A. McCreery[12] gives an approximate solution for the stresses in a notched bar using conformal mapping -- the mapping function being given by a power series expansion.

of stresses along selected sections in a number of Neuber's notches were plotted and from these plots qualitative relationships were deduced. However, because the series of notches associated with Neuber's solution represented a very limited number of combinations of the geometrical parameters characterizing the profile of this type of notch, a method had to be developed which would permit the extension of the available data to a wider range of values of the parameters considered. This was necessary not only to give a better picture of the influence of the different parameters involved but also to provide a method by which the desired correlation for the case of the idealized projecting notch could be obtained on the basis of a relatively few calculated values.

The method developed to extend the results to a wider range of values of the geometrical parameters is based on the so-called "equivalent surface-shear load method."[13,14,15] The effect of the notch is approximated by imposing on a flat bar an equivalent shear stress loading, acting over the full width of the notch. The maximum longitudinal stress along the surface of the bar produced by such a loading is then assumed to be equal to the actual maximum stress produced by the corresponding notch. In effect, it is assumed that the projection on a notched bar is removed by passing a section through the base of the notch and the remaining plain bar loaded with the equivalent stresses acting on the cut section. The stresses along the base section of the notch consist of (1) a shearing stress component of varying intensity and (2) a normal stress component. The normal stress component may reasonably be neglected since it is generally of a smaller magnitude and contributes an insignificant part to the maximum stress along the section, as will be shown in the subsequent development. As in previous papers,[14,15] the shearing stress distribution curve has been approximated by a broken-line surface-shear load curve and the resulting stresses in the plain rectangular bar have been obtained using L. N. G. Filon's solution for this case. However, unlike previous work based on the surface-shear load method, the method of analysis developed in this study does not use directly the maximum stress produced by the "triangular" surface-shear loading to approximate the maximum stress in a notch. Rather it utilizes a series of curves obtained by the surface-shear load method, mainly as a framework of reference and as a means of extending the results of calculations for a limited number of cases to a wider range of values of the parameters.

Using a plot of the maximum stresses derived by the surface-shear load method together with data from Neuber's solution, a correlation was obtained between what appeared to be the most significant geometrical parameters and the stress concentration factor for Neuber's notches.

In order to apply the method developed to obtain a correlation for Neuber's notches to the case of the idealized projecting notch of Figure 1a, a finite-difference solution for the stresses in a rectangular bar with symmetrically disposed projecting notches was applied in a limited number of cases. The method of finite differences permitted the geometrical parameters defining the notch profile to be varied independently of each other so that their separate effects on the stress concentration factor could be determined.

To obtain an experimental check of the resulting relationships for idealized projecting notches, a limited number of tests were made on notched specimens. These test results, as well as available data on bars with shoulder fillets subjected to axial loading, have been compared with values from the theoretical analysis.

III. ANALYSIS OF STRESSES AND RELATIONSHIPS FOR NEUBER'S NOTCHES

A. NEUBER'S SOLUTION[8]

Neuber considered a projecting notch in a half-plane with a profile coincident with a "β = constant" line of the coordinate system defined by the following transformation relationships:

$$x = \alpha + \frac{\alpha}{\alpha^2 + \beta^2}$$

$$y = -\frac{\beta}{\alpha^2 + \beta^2} \qquad (1)$$

Equations (1) determine an orthogonal, isometric* curvilinear coordinate system (α, β). By assigning to β a fixed value, β_o, and allowing α to vary, corresponding values of (x, y) are obtained defining the notch profile. Examples of such profiles, with values of β_o ranging from 0.25 to 1.25, are shown in Figure 2. The characteristic dimensions of the notch profiles are listed in Tables 1-a and 1-b. The above series of notches are referred to as Neuber's notches.

In the two-dimensional case considered here, Neuber gives the following expressions for the stresses along the α and β coordinate axes: (The development of Equations (2), as well as other relationships concerning Neuber's notches, is given in Appendix A).

$$\left.\begin{aligned}
\sigma_\alpha &= \frac{1}{h^2}\frac{\partial^2 F}{\partial \beta^2} + \frac{1}{h^3}\left(\frac{\partial h}{\partial \alpha}\frac{\partial F}{\partial \alpha} - \frac{\partial h}{\partial \beta}\frac{\partial F}{\partial \beta}\right) \\
\sigma_\beta &= \frac{1}{h^2}\frac{\partial^2 F}{\partial \alpha^2} + \frac{1}{h^3}\left(\frac{\partial h}{\partial \beta}\frac{\partial F}{\partial \beta} - \frac{\partial h}{\partial \alpha}\frac{\partial F}{\partial \alpha}\right) \\
\tau_{\alpha\beta} &= -\frac{1}{h^2}\frac{\partial^2 F}{\partial \alpha\, \partial \beta} + \frac{1}{h^3}\left(\frac{\partial h}{\partial \alpha}\frac{\partial F}{\partial \beta} + \frac{\partial h}{\partial \beta}\frac{\partial F}{\partial \alpha}\right)
\end{aligned}\right\} \qquad (2)$$

In the above equations, h is the common scale factor or modulus of the assumed isometric coordinate system; F is a stress function. For the particular coordinate system defined by Equations (1),

$$h^2 = 1 + \frac{2\beta^2 - 2\alpha^2 + 1}{(\alpha^2 + \beta^2)^2} \qquad (2a)$$

and for the problem of the projecting notch with a profile given by $\beta = \beta_o$,

$$F = \frac{p}{2}(\beta - \beta_o)^2\left[1 - \frac{1}{(2\beta_o^2 + 1)(\alpha^2 + \beta^2)}\right]. \qquad (2b)$$

In Equation (2b), p is the applied tensile stress acting across a section parallel to the axis of the notch and sufficiently removed from it to allow for uniform stress. Differentiation of Equations (2a) and (2b) and substitution into Equations (2) give the stress components along the curvilinear coordinate lines α = constant and β = constant. The corresponding x and y components of stress

*See Appendix A.

are obtained by using standard transformation relationships.

The maximum stress (along the profile $\beta = \beta_o$) is given by

$$(\sigma_\alpha)_{max} = \left[1 + \frac{(1 + 4\beta_o^2)\ (\sqrt{1 + \beta_o^2} - \beta_o)}{4\beta_o(1 + 2\beta_o)}\right] p \qquad (3)$$

and occurs at a point defined by

$$\alpha_{(\sigma_\alpha)_{max}} = \left[1 + \beta_o^2 \pm \sqrt{4\beta_o^2 + 4\beta_o^4}\right]^{1/2} . \qquad (4)$$

The rectangular coordinates of the point of maximum stress (x_o, y_o) are readily obtained by substituting the value of α given by Equation (4) and the corresponding β_o into Equations (1).

The minimum radius of curvature of the notch profile is given by

$$R_{min} = 2\beta_o^2\sqrt{1 + \beta_o^2} \qquad (5)$$

and occurs at a point determined by

$$\alpha_{R_{min}} = \sqrt{1 + \beta_o^2} \ . \qquad (6)$$

The corresponding x and y coordinates are again obtained from Equations (1).

The angle which the tangent to the notch profile makes with the x axis at the point (α, β_o) is given by

$$\varphi = \tan^{-1}\left[\frac{2\alpha\beta_o}{(\alpha^2 + \beta_o^2)^2 + (\beta_o^2 - \alpha^2)}\right] . \qquad (7)$$

The angle θ which the tangent to the notch profile makes with the x axis at the point of inflection is defined as the "flank angle."

Definition of Base of Notch

The reader will note that in Figure 2 the curve defining the notch profile does not become horizontal (i.e., parallel to the x axis) at any point except at $x = 0$. It tapers off gradually, becoming almost horizontal for large values of α and x. Equations (1) indicate that α approaches x as α becomes larger, just as β approaches y for large values of β. Because of the absence of a definite horizontal line in the immediate vicinity of the notch, the "base of the notch" is not clearly defined and an appropriate horizontal section $y = y_t$ must be selected which can be taken as the base of the notch. This then determines the width of the notch as well as its height. The following were considered in choosing the section.

(1) Previous experimental measurements on filleted bars[16,17,18] with circular arcs, as well as the results of "Photostress" measurements carried out in connection with this study, have shown that the maximum stress occurs at a point slightly above the toe of the notch -- at a point where the tangent makes an angle of approximately 10 degrees with the axis of the bar.

(2) On the basis of the above observation, the horizontal section to be used in defining the limits of Neuber's notch should intersect the notch profile $\beta = \beta_o$ a short distance beyond the point of maximum stress. Furthermore, this distance should be a function of the minimum radius of curvature of the notch profile.

In view of the above, base sections determined by the relationship

$$x_t = x_o + k \cdot R_{min} \qquad (8)$$

were tried, assuming values of 0.125 and 0.250 for the constant k (corresponding to angles of about 7 degrees and 15 degrees, respectively, for a circular arc fillet). As will be seen later, a variation in the values of k within

the above range does not produce significant changes in the results obtained. In the subsequent discussion, the point on the notch profile defined by the coordinates (x_t, y_t) will be referred to as the toe of the notch.

The relative magnitudes and distributions of the stress components along the base and centerline sections of the notches were calculated using Equations (2) and are plotted in Figures 3 to 6. A value of k = 0.250 was used in Equation (8) to define the base section $y = y_t$. In all of the above-mentioned figures, as well as in the following figures and discussion, the uniform tensile stress p has been taken as unity. With this assumed value of p, the magnitude of the maximum stress $(\sigma_\alpha)_{max}$ is equal to the stress concentration factor.

Discussion of Stress Distributions Along Base and Centerline Sections

A comparison of the distribution curves for the stress components along the base of the notch indicates that the peak of the normal stress intensity curve of Figure 3 occurs slightly to the left of the peak of the corresponding shear stress intensity curve of Figure 4. As will be shown in connection with the surface-shear-load method, this is significant since the longitudinal stress on the surface of a bar produced by a surface-normal stress loading has a distribution similar to that of the load itself. On the other hand, the maximum longitudinal stress on the surface of the bar produced by a surface-shear load lies slightly to the right of the peak of the shear load intensity curve. This relative displacement between the points of maximum longitudinal stress produced by surface-stress loadings corresponding to the normal and shear stress components along the base of the notch, together with the comparatively small magnitude of the longitudinal stress created by the normal component, combine to make the effect of the normal stress component on the maximum longitudinal stress negligible. Neglecting the normal stress component implies that the stress-concentrating effect of the notch is approximated reasonably well by the effect of the shearing stress component.

In the following discussion, therefore, the main emphasis will be placed on the shearing stress component along the base section $y = y_t$. Since this shearing stress component is the predominant factor, a study of the effects of the different shearing stress distributions and the variation of these distributions with the geometrical parameters that characterize the notch profile should lead to a reasonably good correlation between the notch parameters and the theoretical stress concentration factor. This concept underlies the so-called equivalent surface-shear load method of calculating stress concentration factors.

The following additional points are worth noting in connection with the distributions of stresses along the base and centerline sections.

An examination of the shearing stress distribution curves corresponding to the different notch profiles in Figure 4 reveals that these differ principally in two respects, (1) the distance c from the peak of each curve to the toe of the notch (indicated by x/w = 1.0 in Figure 4), and (2) the total area under each curve F_τ/p. The above two quantities, expressed in terms of the dimensionless ratios c/w and F_τ/pw which describe the essential features of the shear distribution curve along the base of the notch, shall be referred to briefly as stress parameters.

Table 2 indicates that the stress parameter F_τ/pw increases with increasing height of notch and decreasing radius of curvature of the notch profile, while the

parameter c/w decreases with decreasing radius of curvature of the notch profile.

It will be noted that in Figure 4 the shearing stress is not equal to zero at the toe of the notch because of the peculiar shape of Neuber's notches and the arbitrary manner in which the base of the notch had to be defined. Thus, the toe of the notch does not mark the point of tangency of a curve and a horizontal line -- as in the idealized notch of Figure 1a. In the idealized projecting notch, the shearing stress is equal to zero at the toe.

Table 2 also lists the dimensionless ratio F_σ/pw, shown equal to F_τ/pw, corresponding to various values of β_o (F_σ being the total force due to σ_x along the centerline section -- for that part of the section above the base of the notch). For equilibrium, the total force F_σ must be equal to the corresponding total force F_τ due to the shearing stress acting along half the width of the base section $y = y_t$. Values of F_σ/pw have been calculated for notches whose widths were determined by using Equation (8) with $k = 0.125$ and $k = 0.250$.

Figure 6 is a plot of the distribution of the longitudinal stress σ_x acting along the centerline section. It shows a decrease in the "efficiency" of the section with an increase in the height of the notch. Efficiency is used here to denote the ratio of the average tensile stress along the centerline section to the maximum tensile stress occurring in the section, for that part of the section above the base of the notch. Values of the efficiency corresponding to various values of β_o are given in Table 2. It is interesting to note that in Figure 6 the stress σ_x becomes compressive in the upper portion of the centerline section for the higher notches.

In order to make a comparison of the total forces (F_σ and F_τ) corresponding to the different notches, all the notches considered were reduced to a "standard width." The data listed in Table 2 correspond to a standard half-width of 4.0 units.

Qualitative Correlation of Stress and Geometrical Parameters

Having decided to eliminate from further consideration the effect of the normal stresses along the base of the notch, the next step was to establish the relationship between the geometrical parameters R_{min}, h, w, and θ and the stress parameters F_τ/pw and c/w. Once such a relationship is established, the stress concentration factor corresponding to a notch of given dimensions may be determined by loading a plain bar with the appropriate shear stress distribution acting over a length equal to the width of the notch. In the subsequent discussion, the geometrical parameters R_{min}, h, and w will be considered in terms of the dimensionless ratios R_{min}/w and h/w.

It must be pointed out that the geometrical parameters characterizing Neuber's notches have fixed relationships so that the parameters are not independent of each other. Each profile in the series is uniquely determined by the value of β_o, which in turn determines the values of the above geometrical parameters. Because of this, a particular notch profile can be described by any single geometrical parameter. In spite of this fixity in the relationships between geometrical parameters, an attempt was made to establish a correlation on the basis of the limited data available and to develop a method by which these results might be extended to a wider range of values of the parameters. In this case, the other combinations of the geometrical parameters would represent notches of approximately the same general shape as the notches in the series considered by Neuber. This was done

mainly as a preliminary step until more definite indications of the relationships between the stress and geometrical parameters could be obtained using the results of a finite-difference solution.

In the following, qualitative relationships between the stress and geometrical parameters are postulated on the basis of observations made in connection with Figure 4 and related data on Neuber's notches. After the qualitative relationships have been established, consideration is given to the problems of determining quantitative relationships between the stress and geometrical parameters and developing a method for extending the results to a wider range of values of the parameters.

The following were considered in determining the geometrical parameter with which to relate the stress parameter c/w.

(1) The parameter c/w exhibits the same variation as the geometrical parameter R_{min}/w, i.e., c/w decreases with decreasing values of R_{min}/w.

(2) As noted previously, the distance from the point of maximum stress (on the surface of the notch) to the toe of the notch is a function of the radius of curvature of the notch profile, the maximum stress occurring at a point where the tangent to the profile makes an angle of approximately 10 degrees with the axis of the bar for the case of notches with circular arcs. The maximum longitudinal stress along the base section of the notch, which may be considered as produced predominantly by the shearing stress component along the same section, occurs at a point only slightly below the point of maximum stress. The location of the point of maximum longitudinal stress along the base section is in turn a function of the position of the peak of the shear stress intensity curve. Hence, the latter, as defined by c/w, must be a function of the radius of curvature of notch profile.

Although the available data do not indicate an exclusive relationship between c/w and R_{min}/w, it was decided to relate c/w to the geometrical parameter R_{min}/w alone, since the latter appears to be the parameter most intimately connected with it.

No clear indication was obtained from the limited data available as to which of the geometrical parameters has the greatest influence on the stress parameter F_τ/pw. However, it was known that for the limiting case when R_{min}/w approaches zero, the maximum stress in the notch theoretically becomes very large, which means that the shearing stresses along the base section also become very large. Thus, F_τ/pw must be a function of R_{min}/w. The geometrical parameters h/w and θ must also influence the parameter F_τ/pw, both of these quantities being measures of the relative magnitude of the discontinuity represented by the notch. Tables 1 and 2 show that F_τ/pw increases with increasing values of h/w and θ. In the limiting case when both h/w and θ are equal to zero (no notch), F_τ/pw is equal to zero. Therefore, the stress parameter F_τ/pw is a function of the geometrical parameters R_{min}/w, h/w, and θ.

The investigation thus far has led to the following qualitative correlation between the stress and geometrical parameters: (1) the relative distance c/w from the point of maximum shearing stress along the base section of the notch to the toe of the notch is directly related to the minimum radius of curvature of the notch profile, as given by the parameter R_{min}/w; and (2) the total shearing force along the half-width of the base section of the notch, as given by the parameter F_τ/pw, is a function of the geometrical parameters R_{min}/w, h/w, and θ.

The next step was to determine quantitative relationships between the stress and geometrical parameters using the data for Neuber's notches. To accomplish this and to develop the method for extending the results

to a wider range of values of the parameters, Filon's solution[19] for the case of a bar of rectangular cross section under an arbitrary surface stress loading has been used.

B. THE SURFACE-SHEAR LOAD METHOD; EFFECT OF NORMAL COMPONENT OF STRESS ALONG BASE SECTION OF NOTCH

Filon's Solution: Expressions for Stresses

In 1902 Filon gave a solution[19] for the stresses and displacements in a bar of rectangular cross section in a state of generalized plane stress subjected to a surface-stress loading of arbitrary distribution. Using Filon's solution for the special case of a surface-shear loading distributed antisymmetrically with respect to both x and y axes, the following expressions are obtained for the resulting stresses:*

$$\sigma_x = -\sum_{n=1}^{\infty} A_n \frac{\cos \alpha a}{\alpha b}$$

$$+\sum_{n=1}^{\infty} 2A_n \frac{2\cos h\alpha b - \alpha b \sin h\alpha b}{\sin h\, 2\alpha b + 2\alpha b} \cos h\alpha y \cos \alpha x$$

$$+\sum_{n=1}^{\infty} 2A_n \frac{\cos h\, \alpha b}{\sin h\, 2\alpha b + 2\alpha b} \alpha y \sin h\alpha y \cos \alpha x.$$

$$\sigma_y = \sum_{n=1}^{\infty} 2A_n \frac{\alpha b \sin h\, \alpha b}{\sin h\, 2\alpha b + 2\alpha b} \cos h\, \alpha y \cos \alpha x$$

$$-\sum_{n=1}^{\infty} 2A_n \frac{\cos h\, \alpha b}{\sin h\, 2\alpha b + 2\alpha b} \alpha y \sin h\, \alpha y \cos \alpha x.$$

$$\tau_{xy} = \sum_{n=1}^{\infty} 2A_n \frac{\cos h\, \alpha b - \alpha b \sin h\, \alpha b}{\sin h\, 2\alpha b + 2\alpha b} \sin h\, \alpha y \sin \alpha x$$

$$+\sum_{n=1}^{\infty} 2A_n \frac{\cos h\, \alpha b}{\sin h\, 2\alpha b + 2\alpha b} \alpha y \cos h\, \alpha y \sin \alpha x.$$

In the above expressions, A_n represents the coefficients in the Fourier series expansion of the surface-shear load distribution curve. Also $\alpha = n\pi/a$, 2a being the total length of the bar considered. The depth of the bar is equal to 2b.

The expressions for the stresses in the bar produced by a surface-normal stress loading distributed symmetrically with respect to both x and y axes follow.

$$\sigma_x = \sum_{n=1}^{\infty} 2C_n \frac{\sin h\, \alpha b - \alpha b \cos h\, \alpha b}{\sin h\, 2\alpha b + 2\alpha b} \cos h\alpha y \cos \alpha x$$

$$+\sum_{n=1}^{\infty} 2C_n \frac{\sin h\, \alpha b}{\sin h\, 2\alpha b + 2\alpha b} \alpha y \sin h\, \alpha y \cos \alpha x.$$

$$\sigma_y = \sum_{n=1}^{\infty} 2C_n \frac{\sin h\, \alpha b + \alpha b \cos h\, \alpha b}{\sin h\, 2\alpha b + 2\alpha b} \cos h\, \alpha y \cos \alpha x$$

$$-\sum_{n=1}^{\infty} 2C_n \frac{\sin h\, \alpha b}{\sin h\, 2\alpha b + 2\alpha b} \alpha y \sin h\, \alpha y \cos \alpha x.$$

$$\tau_{xy} = -\sum_{n=1}^{\infty} 2C_n \frac{\alpha b \cos h\, \alpha b}{\sin h\, 2\alpha b + 2\alpha b} \sin h\, \alpha y \sin \alpha x$$

$$+\sum_{n=1}^{\infty} 2C_n \frac{\sin h\, \alpha b}{\sin h\, 2\alpha b + 2\alpha b} \alpha y \cos h\, \alpha y \sin h\, \alpha x.$$

In the above expressions, C_n represents the coefficients in the Fourier series expansion of the surface-normal load distribution curve.

*A derivation of the expressions which follow is given in Appendix B.

In the analysis which follows, the smooth distribution curves associated with the stress components along the base of the notch are replaced by broken-line approximations. These approximating curves are intended to incorporate the major features of the actual curves, at the same time allowing relatively simple expressions to define them. Thus, instead of the shear distribution curves of Figure 4, the general broken-line approximation of Figure B-1 (Appendix B) is used. The Fourier coefficient A_n corresponding to this approximate distribution curve is given by

$$A_n = \frac{2\,\tau_o}{ac\,\alpha^2 p}\left[\sin\alpha w - \frac{w}{w-c}\sin\alpha(w-c)\right] \quad (11)$$

where the terms involved above have the significance indicated in Figure B-1 (Appendix B).

Similarly, the normal stress distribution curves of Figure 3 are replaced by the general broken-line approximation of Figure B-2b (Appendix B). The corresponding Fourier coefficient, which appears in Equations (10) is given by

$$C_n = \frac{2}{ap}\left[\begin{array}{l} -\dfrac{\sigma_n^{(-)}}{\alpha}\sin\alpha(s-r) + \dfrac{\sigma_n^{(+)}}{\alpha(w-s-g)}\,r\sin\alpha(s-r) \\ \\ +\dfrac{1}{\alpha}\cos\alpha(w-g) - \cos\alpha(s-r) \\ \\ -\dfrac{\sigma_n^{(+)}}{\alpha^2 g}\cos\alpha w - \cos\alpha(w-g) \end{array}\right] \quad (12)$$

Effect of Normal Stress Component Along Base Section of Notch

The longitudinal stresses σ_x along the surface of a rectangular bar due to each component have been calculated, in order to show that the effect of the normal component of stress along the base of the notch on the maximum stress is negligible compared to that of the shear component. The results are shown in Figure 8. The curves of Figure 8 correspond to surface-stress loadings which approximate the stress distribution along the base of Neuber's notch with $\beta_o = 0.60$. In the case of the surface-normal stress loading, the total positive force (i.e., the positive area under the curve) was made equal to that of the corresponding curve of Neuber's notch. (The positive area under the curve must be equal to the negative area under the curve.) In addition, the locations of the point of zero stress and the point of maximum positive stress, with respect to the end of the loaded length (corresponding to the toe of the notch), were made equal to the corresponding quantities for the Neuber notch.

In the case of the surface-shear load, the total area under the approximating shear load "triangle" and the distance c from the point of maximum shearing stress (the apex of the triangle) to the end of the loaded length were made equal to the corresponding quantities for Neuber's notch. Thus, the plot shown in Figure 8 has been based on the following values:

for the normal stress distribution curve --

$$\frac{F_{\sigma_n}^{+}}{pw} = 0.041$$

$$s/w = 0.60$$

$$g/w = 0.180$$

for the shear stress distribution curve --

$$\frac{F_\tau}{pw} = 0.136$$

$$c/w = 0.124$$

with $w = 4.0$.

Values of $a = 4.0$ and $b = 2.0$ were used in Equations (9) and (10) to calculate the longitudinal stress σ_x along the surface of the bar due to the above surface stress loadings.

As mentioned previously, the maximum longitudinal stress along the surface of the bar due to the combined action of the surface-shear load and the uniform tensile stress p lies to the right of the peak of the shear load triangle. In Figure 8, the distance of the peak of the surface-shear load triangle from the centerline of the bar is given by $x/w = 0.876$ (corresponding to a $c/w = 0.124$), while the maximum stress $(\sigma_x)_{max}$ along the surface of the bar due to the surface-shear load and the uniform tensile stress p lies at approximately $x/w = 0.950$. On the other hand, the longitudinal stress along the surface of the bar due to the surface-normal stress loading has the same general pattern of distribution as that of the normal stress load producing it. Thus, the maximum longitudinal stresses produced by the surface-shear load and the surface-normal load generally do not occur at the same point and are, therefore, not directly additive.

For the case shown in Figure 8, the normal stress component contributes 0.086 to the total maximum stress of $\sigma_x/p = 1.55$ (occurring at $x/w = 0.925$). This contribution represents 5.6 per cent of the total maximum stress, or an excess of 5.1 per cent over the maximum stress occurring at $x/w = 0.950$ due to the shearing stress component alone. A similar calculation for the case of Neuber's notch with $\beta_o = 0.30$ shows that the contribution of the normal stress component is only 0.50 per cent of the total maximum stress; for the flatter notch with $\beta_o = 0.90$, the normal stress contribution is 1.6 per cent.

Although based on approximations to the actual distribution curves of the stress components along the base of the notch, the preceding discussion shows that the effect of the normal component of stress may be neglected when calculating the stress concentration factor for a projecting notch.

Comparison of Maximum Stresses for Neuber's Notches and Those Obtained by the Surface-Shear Load Approximation

It will be noted that in Figure 8 the maximum stress produced by the surface-shear and normal loads, together with the uniform stress p, is 16 per cent greater than the maximum stress obtained for a Neuber notch with $\beta_o = 0.60$. This discrepancy is due primarily to the difference in slopes of the stress intensity curves near the toe of the notch, particularly of the shear stress intensity curve, rather than to the replacement of the smooth distribution curves by broken-line approximations. Thus, in the surface-shear load triangle, the shear stress starts from zero at the end of the loaded length (corresponding to the toe of the notch) and increases to its maximum value at a distance c from this end. In Neuber's notch, on the other hand, the shear stress along the base section is generally not zero at $x/w = 1.0$ and increases more gradually to its maximum value at a distance c from the toe. Had the base sections in Neuber's notches been taken slightly below those used in Figure 4, the ordinates to the shear stress intensity curves would have shown a further decrease beyond the point of maximum stress, becoming almost zero as the slope of the profile at the "toe" approached the horizontal. This means that the slope of the shear stress intensity curve at and near the toe of the notch is relatively small, increasing gradually from a value close to zero to a maximum near the peak of the curve as one moves toward the centerline of the notch. This slow increase of the shearing stress near the toe of the notch is a direct reflection of the geometry of the Neuber notch, in which the profile does not become horizontal, i.e., the radius of curvature of the profile decreases gradually from a large value away from the main projection to a minimum

near the point of maximum stress.

In contrast to the Neuber notch, the idealized projecting notch, such as is shown in Figure 1a, has a well-defined base section such that the shear stress along this section becomes zero at the toe of the notch. At the toe of an idealized notch, the radius of curvature of the profile changes abruptly from infinity (for the straight surface of the bar) to the finite (constant) radius of curvature of the circular transition curve. In this case, the shear stress intensity curve would be expected to have a slope at and near the toe of the notch greater than that of a Neuber notch of comparable dimensions (with the base section defined by either k = 0.125 or k = 0.250). In this respect the surface-shear load triangle used here would be a closer approximation to the shear stress intensity curve along the base section of an idealized projecting notch than to that of a Neuber notch.

As will be seen in the next section, the maximum stress produced by a surface-shear loading increases with an increase in the slope of the shear stress intensity curve near the toe of the notch. This difference in geometry between the Neuber notch and the idealized projecting notch -- as reflected in their respective shear stress distribution curves along the base sections -- would lead one to expect a higher stress concentration factor for the idealized projecting notch than for the Neuber notch with the same minimum radius of curvature and the same h/w and θ values.

It must be pointed out that although the maximum stress along the surface of a rectangular bar due to the surface stress loads discussed above is not the same as the maximum stress in the actual notch, the value obtained for a properly distributed surface stress loading should be very close to the actual maximum stress. (As mentioned earlier, the maximum stress in the actual notch occurs along the surface of the notch, at a small distance above the base section). This fact makes the surface-shear load method quite useful as an approximate method of calculating stress concentration factors for projecting notches. For Neuber's notches with the base section defined by k = 0.250 (see Equation 8), the ratio of the actual maximum stress to the maximum longitudinal stress along the base section varies from 1.099 for β_o = 0.40 to 1.003 for β_o = 1.50. The ratio decreases with decreasing notch severity.

However, this difference between the maximum stress along the surface of a notch and the maximum longitudinal stress along the base section of the notch need not cause any difficulty when applying the surface-shear load method. This difference can be allowed for by defining the equivalent surface-shear load as a triangularly distributed surface-shear loading having the same value of F_τ/pw as in the corresponding notch and a value of c/w such that the maximum longitudinal stress along the surface of a plain bar produced by such a loading is equal to the actual maximum stress in the notch. With the above definition of the equivalent surface-shear load, the added effect of the normal stress component along the base section of the notch on the maximum stress is indirectly accounted for. This will become clear in the next section.

Quantitative Relationships Between the Stress and Geometrical Parameters

In order to complete the correlation of the stress and geometrical parameters for Neuber's notches, it was necessary to develop a procedure for determining the essential quantitative relationships which would allow its extension (to the case of idealized projecting notches with appropriate modifica-

tions where indicated). The procedure utilizes a series of curves which give the maximum longitudinal stress in a plain rectangular bar as a function of the parameters F_τ/pw and c/w, characterizing the triangular surface-shear loading. This series of curves is shown in Figure 9. The values of the maximum stress plotted in Figure 9 were obtained by considering 400 terms in the series expression for σ_x (see Equation B-16 and the paragraph immediately following) and by taking w = 4.0, a = 4w, and b = 2w.

The first step in the procedure was to relate the stress parameter F_τ/pw to the geometrical parameters influencing it. Because each of Neuber's notches is characterized by different values of R_{min}/w, h/w, and θ, the available data is insufficient to determine accurately the variation of F_τ/pw with the above geometrical parameters. However, an attempt was made to obtain an approximation of the variation of F_τ/pw with the parameters R_{min}/w and h/w, on the basis of previous observations. This approximation of the relationship between F_τ/pw and the geometrical parameters R_{min}/w and h/w is shown in Figure 11. The parameter θ was not included in Figure 11 since θ varies in the same manner as h/w, and its effect on F_τ/pw may be considered as already included in h/w. This similarity in variation between h/w and θ, which is common to projecting notches with rounded tops, is clearly shown in Figure 7 for the case of Neuber's notches.

Figure 11 was obtained by first preparing a preliminary plot (not shown) which was similar to Figure 11 but whose curves passed through points representing average values of the parameters corresponding to the two values of the constant k used in the foregoing. These F_τ/pw versus h/w curves, corresponding to particular values of R_{min}/w, all pass through the origin (for the limiting case when h/w = 0, i.e., no notch) and become steeper with increasing values of h/w. One such curve corresponding to the notch defined by $\beta_o = 0.50$, with average values $F_\tau/pw = 0.1428$, h/w = 0.824, and $R_{min}/w = 0.250$, (refer to Tables 1 and 2) is shown as a dashed curve marked $R_{min}/w = 0.25$ in Figure 11.

From the above-mentioned preliminary plot the curve of Figure 10, showing the variation of F_τ/pw with R_{min}/w, was obtained. The values plotted in Figure 10 were based on F_τ/pw values corresponding to h/w = 0.80. The ordinate in Figure 10 is expressed in terms of the ratio of the F_τ/pw value corresponding to a particular value of R_{min}/w to that corresponding to $R_{min}/w = 0.250$. By assuming that the variation of F_τ/pw with R_{min}/w shown in Figure 10 applied to all values of h/w, the F_τ/pw versus h/w curves shown in Figure 11 were obtained. These corresponded to values of R_{min}/w in multiples of 0.10. In this figure, the curves were cut off at values of h/w approximately equal to twice the h/w value of the corresponding Neuber notch. This, in effect, limits the applicability of the resulting correlation to projecting notches with h/w ratios no greater than twice the corresponding value of the Neuber notch with the same R_{min}/w value. In connection with Figure 11 it is worth noting that the stress parameter F_τ/pw increases rapidly for the smaller values of h/w and changes much more slowly as h/w increases. This is consistent with the observation made earlier concerning the decrease in the efficiency* of the centerline section with increasing height of notch.

The next step involved determining the relationship between the ratio R_{min}/w of

---

*See page 8 for the special connotation attached to this term.

Neuber's notches and the ratio c/w of the equivalent surface-shear load triangle. This relationship, which is represented by the straight line of Figure 12, was obtained by using the series of curves of Figure 9. The same two values of k used earlier were used to prepare Figure 12.

Using Figure 9 in determining the value of c/w of the equivalent triangular surface-shear load corresponding to R_{min}/w of a particular notch, a value of $(\sigma_x)_{max}/p$ equal to the associated value of $(\sigma_\alpha)_{max}/p$ was assumed. (As mentioned previously, this step obviated the necessity of correcting for the difference between the actual maximum stress and the maximum longitudinal stress along the base section of the notch. At the same time it accounted for the added effect on the maximum stress of the normal stress component along the notch base.) The desired value of c/w was then taken as that value corresponding to the intersection of the appropriate F_τ/pw curve with the line representing the above value of $(\sigma_x)_{max}/p$. As an illustration, Tables 1 and 2 give the following for a Neuber notch defined by $\beta_o = 0.60$. with the base section determined by k = 0.250:

$$\frac{(\sigma_\alpha)_{max}}{p} = 1.335$$

$$\frac{R_{min}}{w} = 0.349$$

$$h/w = 0.632$$

$$\frac{F_\tau}{pw} = 0.136.$$

Using Figure 9, a horizontal line is drawn from a value of

$$\frac{(\sigma_x)_{max}}{p} = \frac{(\sigma_\alpha)_{max}}{p} = 1.335$$

until it intersects the curve corresponding to $F_\tau/pw = 0.136$. A vertical line dropped from this intersection to the c/w axis gives a value of c/w = 0.30. This value of c/w, when plotted against the corresponding value of R_{min}/w (0.349), determines a point in Figure 12. The same procedure has been followed for a number of Neuber's notches in preparing Figure 12.

The points relating the stress parameter c/w to the geometrical parameter R_{min}/w in Figure 12, for both values of k, lie very close to a straight line given by the equation

$$\frac{R_{min}}{w} = 1.25\left(\frac{c}{w}\right). \qquad (13)$$

Equation (13), which has been taken to represent the relationship between the above parameters, indicates that a triangular surface-shear load with c/w equal to 0.100 produces a maximum longitudinal stress $(\sigma_x)_{max}$ along the surface of a plain rectangular bar which is equal to the maximum stress $(\sigma_\alpha)_{max}$ in a Neuber notch with $R_{min}/w = 0.125$ and having the same value of F_τ/pw. Thus, as developed in the foregoing, the equivalent surface-shear load consists in a triangularly distributed surface-shear stress loading having a value of F_τ/pw equal to that along the base section of the corresponding projecting notch. Its value of c/w is such that the maximum longitudinal stress along the surface of a plain rectangular bar produced by such a loading -- acting together with an axial tensile loading of intensity p at the ends of the bar -- is equal to the actual maximum stress occurring in the corresponding notch.

The use of results of the surface-shear load method (which is based on a bar of finite depth with symmetrically disposed projecting notches) in conjunction with Neuber's notches (which are notches in a half-plane) is considered permissible since the final correlation

is independent of the assumed bar depth 2b. This neglect of the effect of the bar depth on the maximum stress is not only demanded by the fact that Neuber's notches have an infinite depth associated with them but is also justified by the fact that the maximum longitudinal stress obtained by the surface-shear load method is affected very little by the depth of the bar. This latter fact is clearly indicated in Table 3, which shows values of $(\sigma_x)_{max}/p$ corresponding to values of b/w ranging from 1.0 to 10.0, $F_\tau/pw = 0.075$, and $F_\tau/pw = 0.150$. The maximum difference between the various values of the maximum stress and those corresponding to b/w = 2.0, the ratio which was used in obtaining the results plotted in Figure 9, is 1.09 per cent.

The final step in obtaining the desired relationship between the stress concentration factor and the geometrical parameters characterizing the profile of Neuber's notches was carried out using Figures 9, 11, and 12. The consolidated results are shown in Figure 13. Thus, the relationship between F_τ/pw, R_{min}/w, and h/w of Figure 11 was replaced by the curves marked A and B in Figure 13, the B curves serving essentially as a curved F_τ/pw scale. It should be noted that a progressively decreasing scale was used for the h/w axis, since the variation of h/w was assumed to be linear between the marked points on the top scale. The relationship between c/w and R_{min}/w of Figure 11 appears in Figure 13 as a change from the c/w scale of Figure 9 to the R_{min}/w scale at the bottom of the figure.

In using Figure 13 to determine the stress concentration factor for a projecting notch of given characteristic dimensions, the procedure is as follows.

(1) From a point representing the given h/w value on the top scale, a vertical line is dropped until it intersects the curve marked A corresponding to the given value of R_{min}/w (estimating intermediate values if necessary).

(2) One then moves from this point in a direction parallel to the curves marked B (again estimating intermediate values when necessary) to the given value of R_{min}/w as indicated on the bottom scale.

(3) A horizontal line drawn from this point to the $(\sigma_\alpha)_{max}/p$ axis gives the stress concentration factor.

A more convenient form of the relationship between the stress concentration factor and the geometrical parameters characterizing the profile of the Neuber notch is shown in Figure 14. This figure, based on Figure 13, represents the final results of the correlation for Neuber's notches. The curve corresponding to h/w = 0.20 in Figure 14 appears as a dashed curve in Figure 13. In both Figures 13 and 14, the dashed lines indicate the use of the graphs for the case of a Neuber notch defined by $\beta_o = 0.60$ and $k = 0.250$.

The values of the stress concentration factor for Neuber's notches (obtained using Figure 14) are compared with the calculated values in Table 4. This table includes only those notches with characteristic dimensions which fall within the range of the respective parameters in Figure 14. A maximum error of 6.0 per cent occurs for the higher notches, with smaller errors corresponding to the flatter notches.

The larger errors in the values of the stress concentration factor obtained from Figure 14 occur for the notches defined by $\beta_o = 0.25$ and $\beta_o = 0.30$. The profiles of these notches have flank angles exceeding 90 degrees, i.e., the notch profile in each

case flares out above the point of minimum radius of curvature so that a vertical line intersects the profile at three distinct points (see Figure 2). Had the points corresponding to the above two notches been plotted in the $(\sigma_\alpha)_{max}/p$ versus θ graph of Figure 7, (these points would fall beyond the limits of Figure 7) they would lie farther from the straight line representing the variation of the maximum stress with the flank angle θ than the points on the plot corresponding to the other notch profiles. In contrast, the points corresponding to these same two notch profiles in the $(\sigma_\alpha)_{max}/p$ versus h/w plot of Figure 7 lie along the straight line representing the variation of the maximum stress with the ratio h/w. This indicates that for these two particular profiles, the flank angle does not vary in the same manner as does the ratio h/w for the other notch profiles, and that the effect of the flank angle on the maximum stress cannot be considered as being directly reflected in the ratio h/w. Thus, the difference between the calculated values of the stress concentration factor and the corresponding values obtained from Figure 14 for notch profiles with flank angles exceeding 90 degrees is the result of an increased effect of the flank angle.

• • •

IV. ANALYSIS OF STRESSES FOR IDEALIZED PROJECTING NOTCHES

A. FINITE-DIFFERENCE SOLUTION

In order to arrive at a correlation between the stress concentration factor and the geometrical parameters for the case of the idealized projecting notch of Figure 1a, using the same method employed in connection with Neuber's notches, a finite-difference solution was employed. The finite-difference method, although approximate, allows a controlled variation of the geometrical parameters defining the notch profile, a requirement essential in this study. Thus, although the geometrical parameters characterizing the profiles of Neuber's notches have fixed relationships, the finite-difference method made it possible to specify the dimensions of the notch profile and to vary the parameters independently of each other. This flexibility allowed the effect of each parameter to be ascertained more fully.

A brief description of the method of finite differences and a derivation of the boundary conditions in terms of Airy's stress function for the particular case considered here is given in Appendix C. Because of the two-fold symmetry of the notched bar section, only one-fourth of the entire section was considered in the solution. This is shown in Figure C-1 of Appendix C. A value of w equal to 4.0 units has been used.

Using the finite-difference method, values of the stress concentration factor were obtained as well as the stress parameters F_τ/pw and c/w, corresponding to a number of notch profiles. All calculations made in this study were carried out on the University of Illinois' IBM 7094 electronic digital computer. The limited storage space in the computer is a major problem which must be considered in using the method of finite differences. The storage space available in the computer memory limits the number of equations which may be solved and hence the fineness of the grid which may be used for a given area. This is particularly important since accuracy is heavily dependent upon the fineness of the grid used.

By solving the resulting set of simultaneous equations by iteration rather than by a direct method and by taking advantage of the sparseness of the associated matrix of coefficients, it was possible to write a computer program capable of handling 1000 points on a 40 x 45 mesh grid.

The complete solution involved three steps. The first employed a relatively coarse grid, the starting values of the stress function for the iterative solution being taken to equal zero. The values of the function obtained from this coarse-grid solution (with values at intermediate points calculated by linear interpolation) were then used as starting values for the iterative process of the second step. In the second step, a grid spacing equal to one-half that of the first step was used. By thus obtaining rough

approximations of the values of the function with the coarse-grid solution of the first step and using these as starting values for the second step, the convergence of the iterative process in the latter was hastened considerably.

A further refinement of the grid spacing was carried out in the third step of the solution, which used a mesh interval equal to one-half that of the second step and included only a portion of the area considered in the first two steps. For this final step, the area considered was bounded by a horizontal line a few mesh intervals below the base of the notch and a vertical line a few mesh intervals beyond the toe of the notch. This new boundary is indicated by the dashed line marked S in Figure C-1 of Appendix C. Values of the stress function along this new boundary as obtained in the second step -- with intermediate values calculated by parabolic interpolation -- were used as the new boundary values for the third step.

In addition to the values of the stress function obtained in the preceding coarser-mesh solution as starting values for the second- and third-step iterations, systematic over-relaxation[20,21] was used to improve the convergence of the Gauss-Seidel method. The optimum value of the over-relaxation factor (corresponding to the maximum rate of convergence) was determined by trial and ranged from 1.65 to 1.75, decreasing with the closeness of the starting values to the true solution and increasing with the number of equations involved (the factor can vary theoretically from 1.0 to 2.0). The convergence criterion used required that the absolute value of the residual in 99 per cent of the equations involved be equal to or less than a specified value. The results given below were obtained using a maximum allowable residual of 0.05 for the first step and 0.01 for the second and third steps. The magnitudes of these residuals were selected with the aim of obtaining a solution requiring only a reasonable amount of computer time and are believed to have resulted in relatively small errors in the calculated values of the stress function. With the above criteria, convergence was achieved after an average of 340 cycles of iteration for the first step, 80 cycles for the second step, and 40 cycles for the third step. These correspond to an average of 150 points (or unknowns) for the first step, 550 points for the second step, and 700 points for the final step. In all cases, there was a slight increase in F_τ/pw and a comparatively greater increase in σ_{max}/p with each refinement of the grid spacing, corresponding to each step of the solution.

Because of the limited capacity of the program, the total length a of the section considered was limited to a value slightly greater than twice the half-width of the notch w; the depth of the section below the base of the notch b was limited to a value slightly greater than w. The results of the calculations listed in Table 5 were obtained using $a/w = 2.10$ and $b/w = 1.05$ for the first two steps of the solution, and $a'/w = 1.425$ and $b'/w = 0.375$ for the final step. The restriction on the number of unknowns capable of being handled by the program eliminated the possibility of studying the effect of the depth of the bar 2b on the stress concentration factor. However, the results of a limited number of two-step solutions carried out to check this effect indicate a slight decrease in both F_τ/pw and σ_{max}/p with an increase in b/w. A solution using a value of $a/w = 3.00$ did not show any significant difference from the stress values corresponding to $a/w = 2.10$.

B. CORRELATION OF STRESS AND GEOMETRICAL PARAMETERS

To carry out the desired correlation, the stresses at points along the surface of the notch as well as those along the base and centerline sections were calculated for notches with flank angles of 30 degrees, 60 degrees, and 90 degrees. The ratio R/w was given values of 0.30, 0.40, 0.50, and 0.60, while h/w was varied from 0.30 to a maximum of 0.90. The results of the calculations are given in Table 5.

Using Simpson's rule, the values of F_τ/pw and F_σ/pw in Table 5 were calculated from the values of the stresses along the respective sections. It is worth noting the close agreement between the values of these two quantities for the different notches considered. The values of the ratio c/w, as well as those of σ_{max}/p, were obtained graphically, i.e., by passing smooth curves through points representing calculated values. Examples of such plots are shown in Figures 15 and 16. In all cases considered, the maximum stress occurred at a point along the circular arc where the tangent made an angle of between 5 and 15 degrees with the axis of the bar.

Although approximate, the results of the calculations are in general reasonably consistent and provide a good indication of the relative effects of the different parameters considered. The calculated values along the boundary, where interpolation equations had to be used, are likely to be in greater error than those corresponding to interior points.

Notches with θ = 90 Degrees

Stresses for notches with flank angles equal to 90 degrees were calculated for values of h/w equal to 0.30, 0.45, 0.60, 0.75, and 0.90. These values of h/w were chosen to maintain the same grid spacing throughout. Thus, for the notch with h/w = 0.60, the height of the notch h was divided into four equal parts in the first step of the solution; for the notch with h/w = 0.75, it was divided into five equal parts, etc. The program was written so that the mesh interval for the first-step solution was determined by dividing the height of the notch into a number of equal parts, the minimum number being three. Because of this limitation on the number of parts into which the height of the notch could be subdivided and in order to maintain the same grid spacing in the final step of the solution for all the notches considered, the stresses for notches with h/w = 0.30 were obtained by using only the first and final steps of the complete solution. For this particular value of h/w, the height of the notch was divided into four equal parts and a maximum allowable residual of 0.01 was used for the iterative solution in the first step. With the height of the notch divided as indicated above, a grid spacing of 0.150 units was obtained for the third-step solution. This gave values of the ratio of the mesh interval to the radius of curvature Δ/R of 0.125, 0.094, 0.075, and 0.062 corresponding to R/w values of 0.30, 0.40, 0.50, and 0.60.

Essentially the same procedure as that used for the case of Neuber's notches was employed to obtain the desired relationship between the stress concentration factor and the geometrical parameters defining the notch profile.

A plot of the variation of the shearing stress parameter F_τ/pw with h/w for different values of R/w is shown in Figure 17. The values of F_τ/pw used in Figure 17 have been taken as the average of the calculated values of F_τ/pw and F_σ/pw. Since, for equilibrium, these two values should be equal, their average appears to provide the most representative value. The curves through the plotted points corresponding to different values of

SUPPORTING DATA

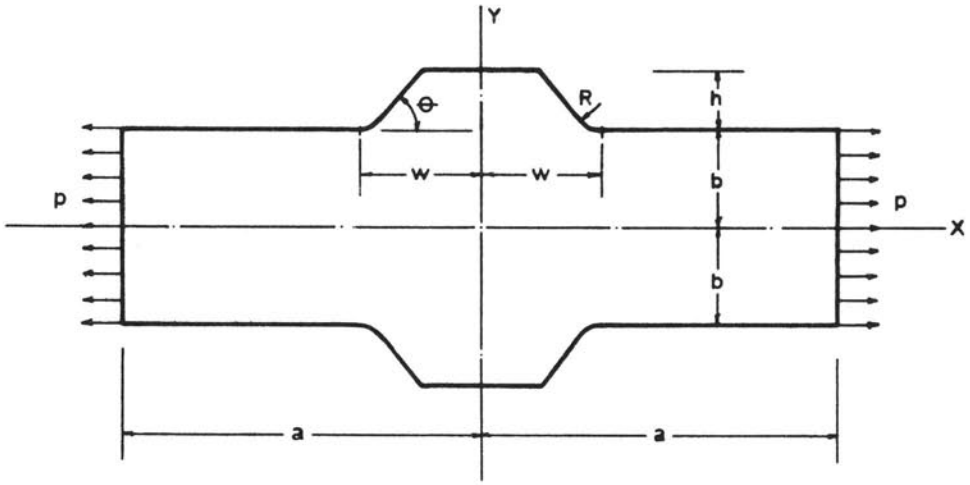

FIGURE 1a. SYMMETRICALLY DISPOSED PROJECTING NOTCHES IN A BAR OF RECTANGULAR CROSS SECTION

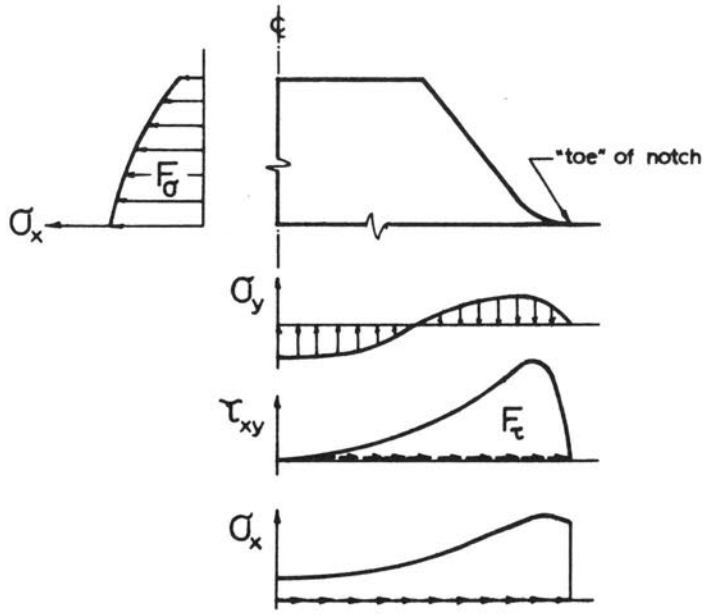

FIGURE 1b. TYPICAL DISTRIBTUIONS OF STRESSES ALONG CENTERLINE AND BASE SECTIONS

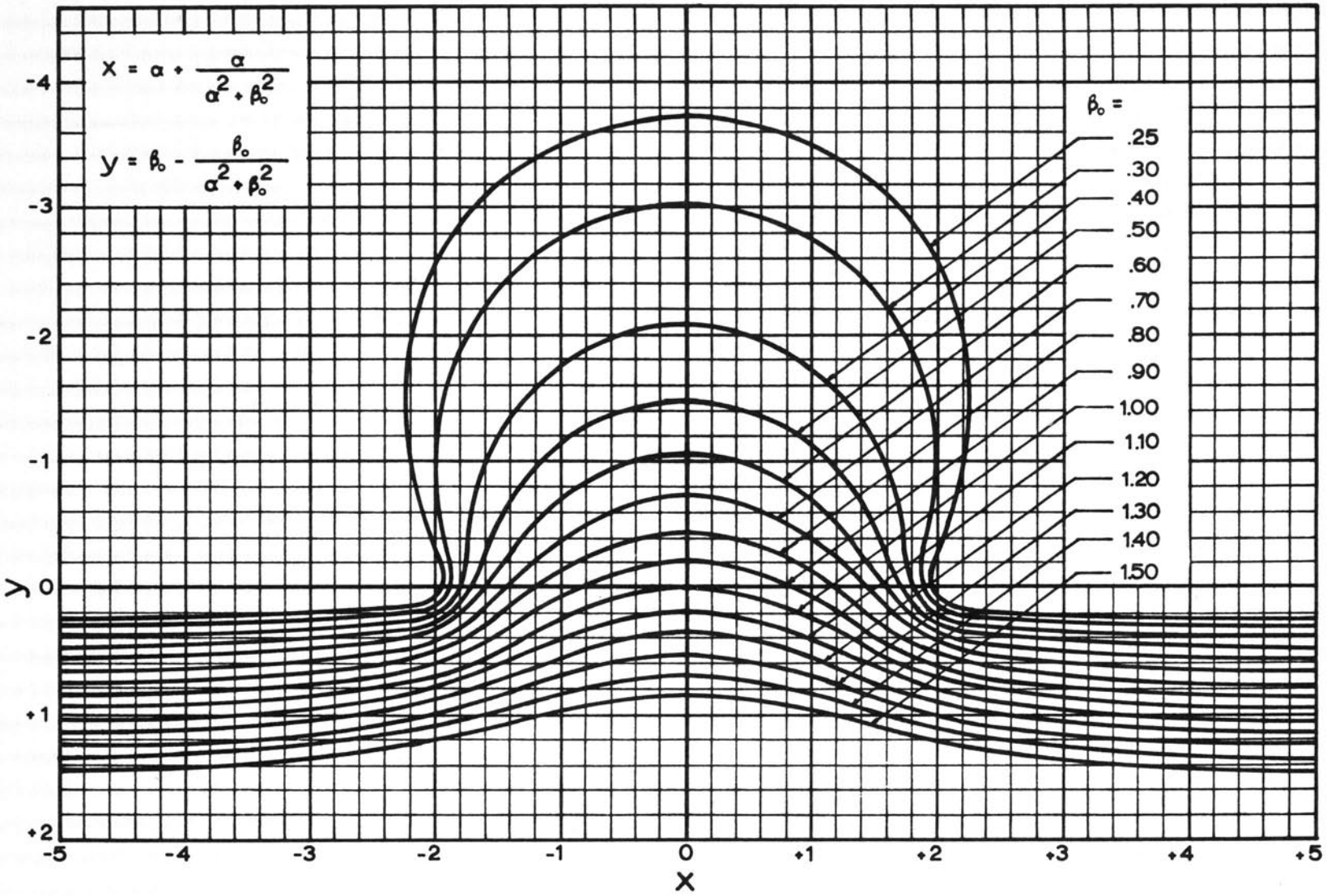

FIGURE 2. PROFILES OF NEUBER'S PROJECTING NOTCHES

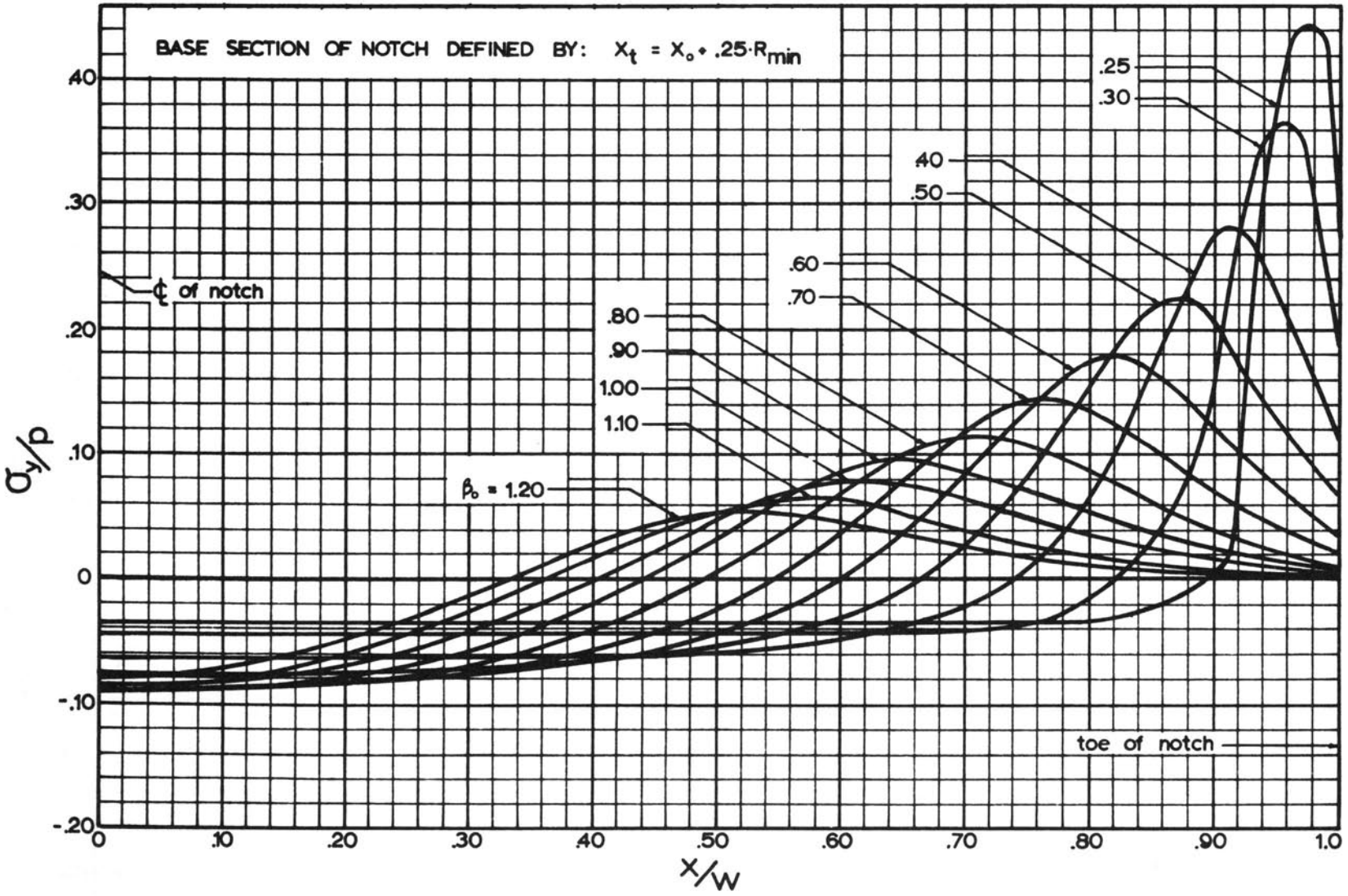

FIGURE 3. DISTRIBUTIONS OF NORMAL STRESSES ALONG THE BASES OF NEUBER'S NOTCHES

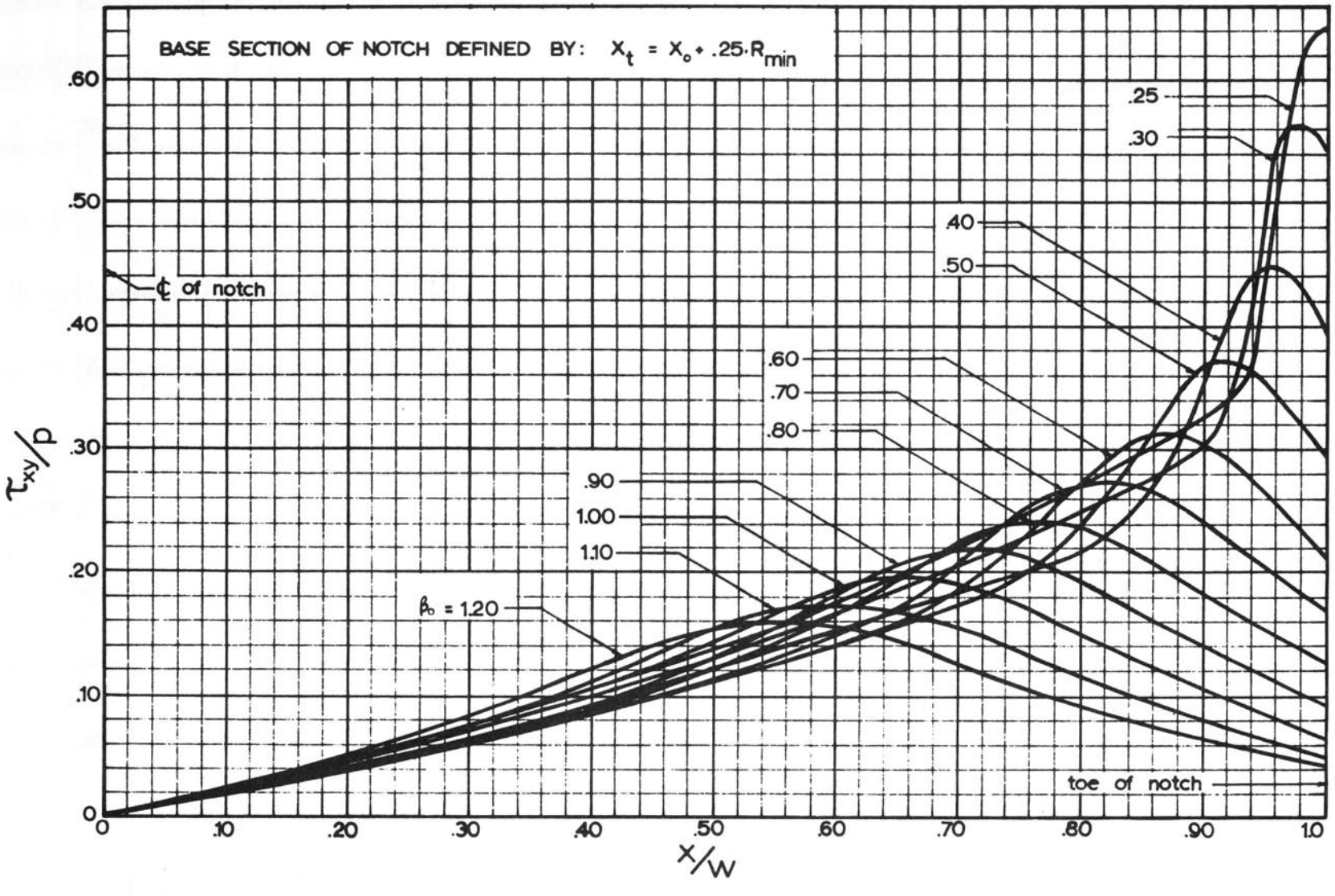

FIGURE 4. DISTRIBUTIONS OF SHEARING STRESSES ALONG THE BASES OF NEUBER'S NOTCHES

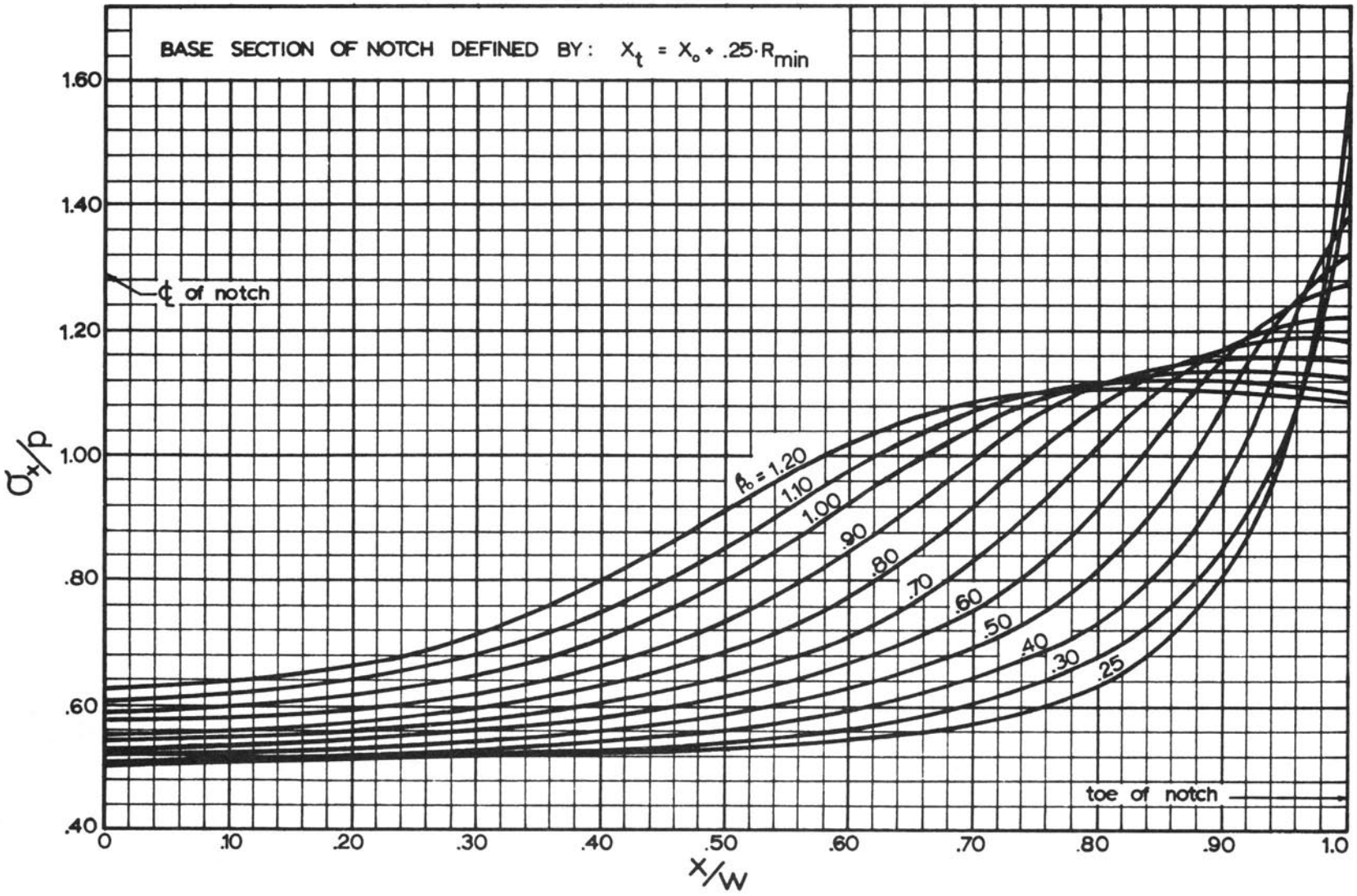

FIGURE 5. DISTRIBUTIONS OF LONGITUDINAL STRESSES ALONG THE BASES OF NEUBER's NOTCHES

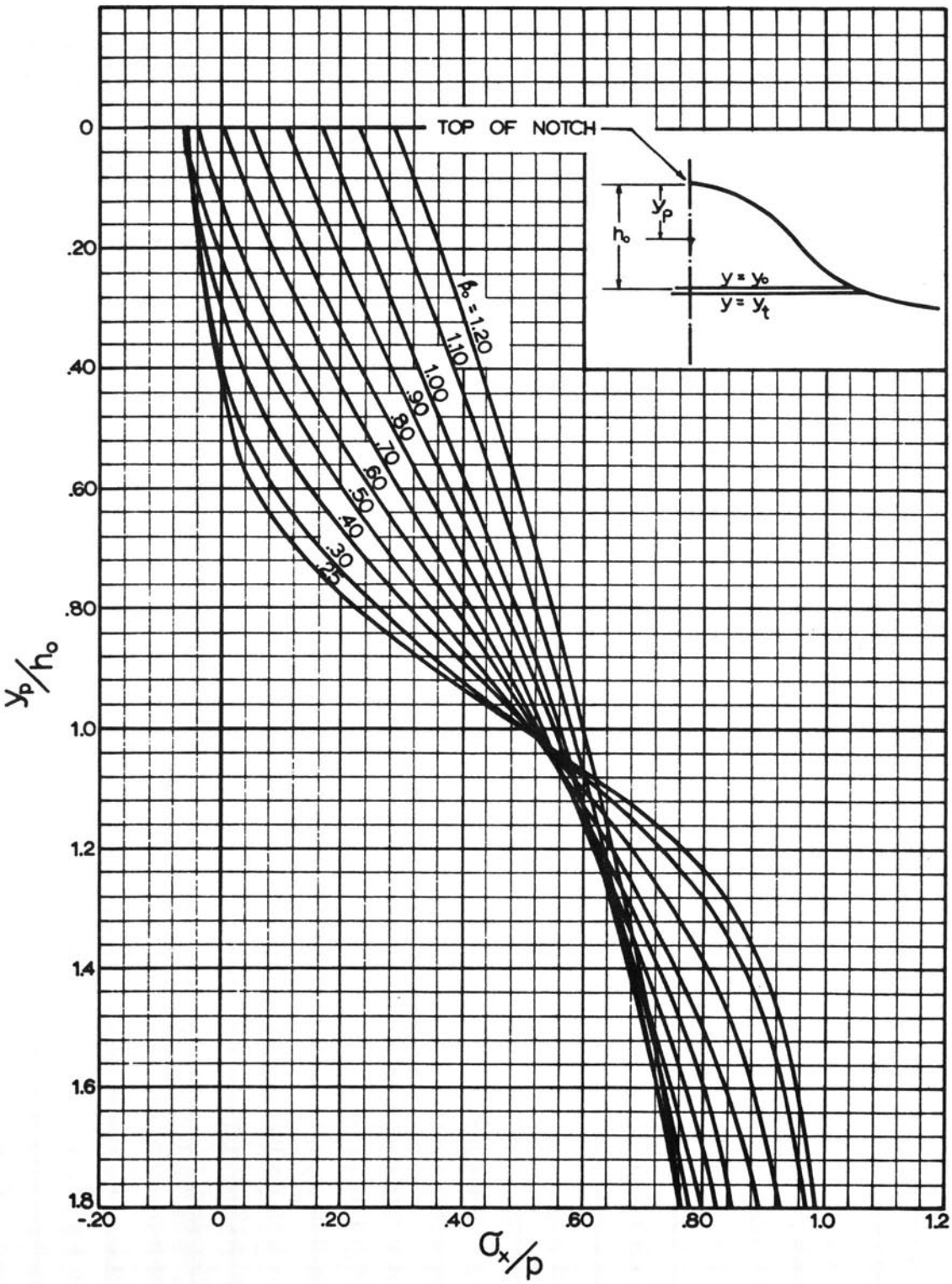

FIGURE 6. DISTRIBUTIONS OF LONGITUDINAL STRESSES ALONG THE CENTERLINE OF NEUBER'S NOTCHES

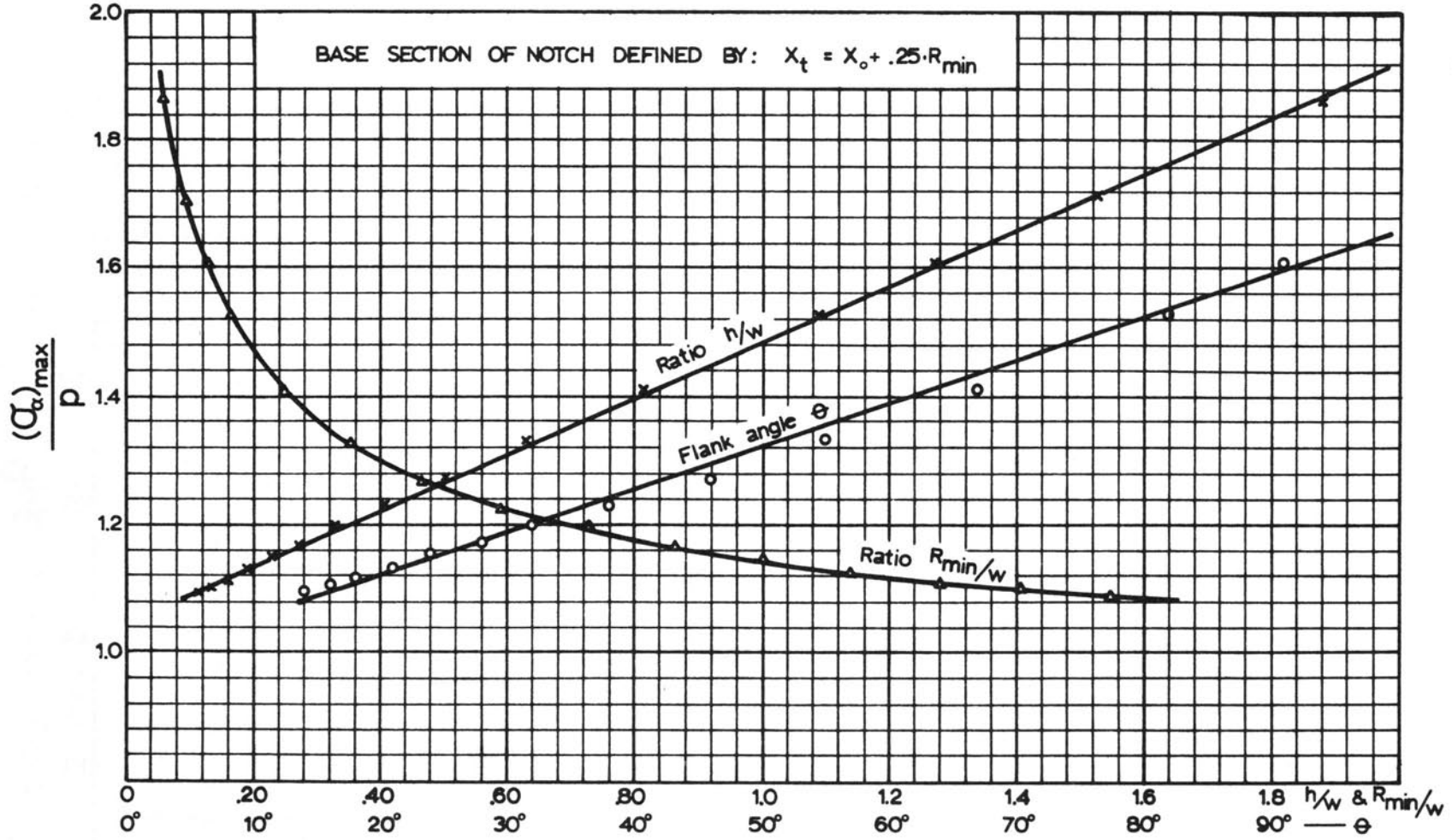

FIGURE 7. VARIATION OF STRESS CONCENTRATION FACTOR WITH PARAMETERS h/w, R_{min}/w, and θ FOR NEUBER'S NOTCHES

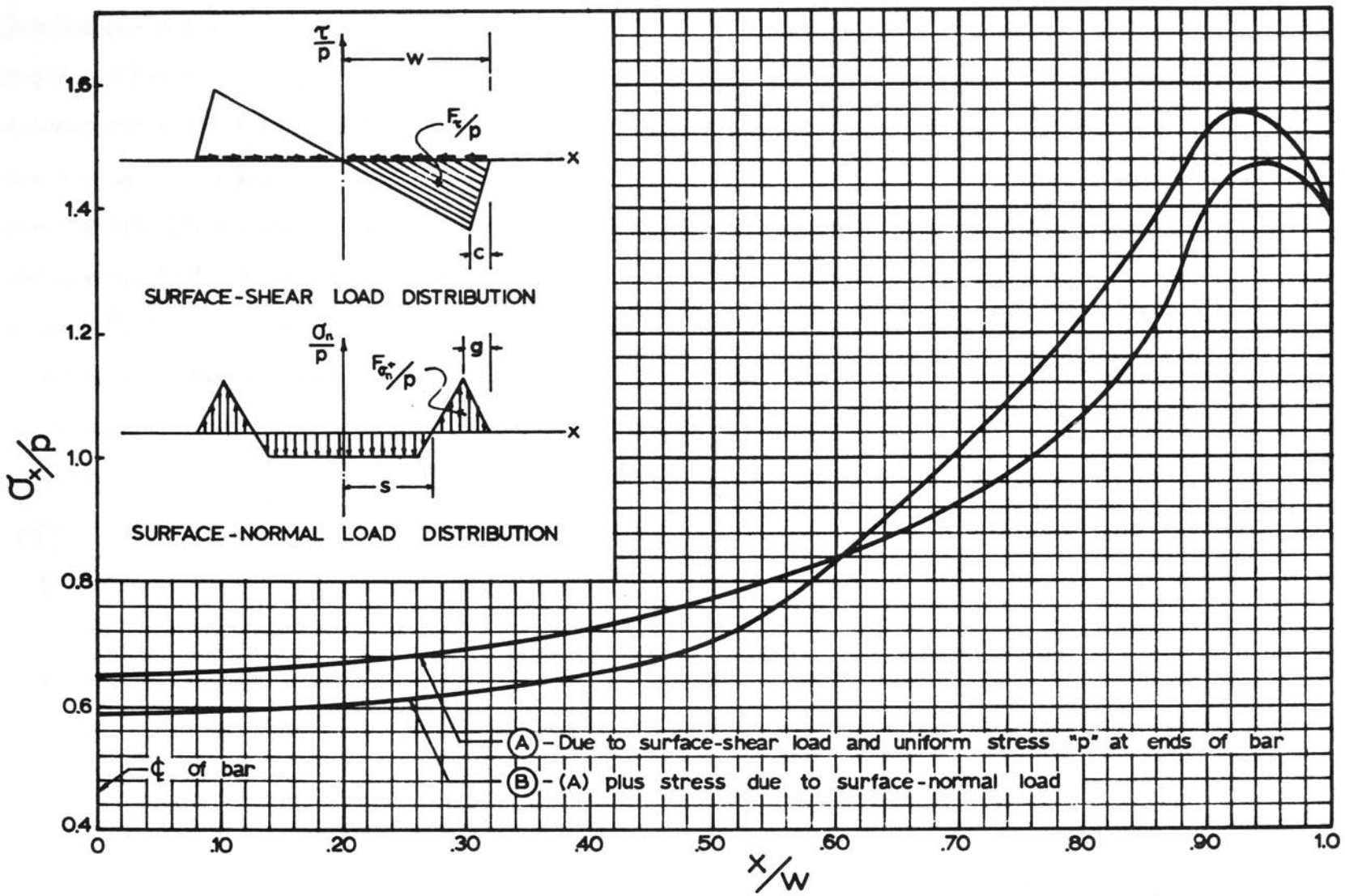

FIGURE 8. LONGITUDINAL STRESS ALONG SURFACE OF RECTANGULAR BAR DUE TO SURFACE STRESS LOADINGS

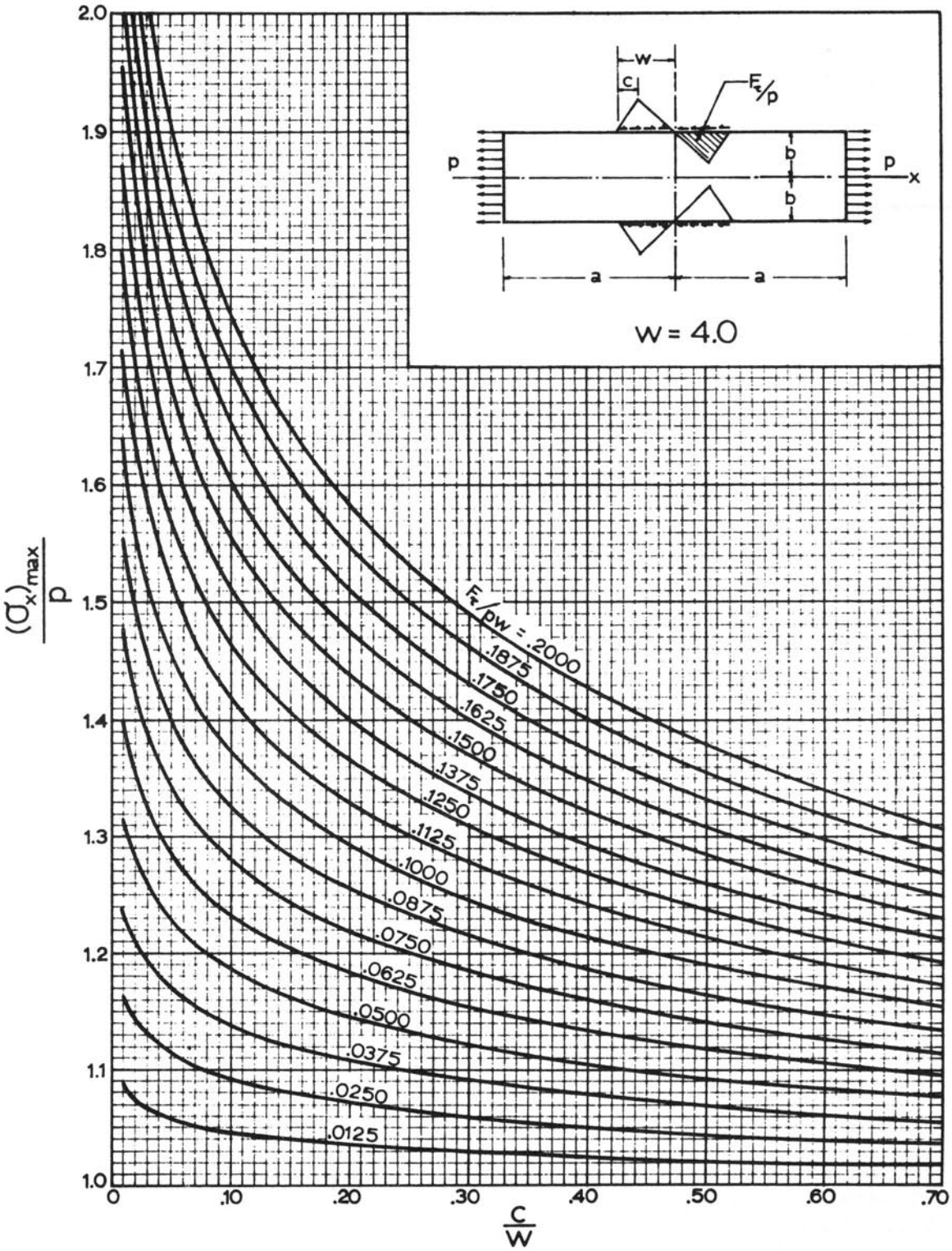

FIGURE 9. MAXIMUM STRESS IN A RECTANGULAR BAR DUE TO SURFACE-SHEAR LOAD AND UNIFORM STRESS ACROSS ENDS

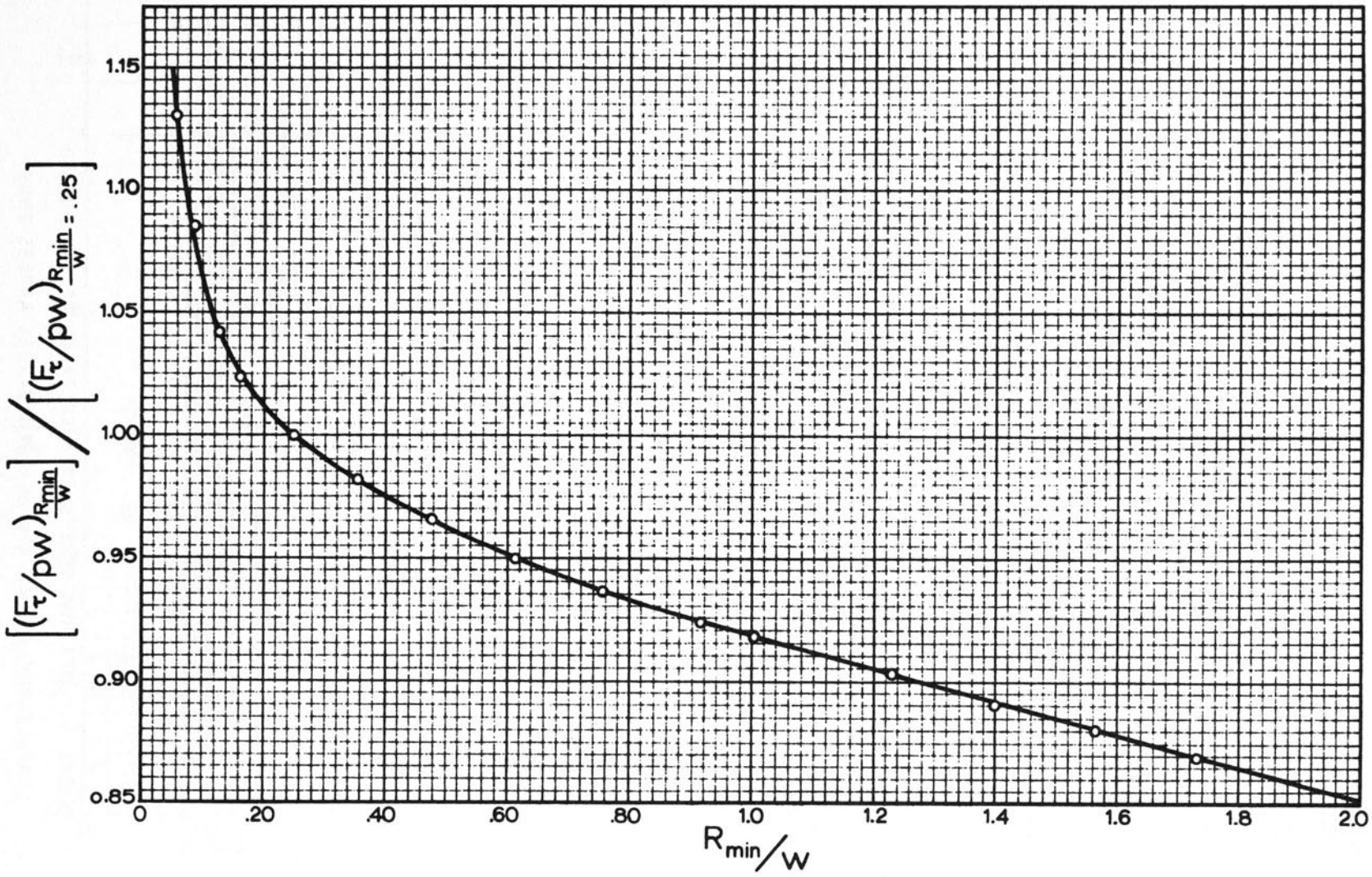

FIGURE 10. APPROXIMATE VARIATION OF SHEARING STRESS PARAMETER, F_τ/pw, WITH R_{min}/w NEUBER'S NOTCHES

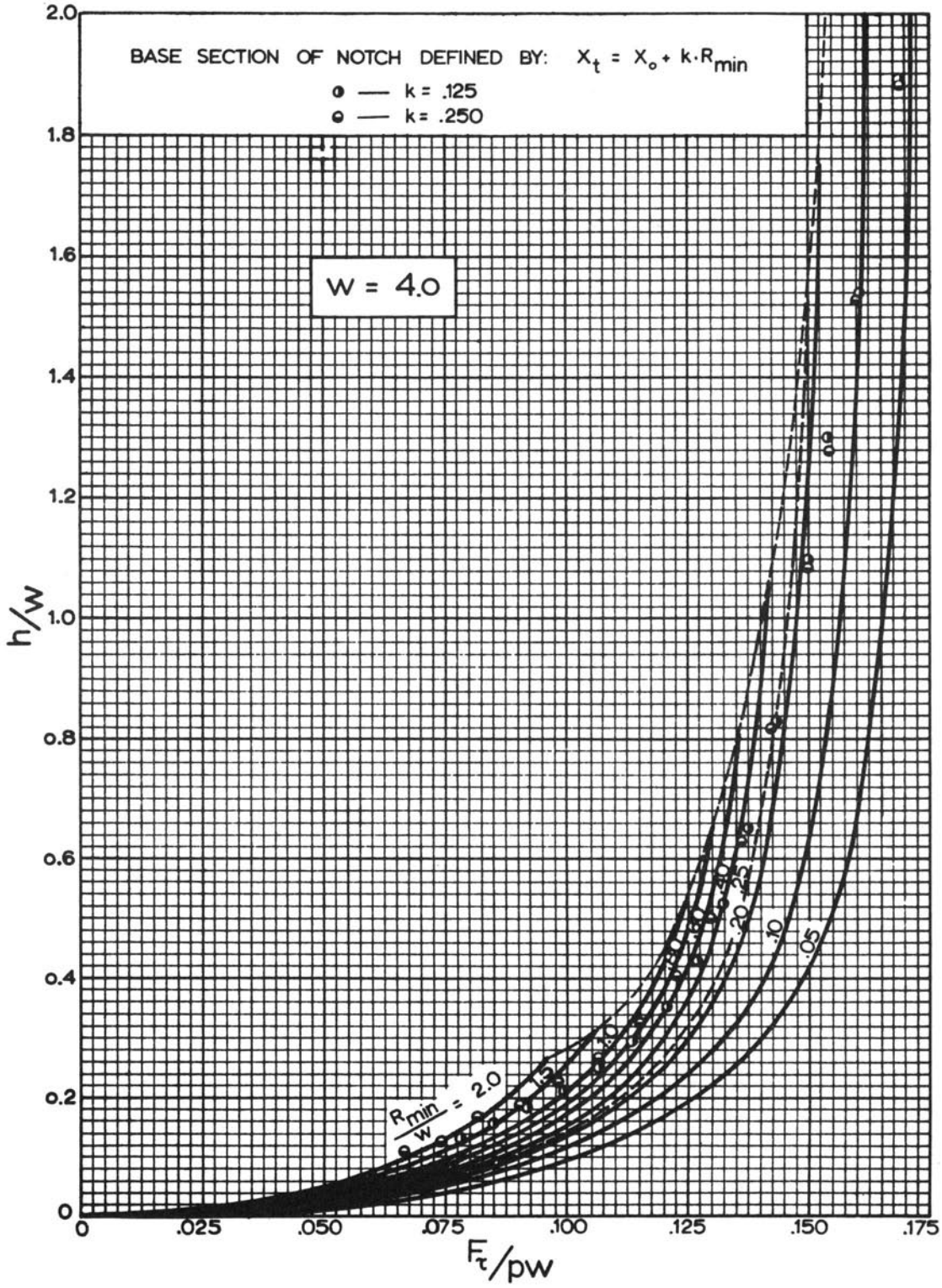

FIGURE 11. SHEARING STRESS PARAMETER F_τ/pw AS A FUNCTION OF R_{min}/w AND h/w FOR NEUBER'S NOTCHES

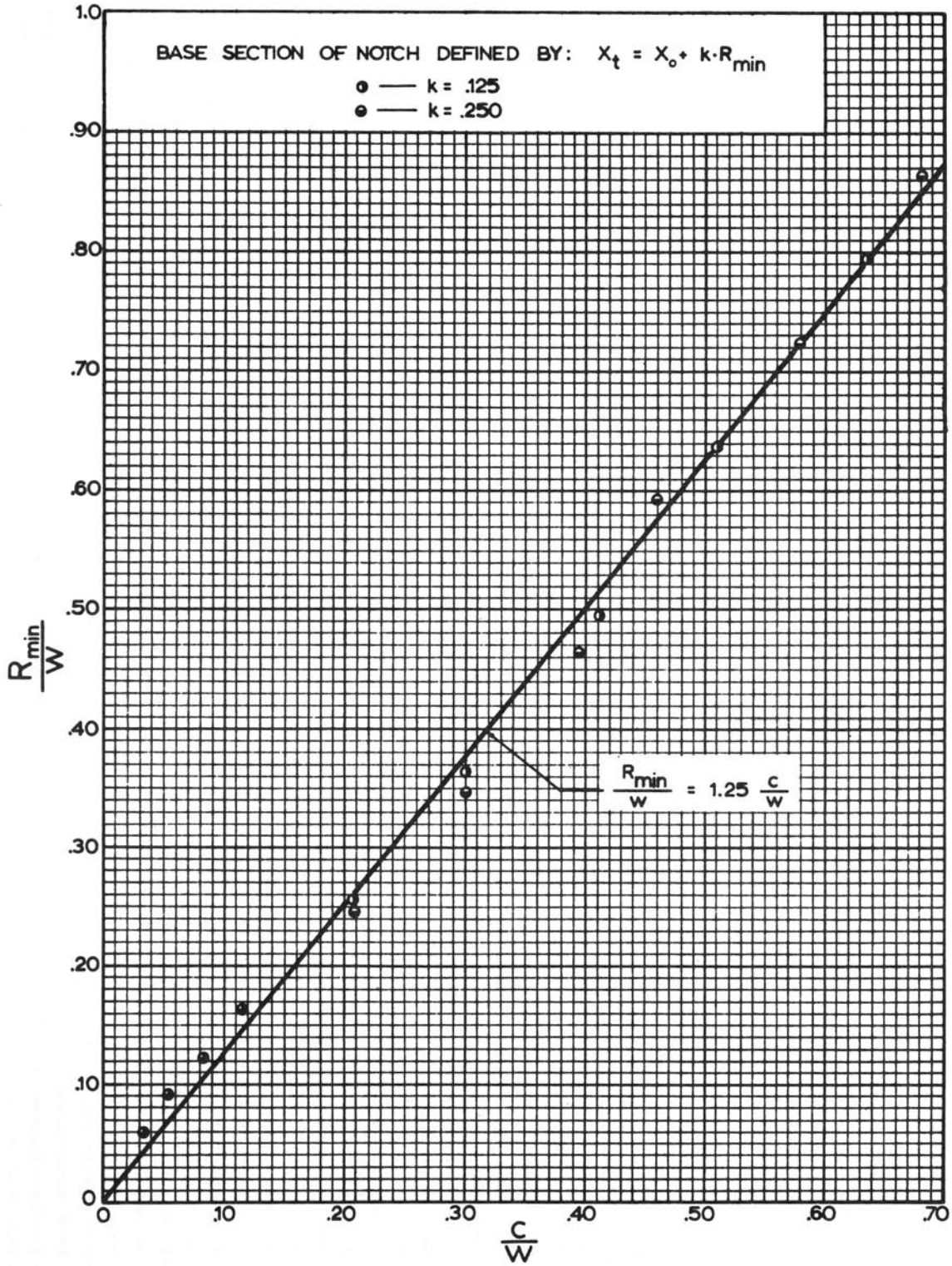

FIGURE 12. CORRELATION OF R_{min}/w OF NEUBER'S NOTCHES WITH c/w OF TRIANGULAR SURFACE-SHEAR LOAD

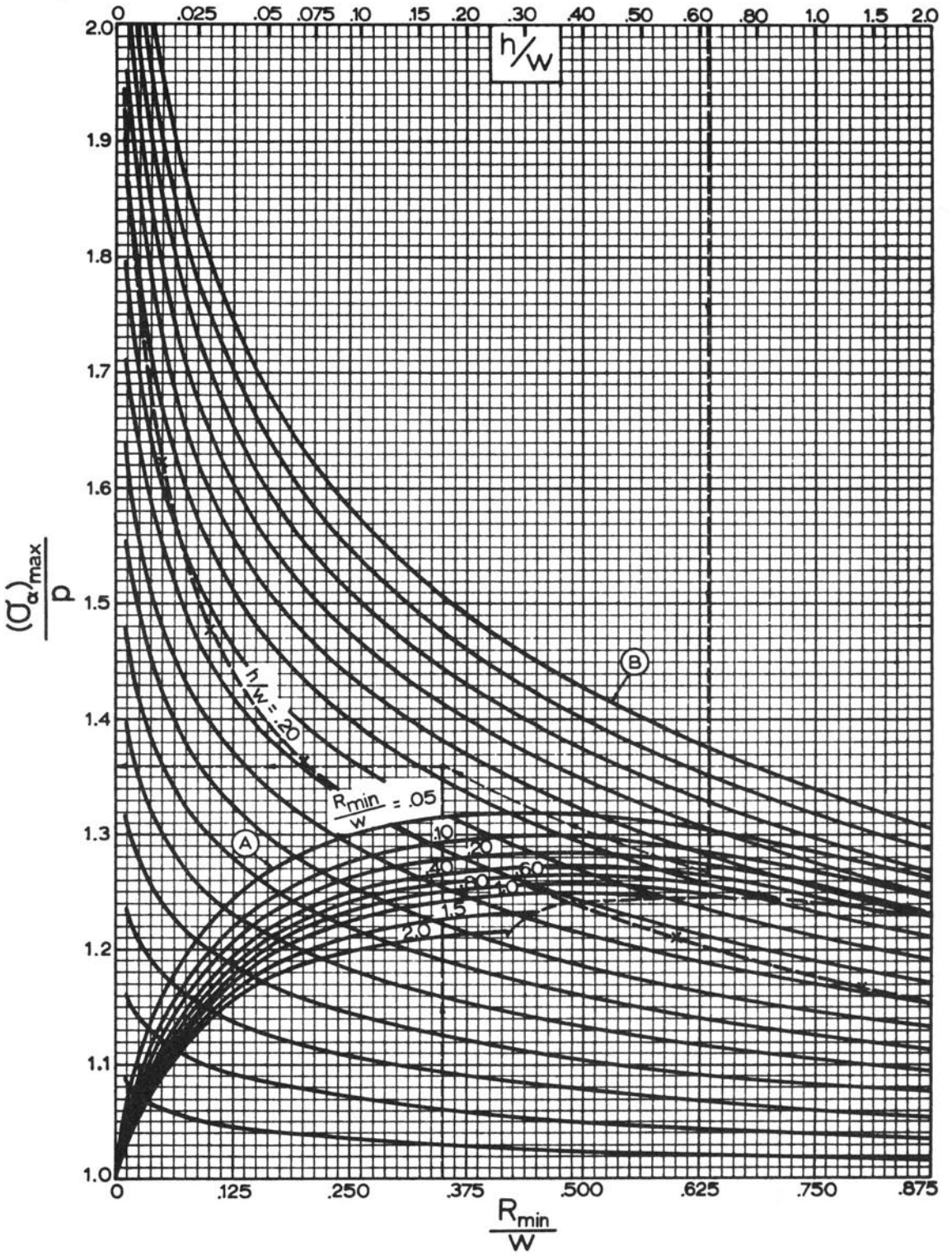

FIGURE 13. THE STRESS CONCENTRATION FACTOR AS A FUNCTION OF h/w AND R_{min}/w FOR NEUBER'S NOTCHES

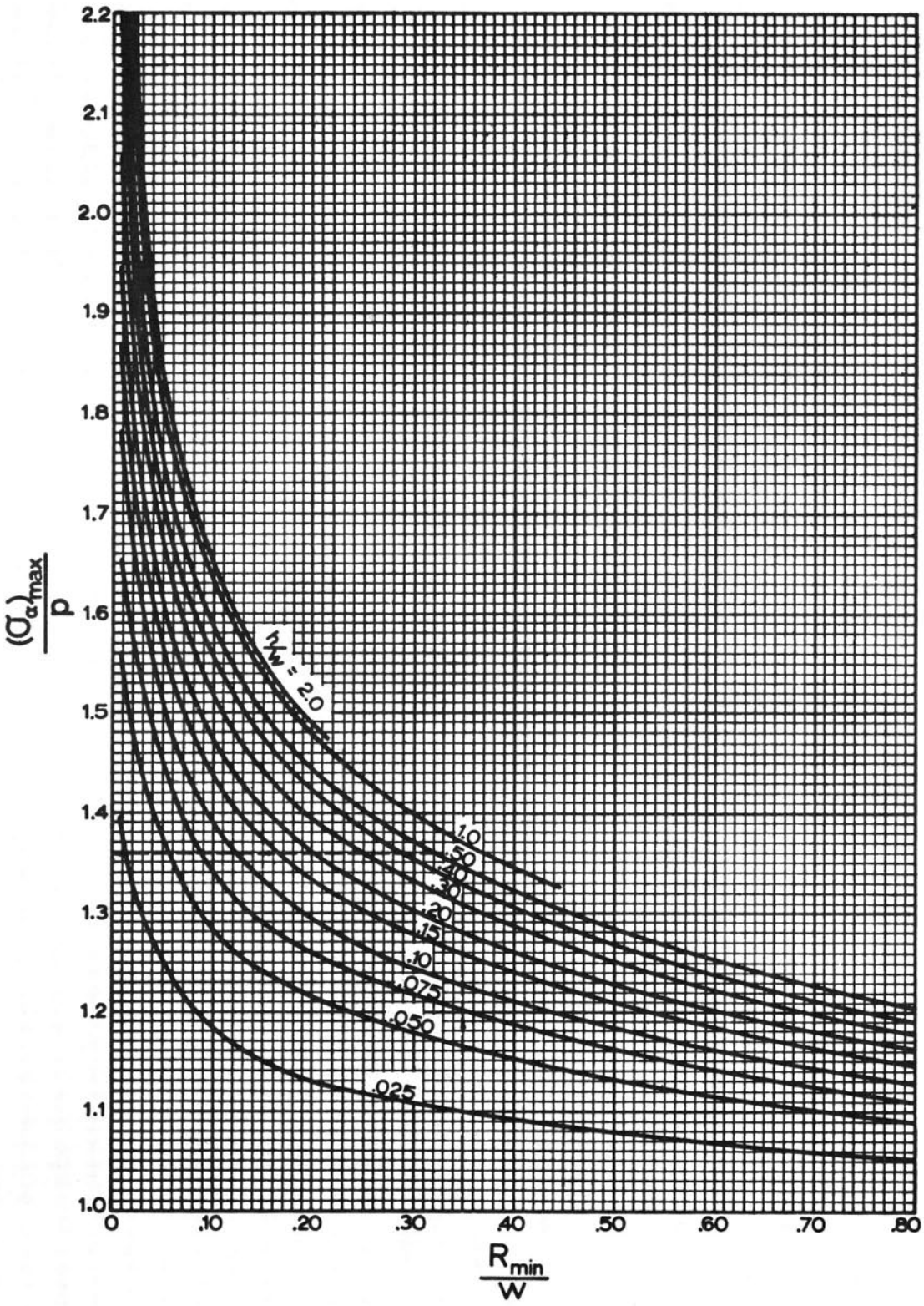

FIGURE 14. STRESS CONCENTRATION FACTORS FOR NEUBER'S NOTCHES

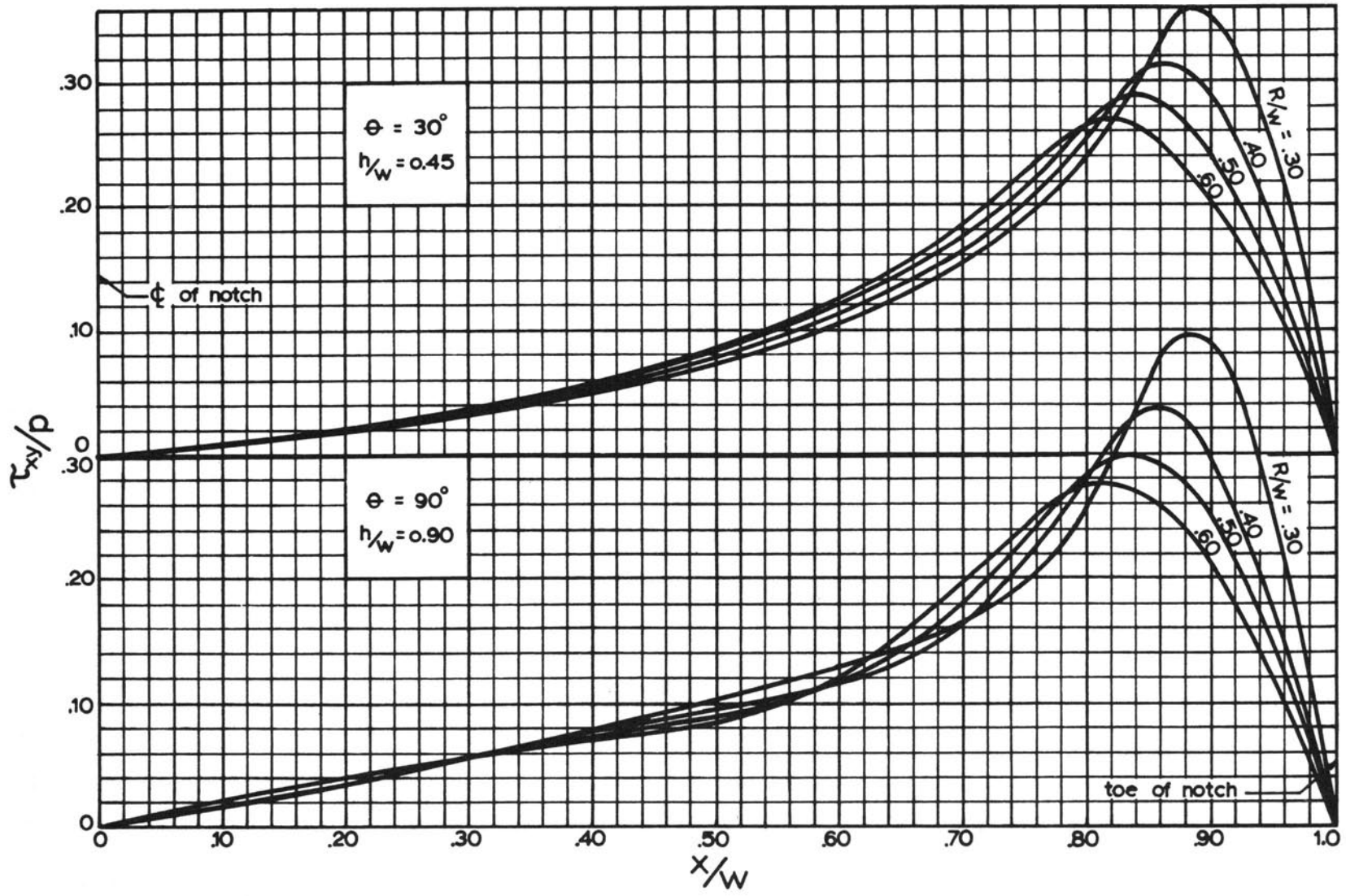

FIGURE 15. DISTRIBUTIONS OF SHEARING STRESSES ALONG THE BASES OF IDEALIZED PROJECTING NOTCHES

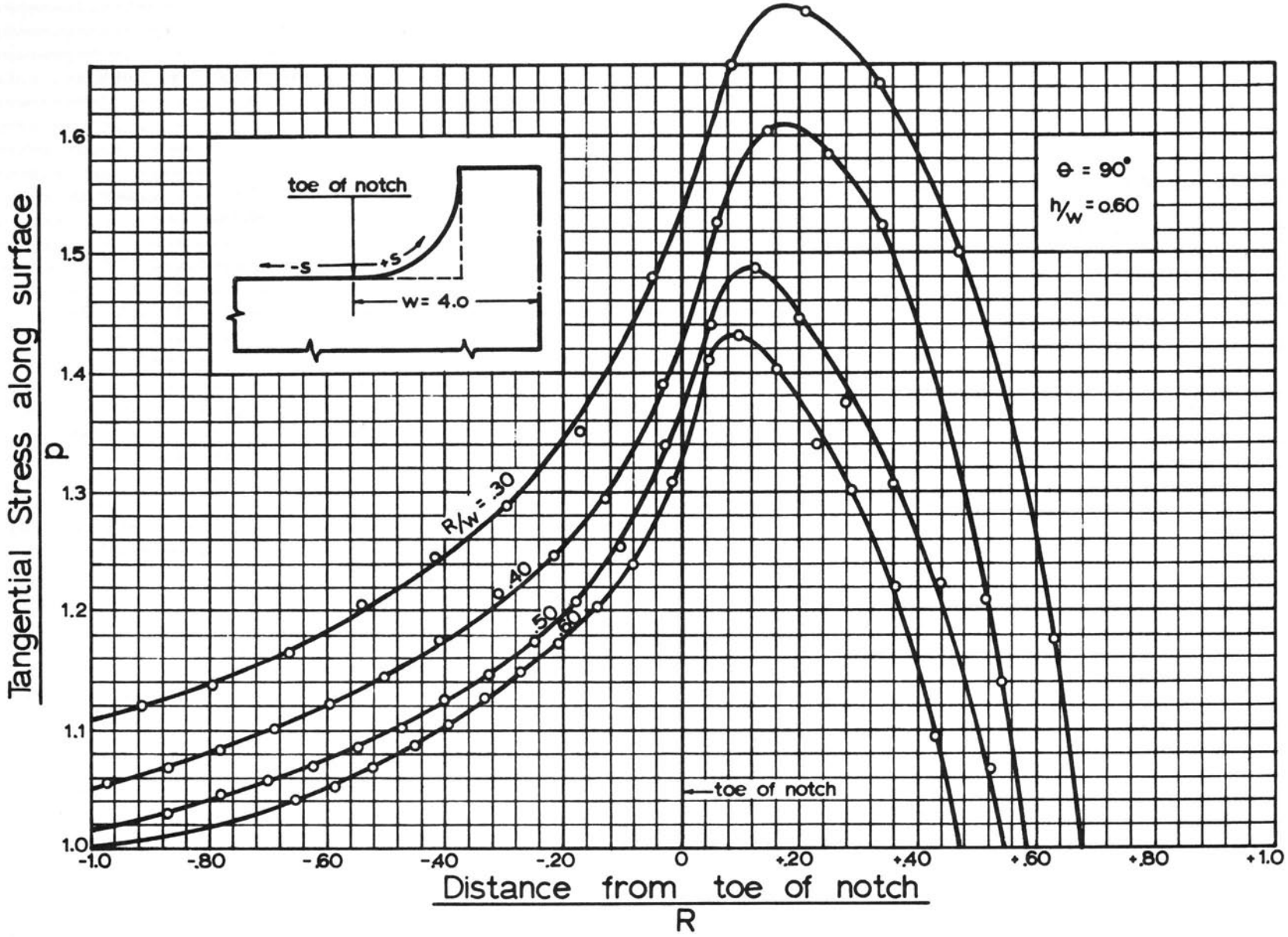

FIGURE 16. GRAPHICAL ESTIMATION OF MAXIMUM STRESSES

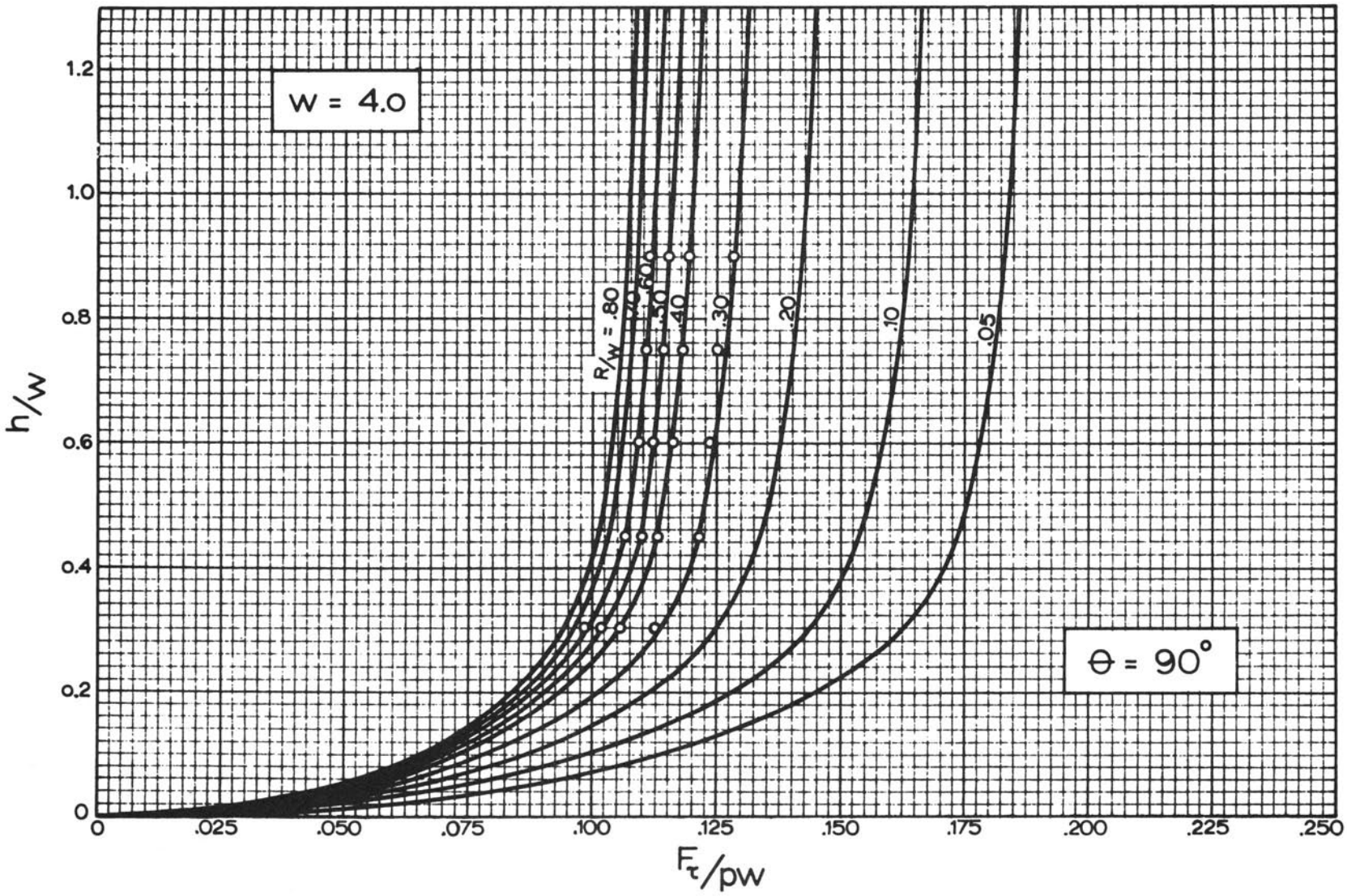

FIGURE 17. SHEARING STRESS PARAMETER, F_τ/pw, AS A FUNCTION OF h/w AND R/w, FOR IDEALIZED PROJECTING NOTCHES WITH θ = 90 DEGREES

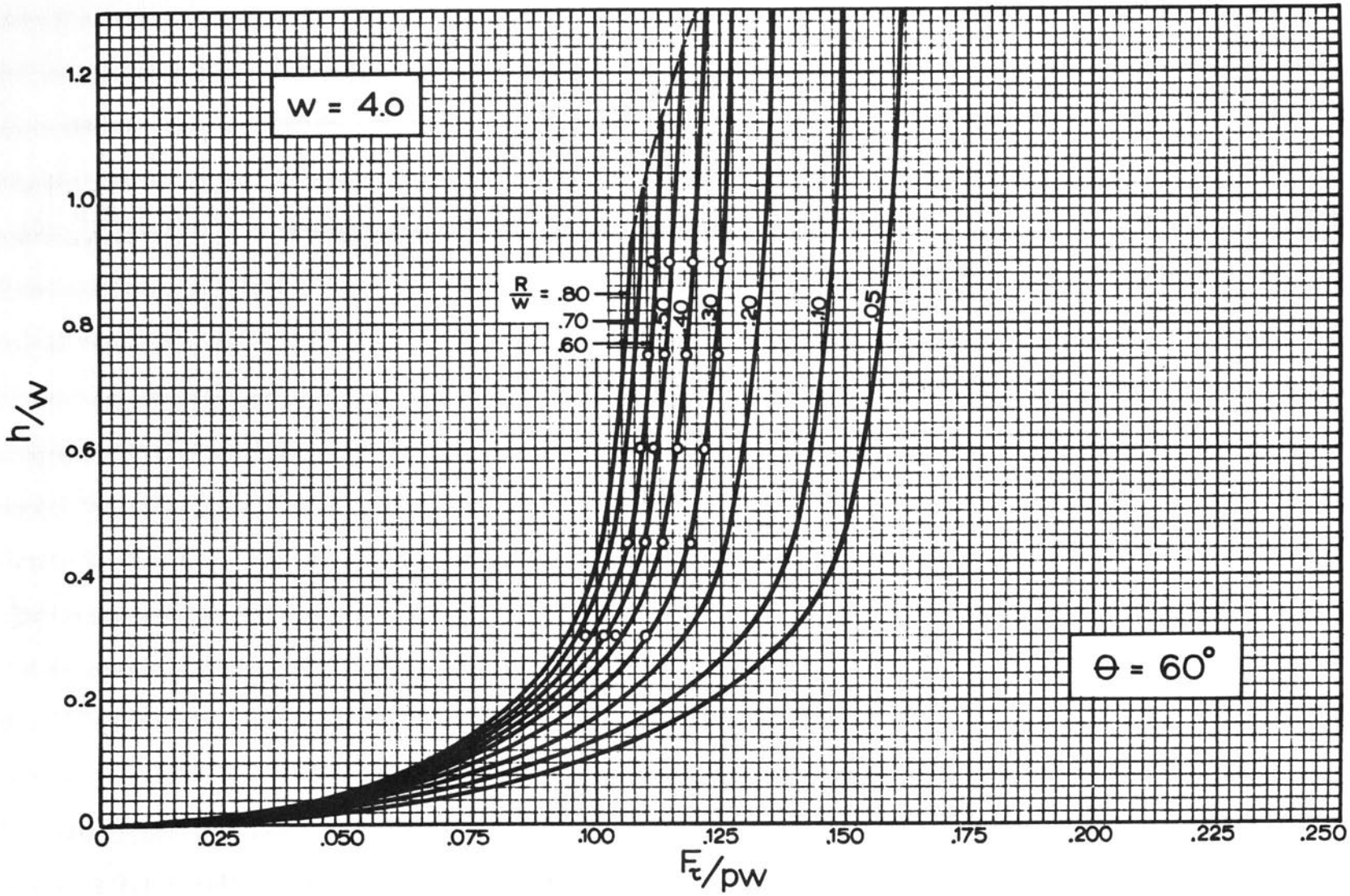

FIGURE 18. SHEARING STRESS PARAMETER, F_τ/pw, AS A FUNCTION OF h/w AND R/w, FOR IDEALIZED PROJECTING NOTCHES WITH θ = 60 DEGREES

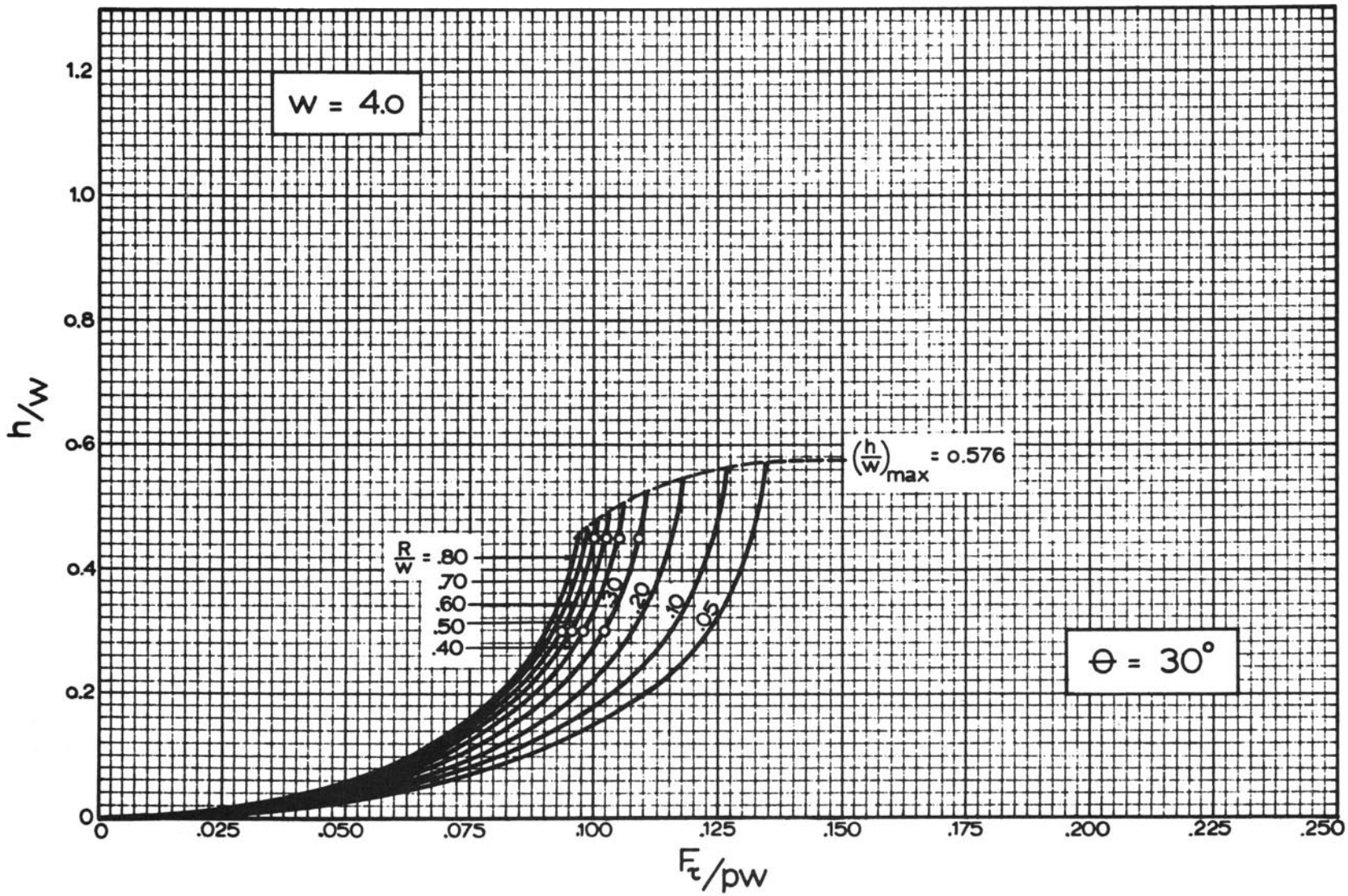

FIGURE 19. SHEARING STRESS PARAMETER, F_τ/pw, AS A FUNCTION OF h/w AND R/w, FOR IDEALIZED PROJECTING NOTCHES WITH θ = 30 DEGREES

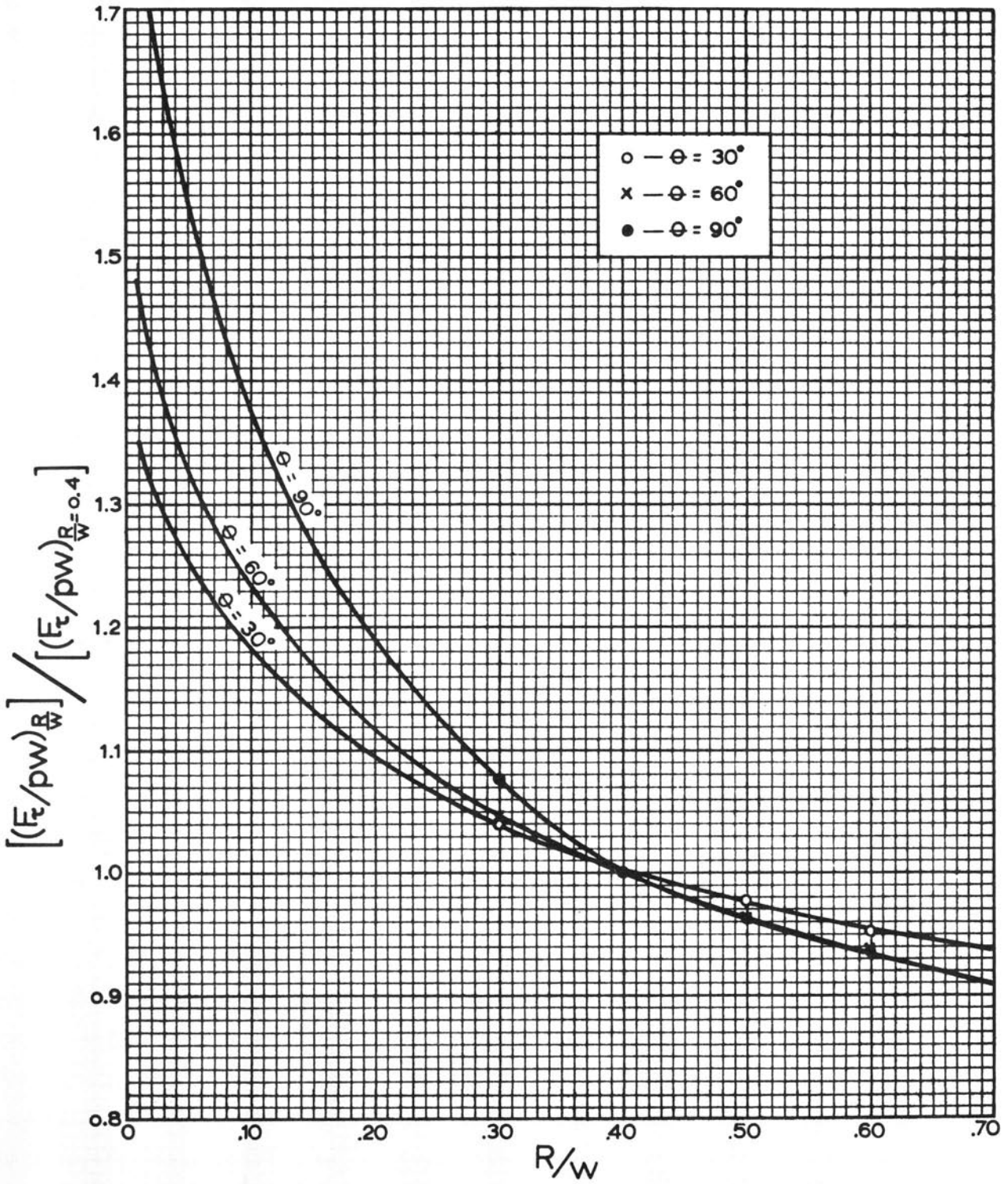

FIGURE 20. EXTRAPOLATION CURVES FOR F_τ/pw — h/w RELATIONSHIPS

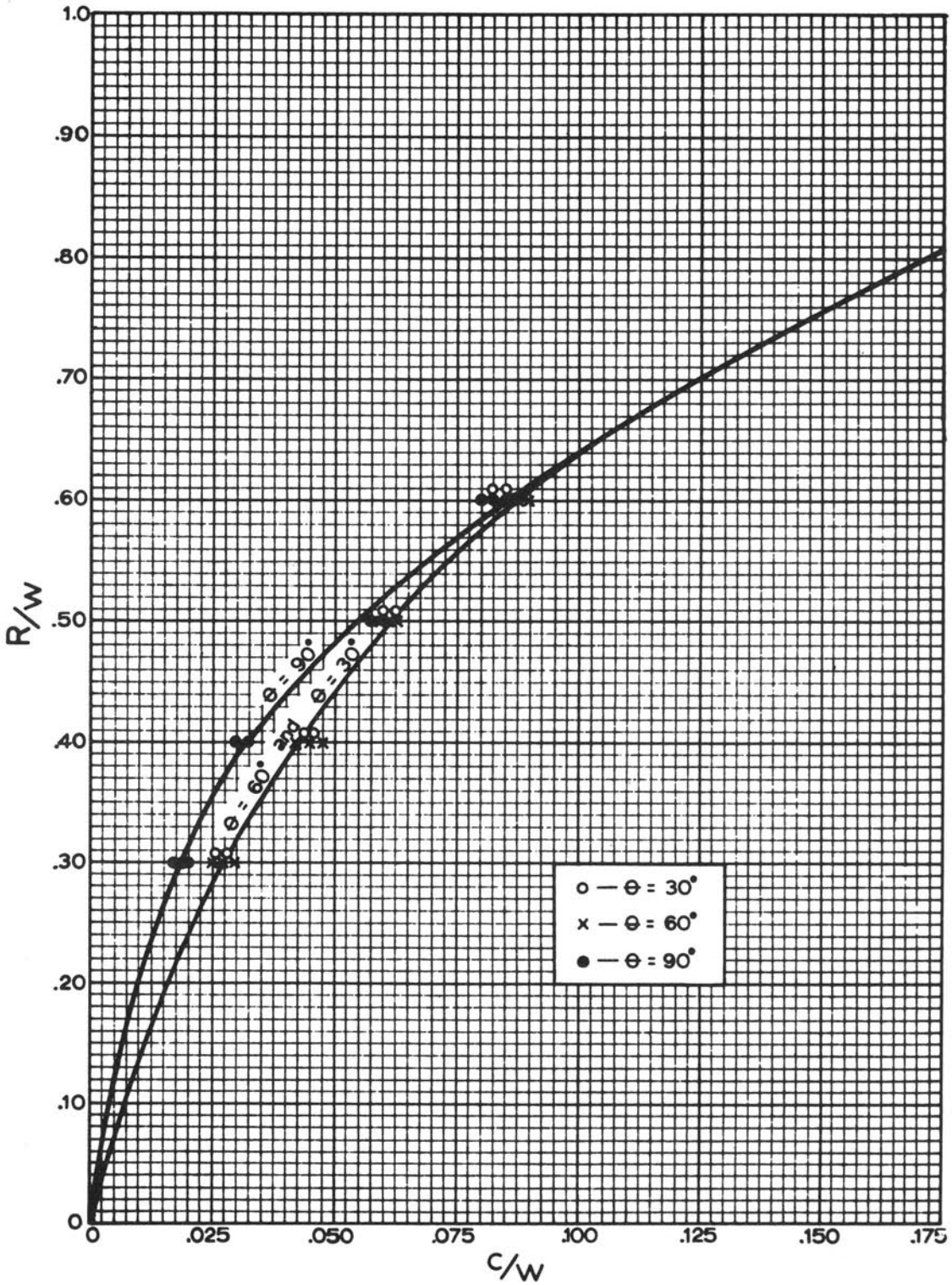

FIGURE 21. CORRELATION OF R/w OF IDEALIZED PROJECTING NOTCH WITH c/w OF TRIANGULAR SURFACE-SHEAR LOAD

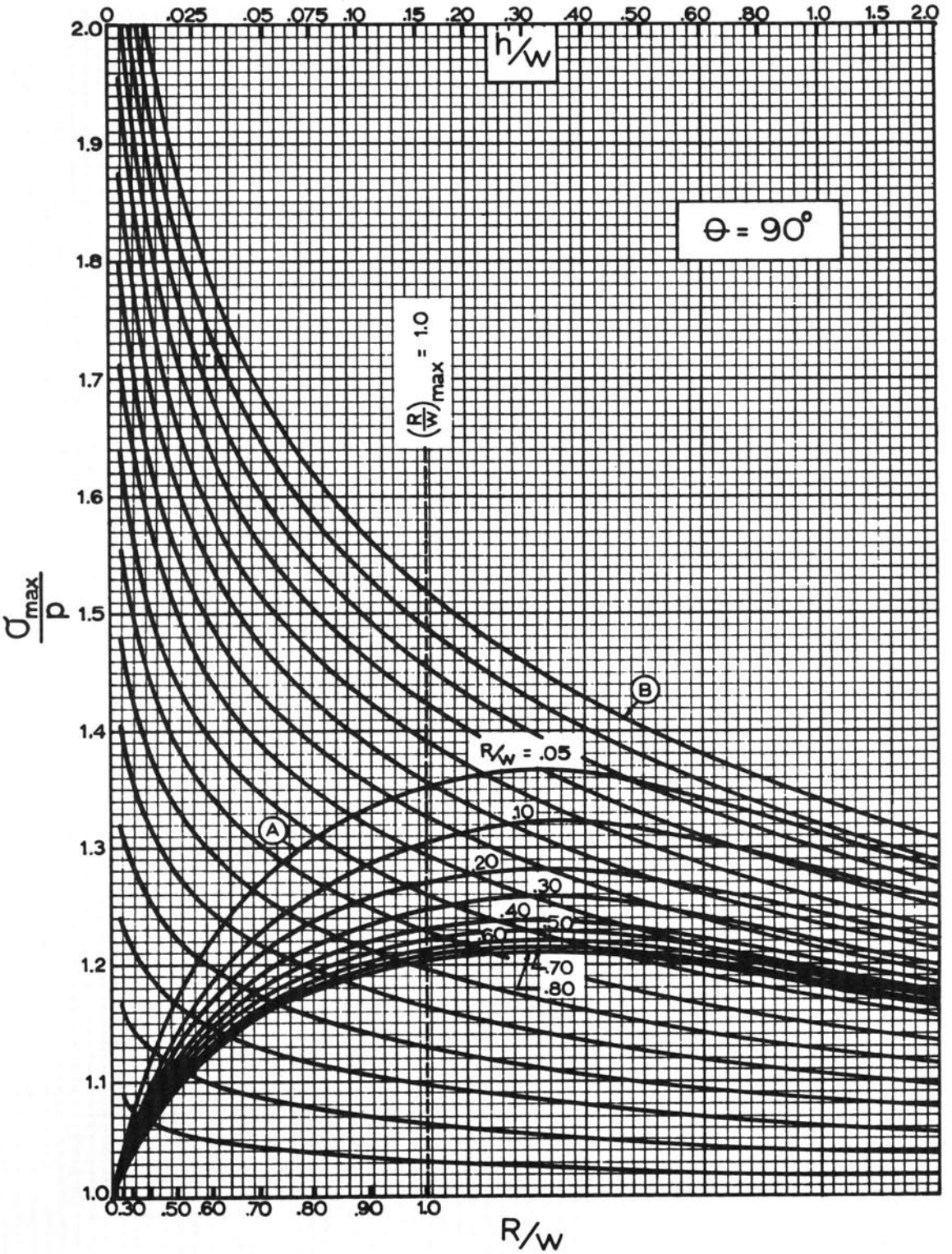

FIGURE 22. THE STRESS CONCENTRATION FACTOR AS A FUNCTION OF h/w AND R/w FOR IDEALIZED PROJECTING NOTCHES WITH θ = 90 DEGREES

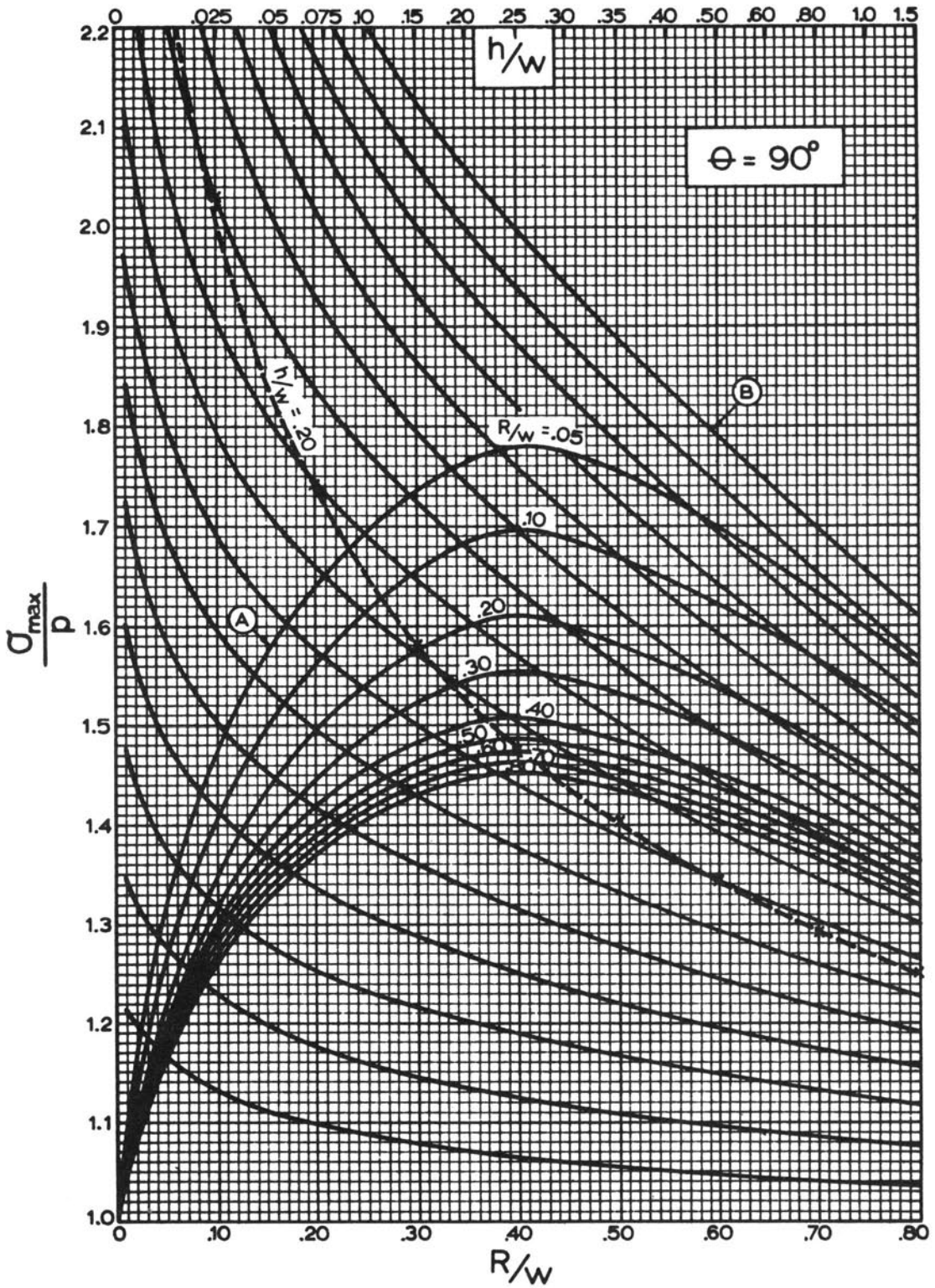

FIGURE 22a. FIGURE 22 WITH R/w SCALE EXPANDED AND LINEARIZED

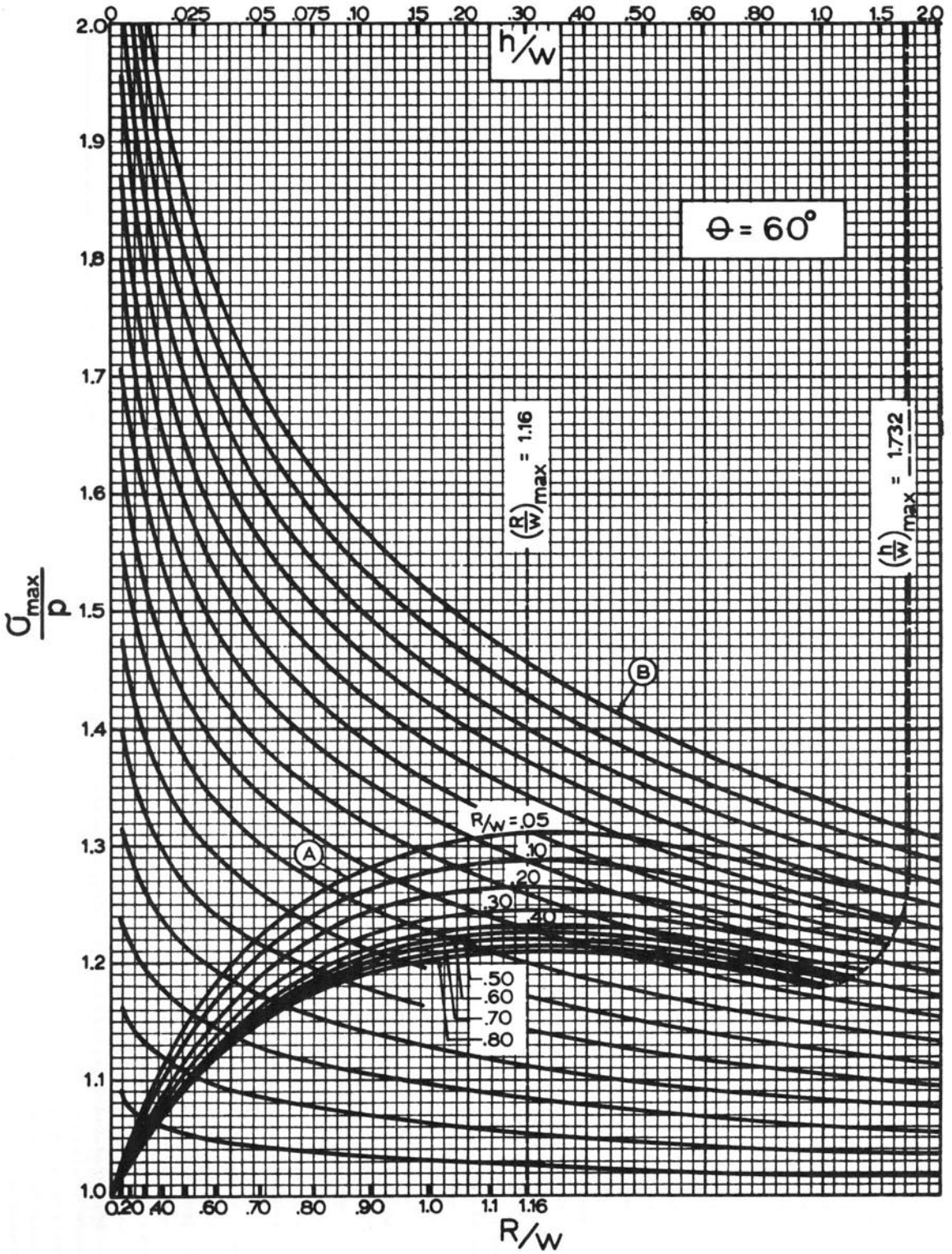

FIGURE 23. THE STRESS CONCENTRATION FACTOR AS A FUNCTION OF h/w AND R/w FOR IDEALIZED PROJECTING NOTCHES WITH θ = 60 DEGREES

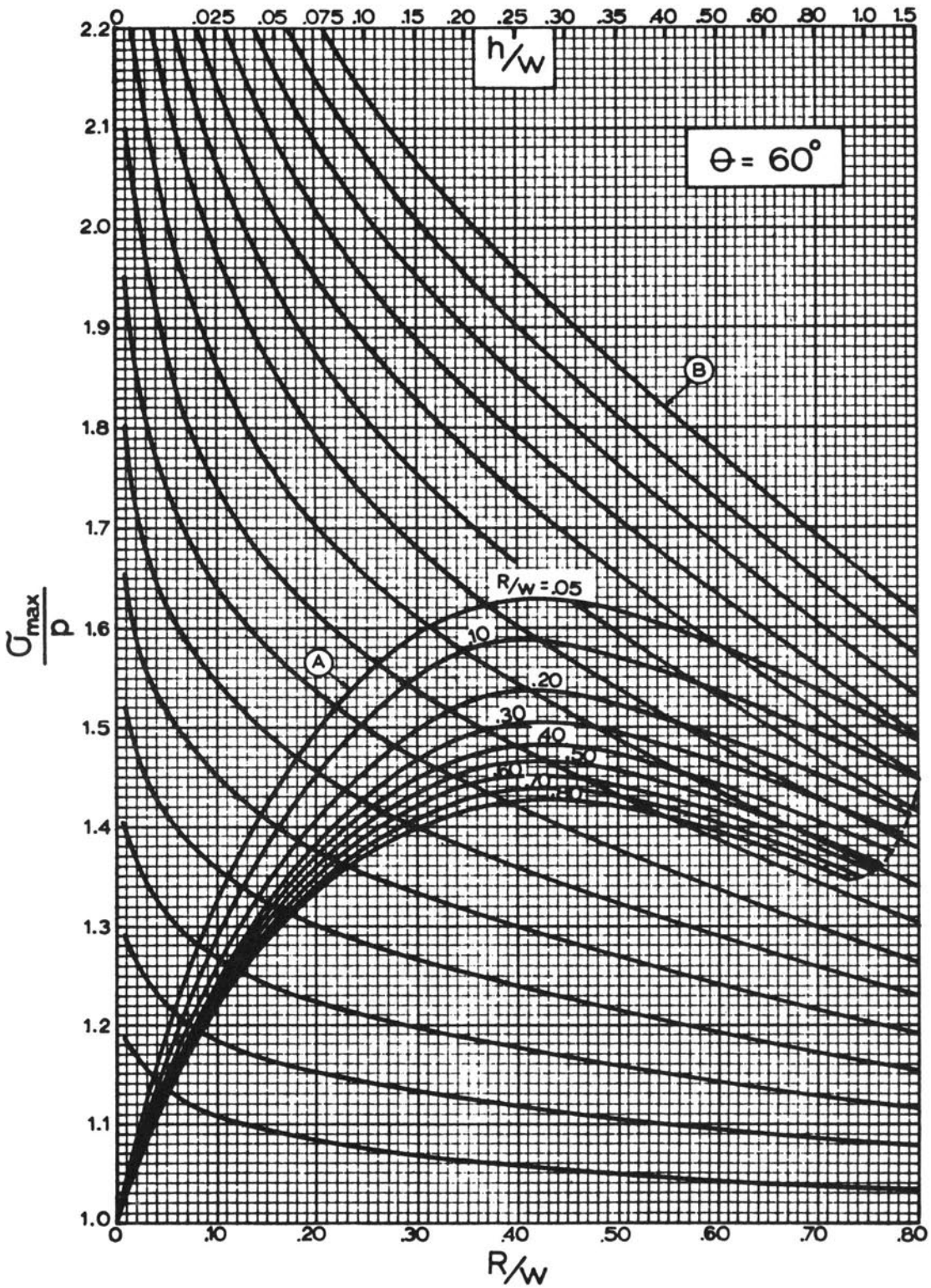

FIGURE 23a. FIGURE 23 WITH R/w SCALE EXPANDED AND LINEARIZED

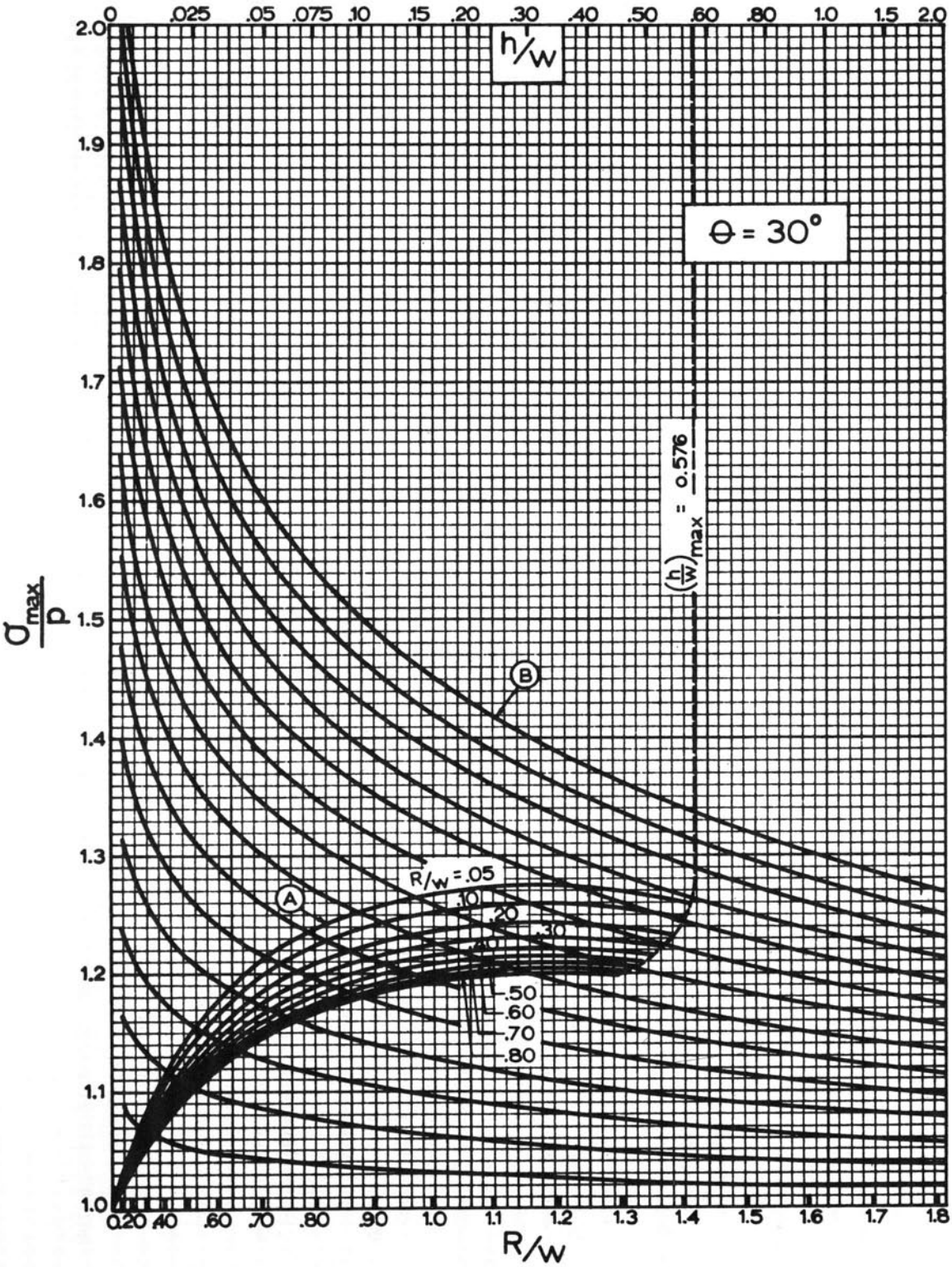

FIGURE 24. THE STRESS CONCENTRATION FACTOR AS A FUNCTION OF h/w AND R/w FOR IDEALIZED PROJECTING NOTCHES WITH θ = 30 DEGREES

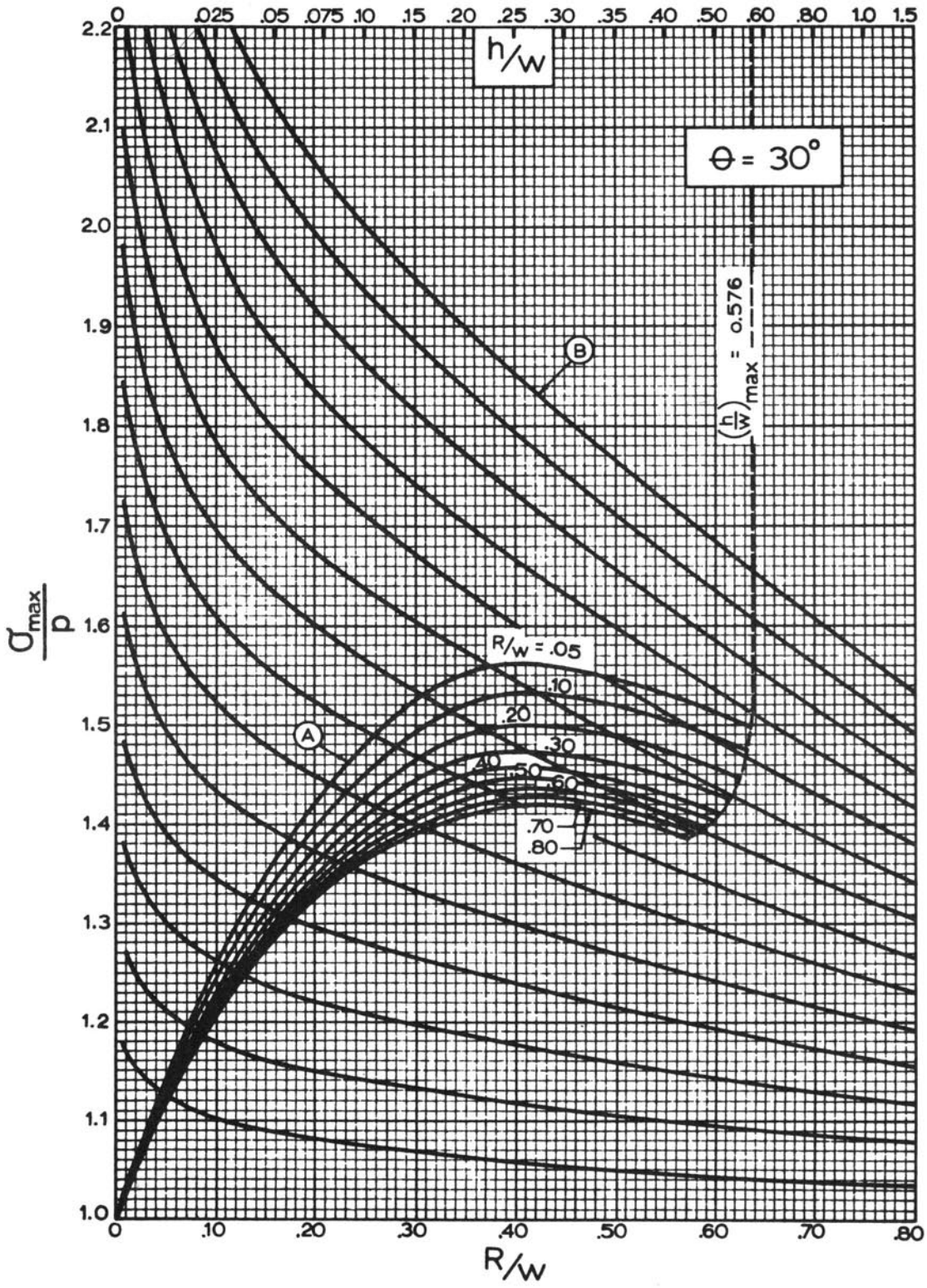

FIGURE 24a. FIGURE 24 WITH R/w SCALE EXPANDED AND LINEARIZED

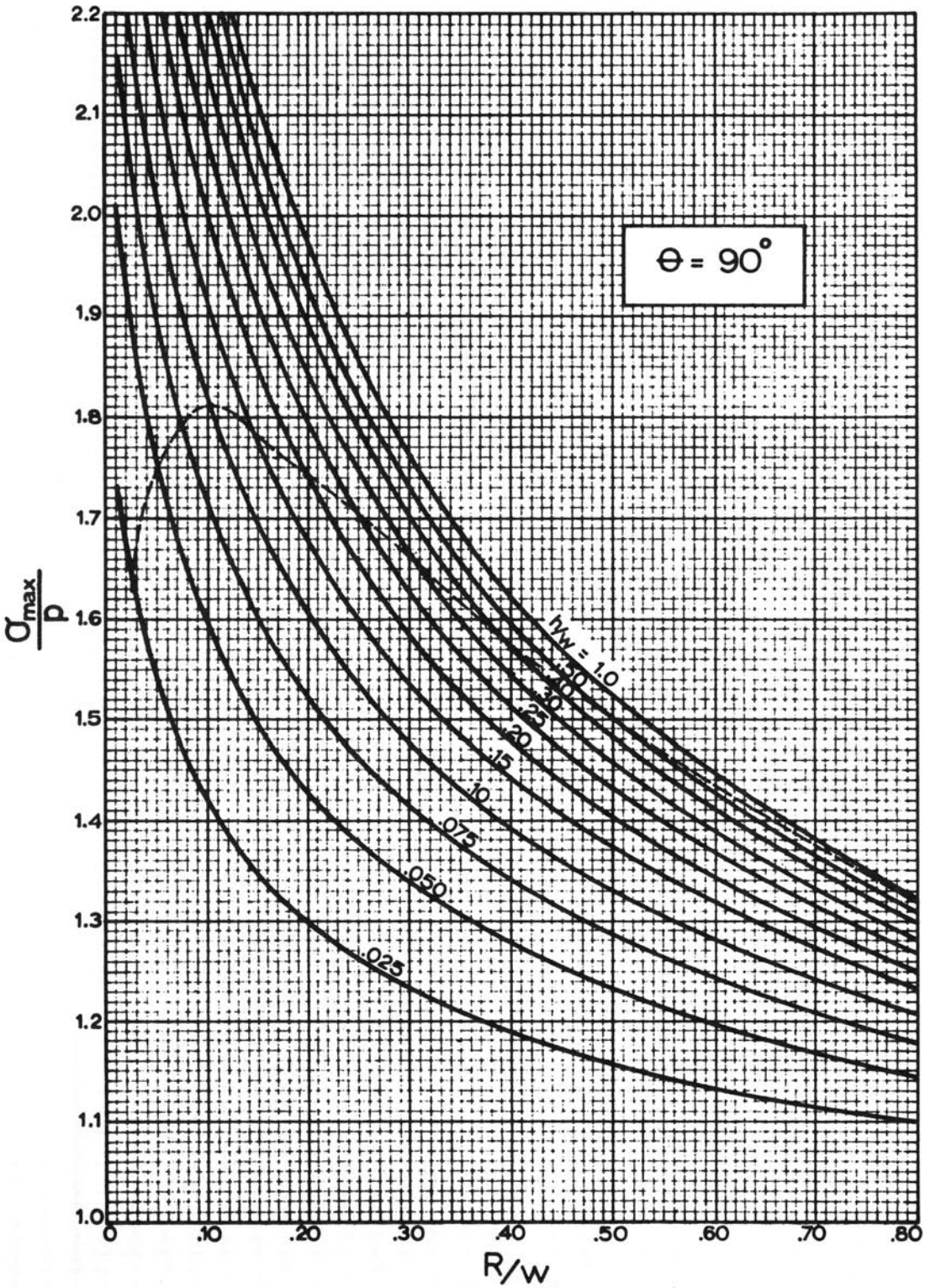

FIGURE 25. STRESS CONCENTRATION FACTORS FOR IDEALIZED PROJECTING NOTCHES WITH θ = 90 DEGREES

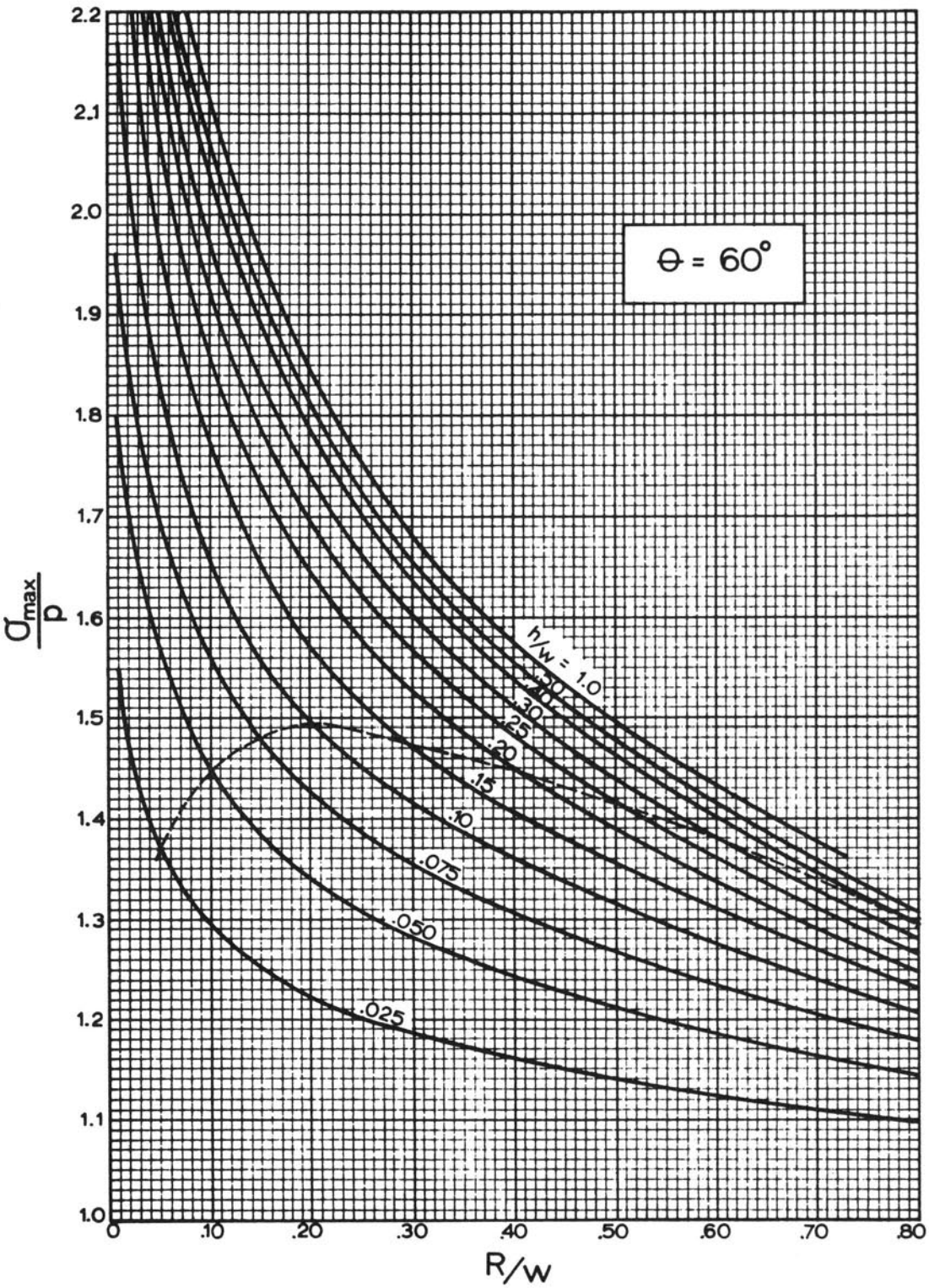

FIGURE 26. STRESS CONCENTRATION FACTORS FOR IDEALIZED PROJECTING NOTCHES WITH θ = 60 DEGREES

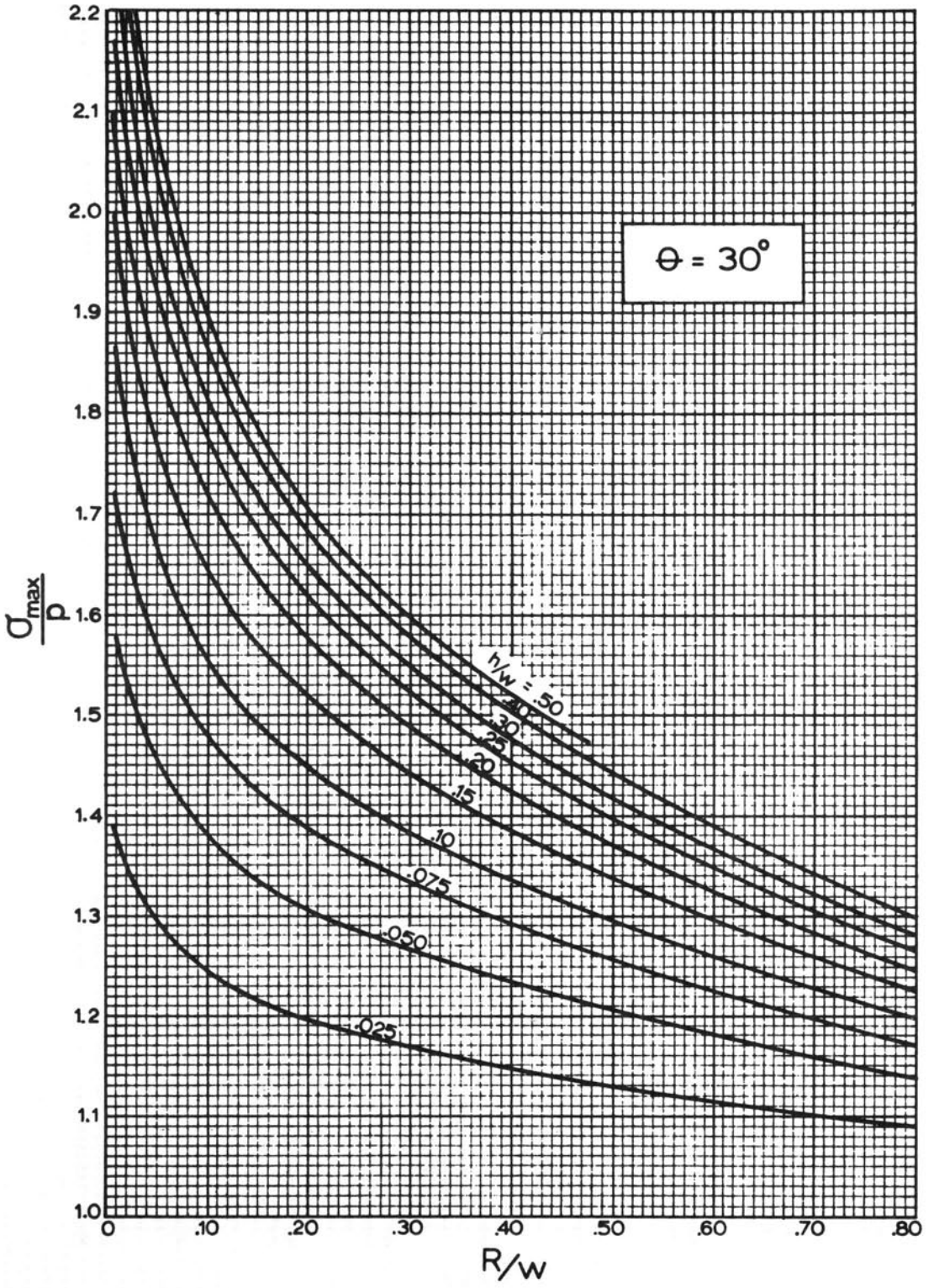

FIGURE 27. STRESS CONCENTRATION FACTORS FOR IDEALIZED PROJECTING NOTCHES WITH θ = 30 DEGREES

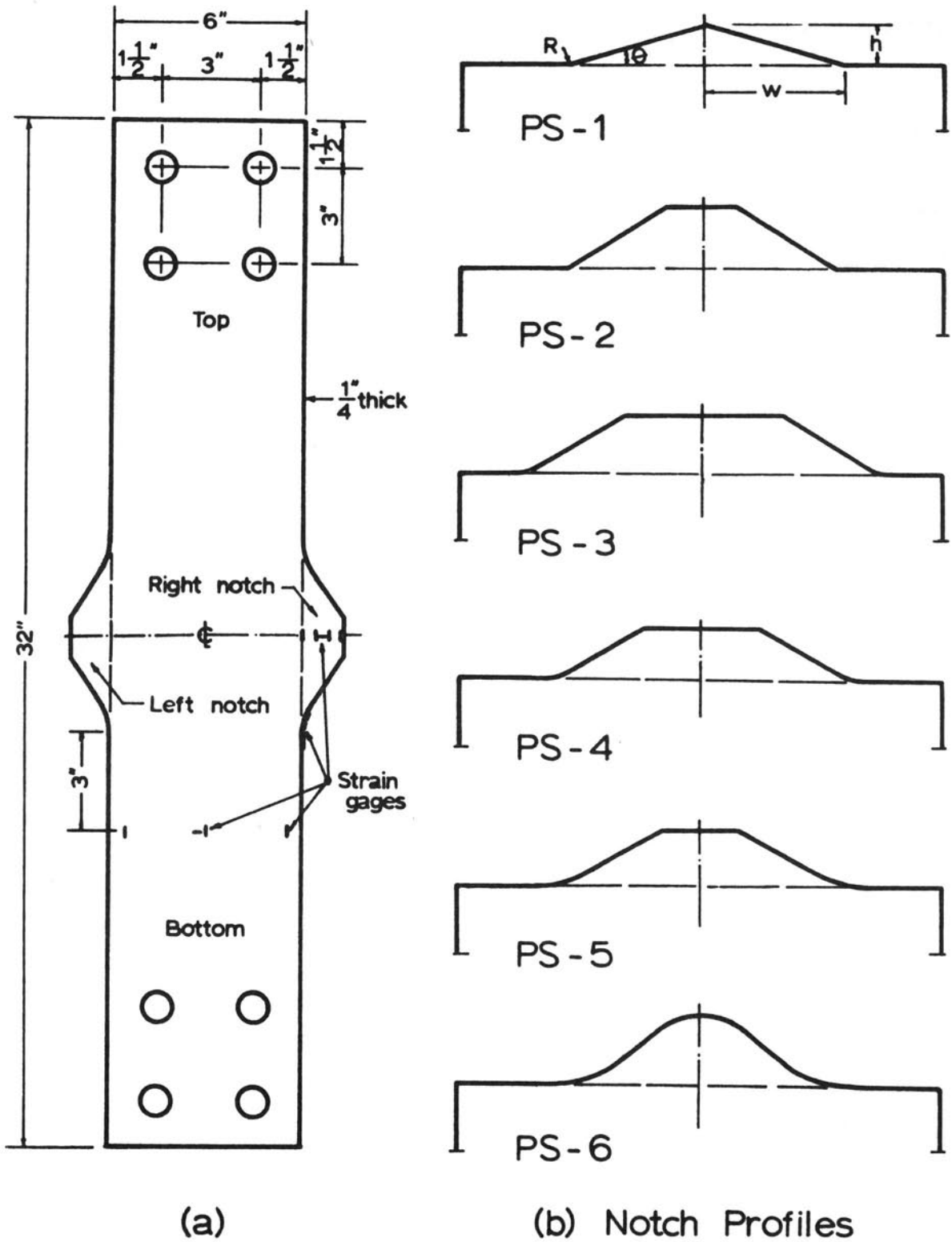

FIGURE 28. DETAILS OF TEST SPECIMENS

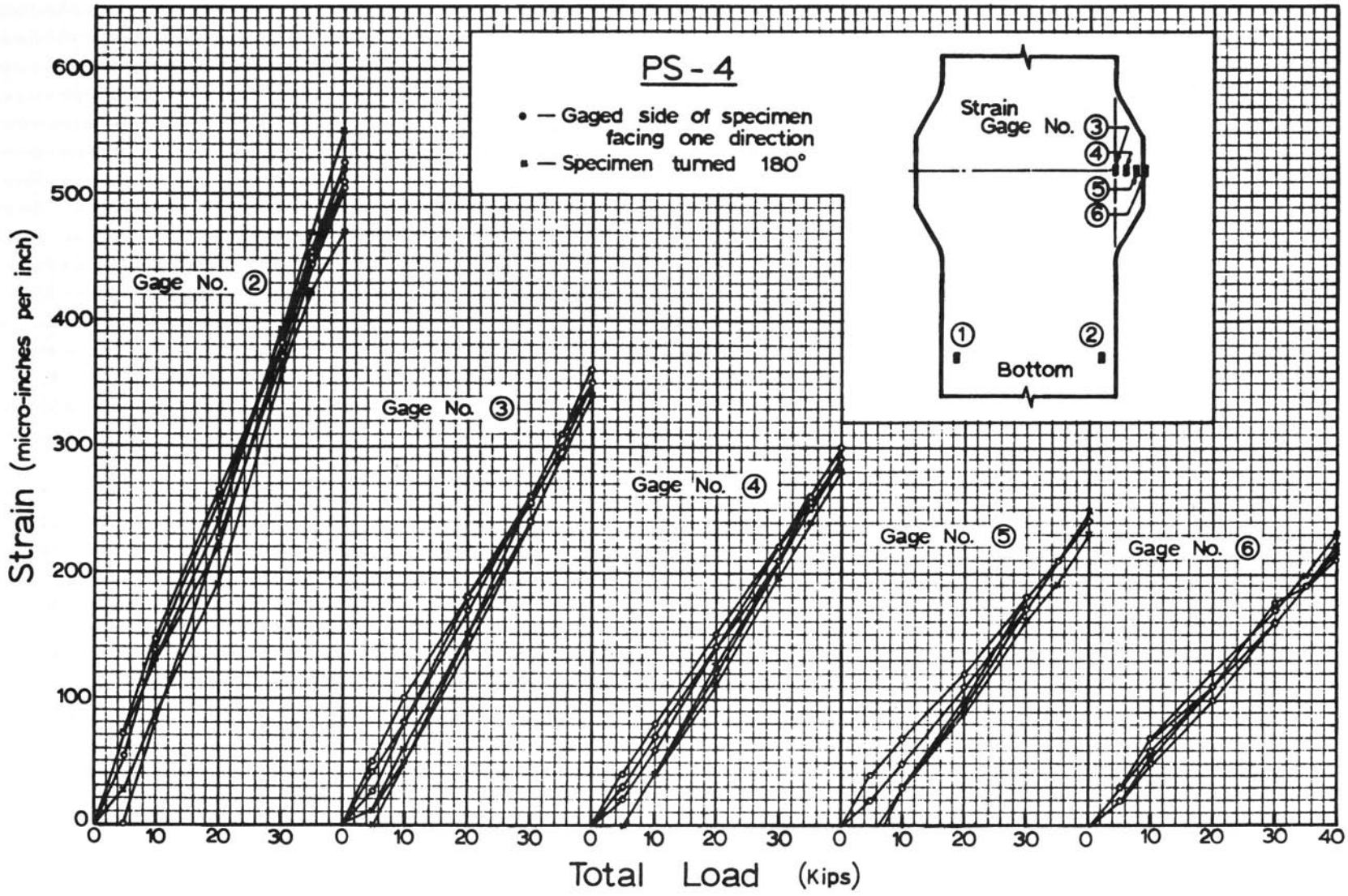

FIGURE 29. STRAIN VERSUS TOTAL LOAD PLOTS FOR SOME GAGES ON SPECIMEN PS-4

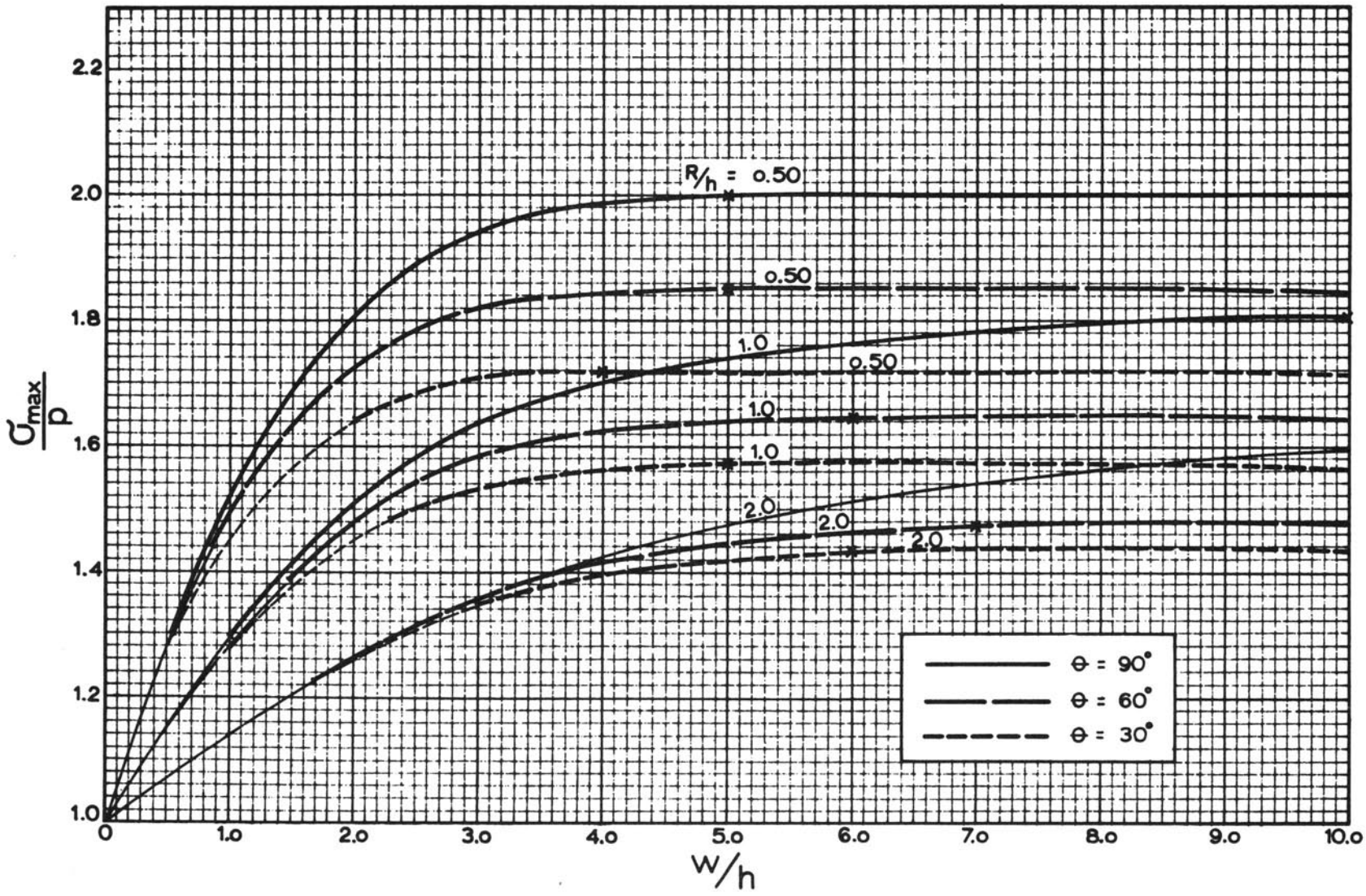

FIGURE 30. VARIATION OF STRESS CONCENTRATION FACTOR WITH w/h

FOR DIFFERENT θ and R/h IDEALIZED PROJECTING NOTCHES

This page is intentionally blank.

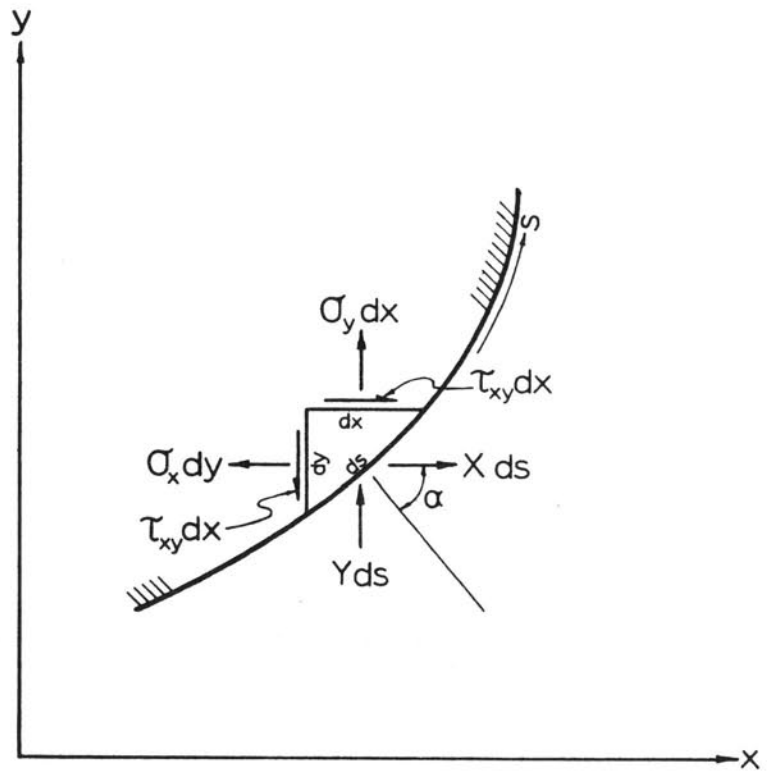

FIGURE A-1. AN ELEMENT ON A CURVED BOUNDARY

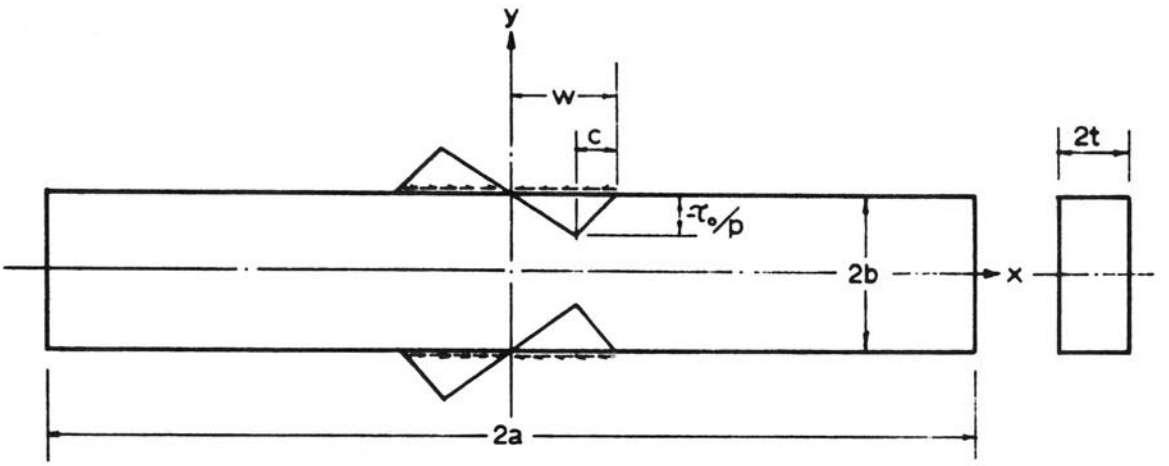

FIGURE B-1. TRIANGULAR SURFACE-SHEAR LOAD

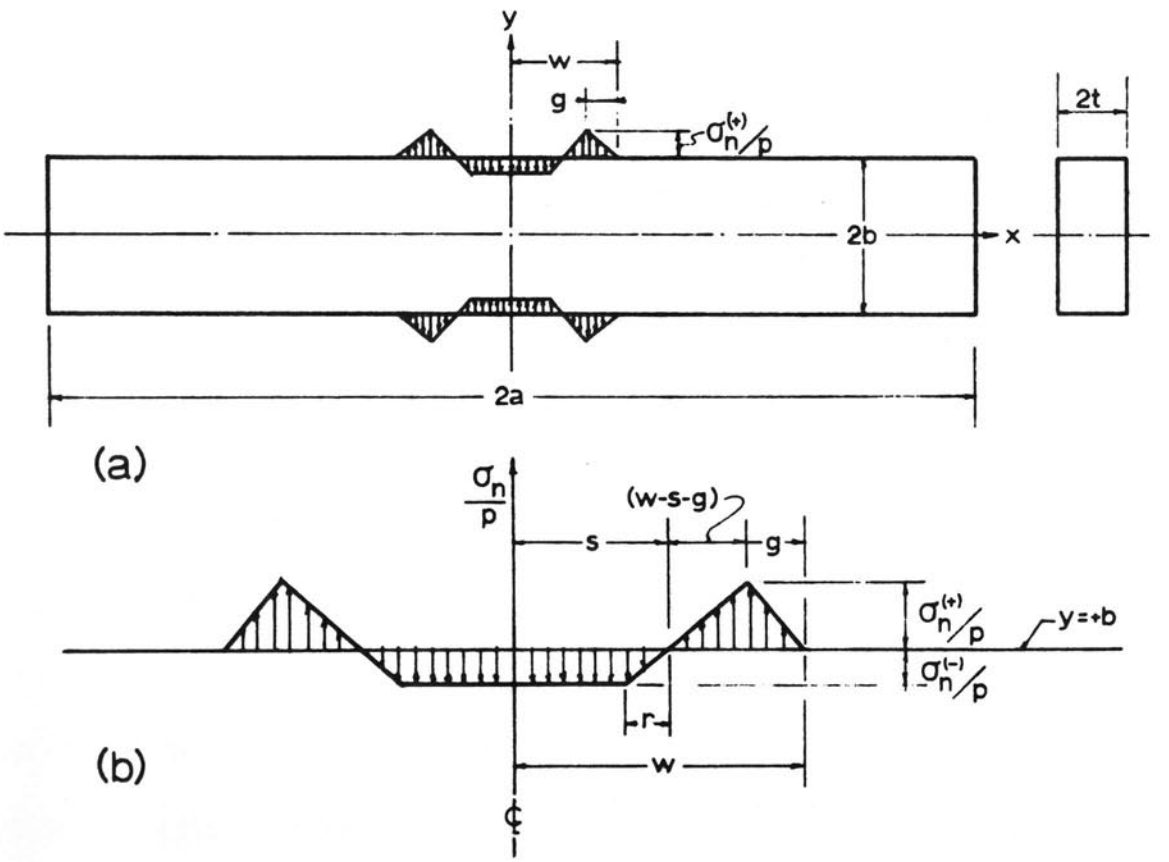

FIGURE B-2. LINEARLY VARYING SURFACE-NORMAL LOAD

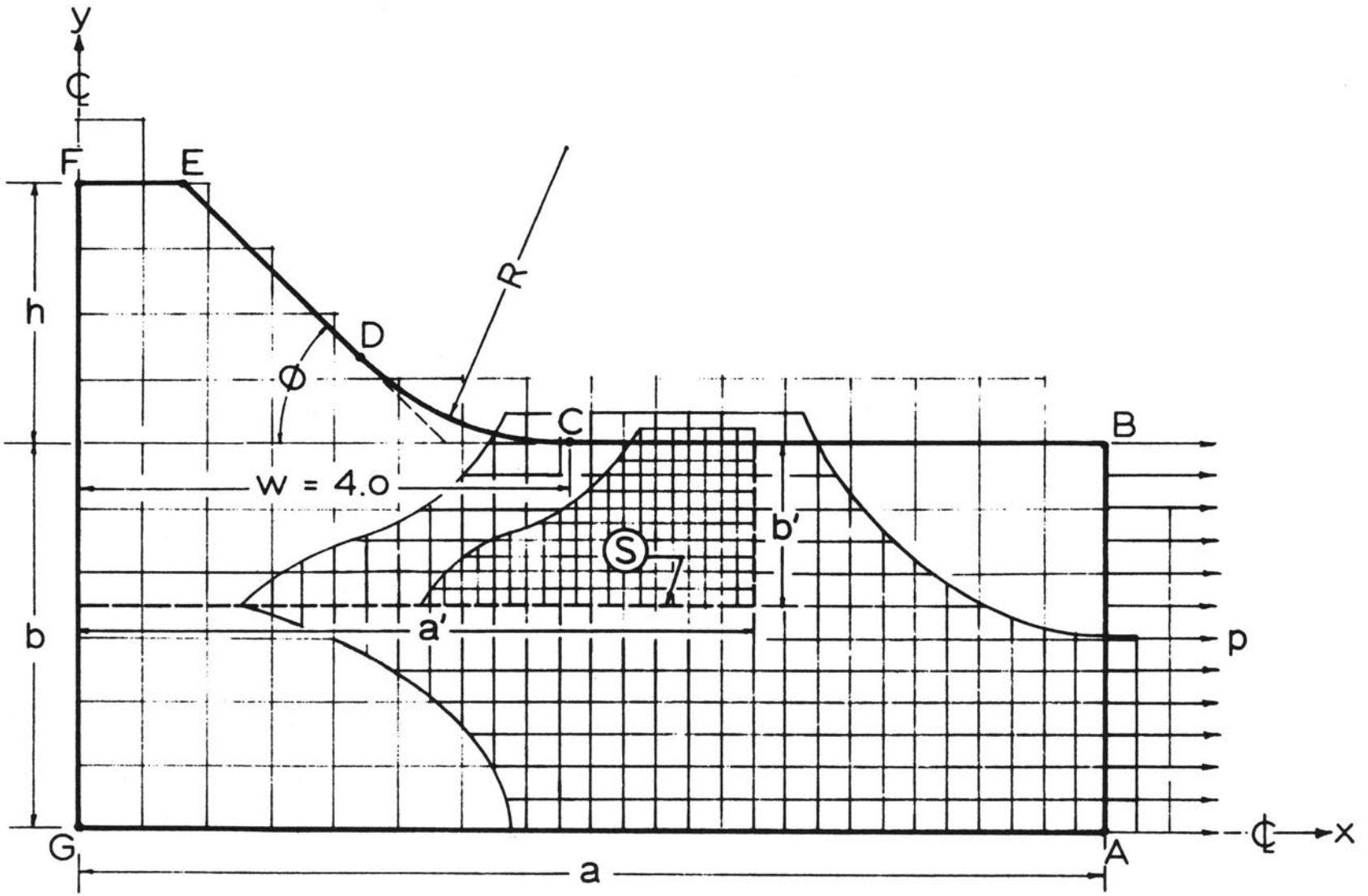

FIGURE C-1. TYPICAL SECTION CONSIDERED IN FINITE DIFFERENCE SOLUTION

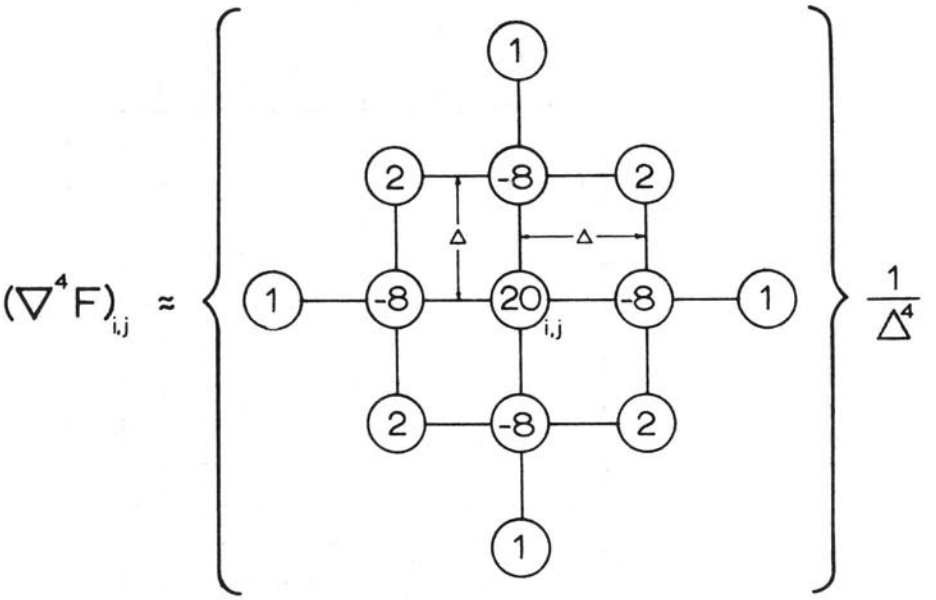

FIGURE C-2. FINITE DIFFERENCE BIHARMONIC OPERATOR

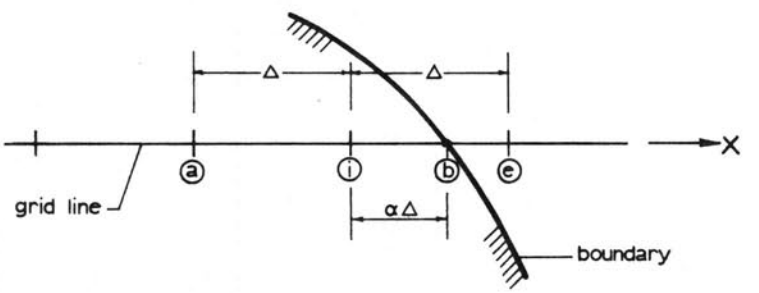

FIGURE C-3. NOTATION USED IN INTERPOLATION EQUATIONS

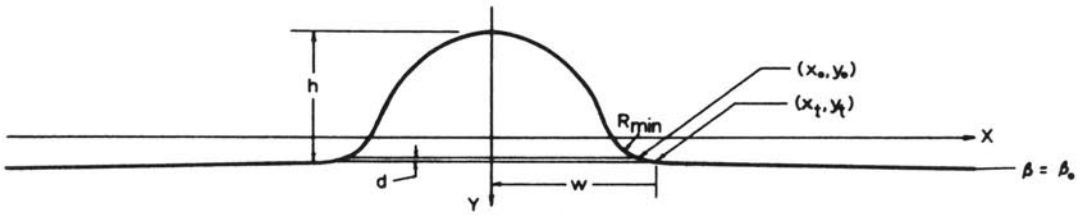

β_o	$(\sigma_\alpha)_{max}/p$	d	h	w	R_{min}	h/w	R_{min}/w	θ (degrees)	$x_o/x_{R_{min}}$
.25	1.868	.008	3.856	2.038	.129	1.892	.063	112	1.038
.30	1.715	.010	3.178	2.059	.188	1.543	.091	101	1.055
.35	1.607	.013	2.694	2.085	.260	1.292	.124	91	1.075
.40	1.526	.015	2.332	2.117	.345	1.102	.163	82	1.096
.50	1.412	.021	1.830	2.197	.559	.833	.255	67	1.142
.60	1.335	.025	1.500	2.299	.840	.652	.365	55	1.190
.70	1.278	.030	1.269	2.423	1.196	.524	.494	46	1.237
.80	1.235	.034	1.100	2.569	1.639	.428	.638	38	1.283
.90	1.200	.038	.971	2.738	2.179	.355	.796	32	1.326
1.00	1.173	.042	.870	2.928	2.828	.297	.966	28	1.365
1.10	1.150	.045	.790	3.141	3.598	.252	1.145	24	1.401
1.20	1.131	.048	.724	3.376	4.499	.215	1.332	21	1.432
1.30	1.116	.051	.670	3.635	5.544	.184	1.525	18	1.460
1.40	1.103	.054	.624	3.918	6.744	.159	1.721	16	1.486
1.50	1.092	.056	.585	4.226	8.112	.138	1.920	14	1.507

TABLE 1-a. MAXIMUM STRESSES AND CHARACTERISTIC DIMENSIONS FOR NEUBER'S NOTCHES WITH BASE SECTIONS DEFINED BY k=0.125 IN EQUATION (8)

β_o	$(\sigma_\alpha)_{max}/p$	d	h	w	R_{min}	h/w	R_{min}/w	θ (degrees)	$x_o/x_{R_{min}}$
.25	1.868	.015	3.863	2.054	.129	1.880	.063	112	1.038
.30	1.715	.020	3.187	2.082	.188	1.530	.090	101	1.055
.35	1.607	.024	2.705	2.117	.260	1.277	.123	91	1.075
.40	1.526	.029	2.345	2.160	.345	1.086	.160	82	1.096
.50	1.412	.037	1.846	2.266	.559	.815	.247	67	1.142
.60	1.335	.046	1.520	2.404	.840	.632	.349	55	1.190
.70	1.278	.053	1.292	2.572	1.196	.502	.465	46	1.237
.80	1.235	.060	1.125	2.774	1.639	.405	.591	38	1.283
.90	1.200	.065	.998	3.010	2.179	.332	.724	32	1.326
1.00	1.173	.070	.899	3.281	2.828	.274	.862	28	1.365
1.10	1.150	.074	.819	3.590	3.598	.228	1.002	24	1.401
1.20	1.131	.078	.754	3.939	4.499	.191	1.142	21	1.432
1.30	1.116	.080	.699	4.328	5.544	.162	1.281	18	1.460
1.40	1.103	.082	.653	4.761	6.744	.137	1.416	16	1.486
1.50	1.092	.084	.613	5.240	8.112	.117	1.548	14	1.507

TABLE 1-b. MAXIMUM STRESSES AND CHARACTERISTIC DIMENSIONS FOR NEUBER'S NOTCHES WITH BASE SECTIONS DEFINED BY k=0.250 IN EQUATION (8)

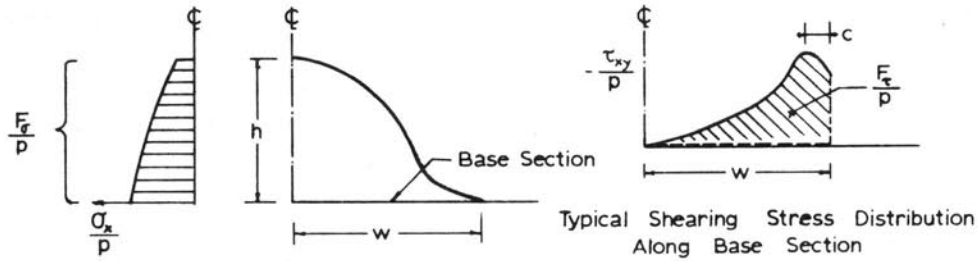

Typical Shearing Stress Distribution Along Base Section

β_o	Base Section Defined by k = 0.125				Base Section Defined by k = 0.250			
	$\frac{F_\tau}{pw} = \frac{F_\sigma}{pw}$ (a)	c/w	c/R_{min}	Efficiency (b)	$\frac{F_\tau}{pw} = \frac{F_\sigma}{pw}$ (a)	c/w	c/R_{min}	Efficiency (b)
.25	.1683	0	0	.177	.1688	.004	.071	.178
.30	.1605	.002	.021	.206	.1608	.013	.146	.206
.35	.1543	.014	.116	.236	.1548	.025	.202	.237
.40	.1500	.024	.150	.266	.1500	.039	.246	.269
.50	.1430	.051	.199	.333	.1425	.080	.324	.335
.60	.1378	.089	.243	.403	.1363	.124	.356	.405
.70	.1328	.131	.266	.474	.1298	.178	.382	.474
.80	.1270	.177	.277	.542	.1228	.230	.390	.544
.90	.1208	.224	.281	.603	.1150	.287	.397	.604
1.00	.1138	.271	.280	.659	.1068	.343	.398	.657
1.10	.1068	.317	.277	.708	.0983	.397	.396	.707
1.20	.0993	.362	.271	.755	.0898	.448	.392	.748
1.30	.0920	.404	.265	.786	.0815	.493	.388	.783
1.40	.0850	.442	.257	.824	.0740	.537	.379	.811
1.50	.0783	.481	.250	.849	.0668	.575	.372	.837

(a) - p = 1.0. (b) - at centerline section; equal to ratio of average to maximum stress, for portion above base

TABLE 2. STRESS PARAMETERS F_τ/pw and c/w, AND EFFICIENCY OF CENTERLINE SECTION OF NEUBER'S NOTCHES WITH BASE SECTIONS DEFINED BY k=0.125 AND k=0.250

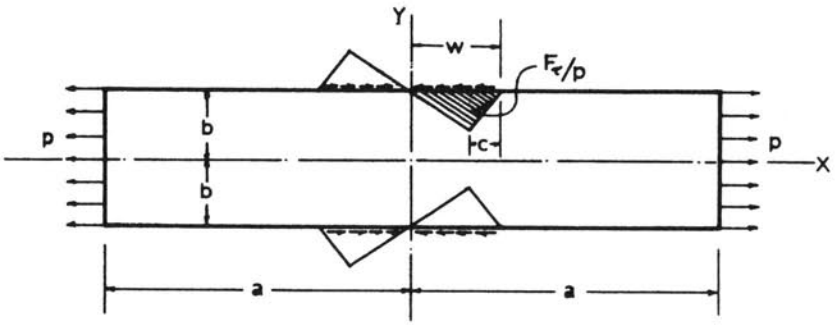

	c/w	b/w					
		1.0	2.0	4.0	6.0	8.0	10.0
$F_\tau/pw = 0.075$	.02	1.435	1.434	1.428	1.426	1.426	1.425
	.10	1.281	1.280	1.274	1.272	1.272	1.271
	.20	1.221	1.220	1.214	1.212	1.212	1.211
	.30	1.187	1.185	1.179	1.178	1.178	1.177
	.40	1.163	1.161	1.156	1.154	1.154	1.154
	.50	1.145	1.143	1.138	1.136	1.136	1.136
	.60	1.130	1.128	1.123	1.122	1.122	1.121
	.70	1.117	1.115	1.111	1.110	1.109	1.109
	Max. % Variation [a]	+ 0.18	0	-0.51	-0.66	-0.66	-0.74
$F_\tau/pw = 0.150$	.02	1.871	1.868	1.855	1.852	1.851	1.851
	.10	1.562	1.559	1.547	1.544	1.543	1.543
	.20	1.443	1.439	1.427	1.425	1.424	1.423
	.30	1.374	1.370	1.359	1.356	1.355	1.355
	.40	1.326	1.322	1.311	1.309	1.308	1.307
	.50	1.290	1.286	1.275	1.273	1.272	1.272
	.60	1.260	1.256	1.246	1.244	1.243	1.243
	.70	1.235	1.231	1.222	1.219	1.219	1.218
	Max. % Variation [a]	+ 0.32	0	-0.85	-1.01	-1.09	-1.09

(a) from b/w = 2.0 value.

TABLE 3. VARIATION OF $(\sigma_x)_{max}/p$ ALONG SURFACE OF RECTANGULAR BAR DUE TO TRIANGULAR SURFACE-SHEAR LOAD, WITH THE DEPTH 2b OF THE BAR

β_o	$\frac{\sigma_{max}}{p}$ Calculated	Base Section Defined by k = 0.125				Base Section Defined by k = 0.250			
		R_{min}/w	h/w	$\frac{\sigma_{max}}{p}$ (Fig. 14)	Percent Error	R_{min}/w	h/w	$\frac{\sigma_{max}}{p}$ (Fig. 14)	Percent Error
.25	1.87	.063	1.89	1.76	- 5.9	.063	1.88	1.76	- 5.9
.30	1.72	.091	1.54	1.66	- 3.5	.090	1.53	1.66	- 3.5
.35	1.61	.124	1.29	1.58	- 1.8	.123	1.28	1.57	- 2.5
.40	1.53	.163	1.10	1.53	0	.160	1.09	1.53	0
.50	1.41	.255	0.83	1.42	+ 0.7	.247	0.82	1.42	+ 0.7
.60	1.34	.365	0.65	1.35	+ 0.7	.349	0.63	1.36	+ 1.5
.70	1.28	.494	0.52	1.29	+ 0.8	.465	0.50	1.30	+ 1.6
.80	1.26	.638	0.42	1.24	- 1.6	.591	0.41	1.24	- 1.6
.90	1.20	.796	0.36	1.19	- 0.8	.724	0.33	1.20	- 0

TABLE 4. COMPARISON OF VALUES OF THE STRESS CONCENTRATION FACTOR FOR NEUBER'S NOTCHES AS OBTAINED FROM FIGURE 14 WITH CALCULATED VALUES

Flank Angle θ	R/w	h/w	$\frac{F_\tau}{pw}$	$\frac{F_\sigma}{pw}$	c/w	$\frac{\sigma_{max}}{p}$
90^o	.30	.30	- .1120	.1136	.12	1.66
		.45	- .1212	.1220	.12	1.71
		.60	- .1228	.1241	.12	1.71
		.75	- .1243	.1254	.12	1.72
		.90	- .1285	.1294	.12	1.74
	.40	.30	- .1053	.1062	.14	1.55
		.45	- .1127	.1135	.14	1.60
		.60	- .1156	.1165	.14	1.61
		.75	- .1178	.1187	.14	1.61
		.90	- .1188	.1196	.14	1.62
	.50	.30	- .1016	.1028	.16	1.44
		.45	- .1098	.1105	.16	1.47
		.60	- .1119	.1125	.16	1.48
		.75	- .1134	.1138	.16	1.49
		.90	- .1146	.1147	.16	1.50
	.60	.30	- .0978	.0984	.18	1.39
		.45	- .1065	.1071	.18	1.42
		.60	- .1094	.1094	.18	1.43
		.75	- .1102	.1100	.18	1.43
		.90	- .1107	.1110	.18	1.43
60^o	.30	.30	- .1095	.1101	.12	1.59
		.45	- .1187	.1189	.12	1.63
		.60	- .1205	.1216	.12	1.63
		.75	- .1236	.1247	.12	1.64
		.90	- .1241	.1253	.12	1.64

TABLE 5. SUMMARY OF RESULTS OF FINITE-DIFFERENCE SOLUTION FOR THE IDEALIZED PROJECTING NOTCH

Flank Angle θ	R/w	h/w	$\frac{F_\tau}{pw}$	$\frac{F_\sigma}{pw}$	c/w	$\frac{\sigma_{max}}{p}$
60°	.40	.30	- .1048	.1055	.14	1.50
		.45	- .1128	.1136	.14	1.54
		.60	- .1156	.1165	.14	1.55
		.75	- .1177	.1185	.14	1.55
		.90	- .1191	.1202	.14	1.56
	.50	.30	- .1011	.1024	.16	1.44
		.45	- .1095	.1101	.16	1.47
		.60	- .1108	.1118	.16	1.48
		.75	- .1130	.1135	.16	1.48
		.90	- .1141	.1144	.16	1.49
	.60	.30	- .0975	.0981	.18	1.39
		.45	- .1063	.1068	.18	1.41
		.60	- .1087	.1089	.18	1.42
		.75	- .1100	.1101	.18	1.43
		.90	- .1106	.1110	.18	1.43
30°	.30	.30	- .0988	.1015	.12	1.54
		.45	- .1088	.1098	.12	1.59
	.40	.30	- .0972	.0990	.14	1.46
		.45	- .1048	.1056	.14	1.50
	.50	.30	- .0950	.0963	.16	1.42
		.45	- .1023	.1034	.16	1.46
	.60	.30	- .0930	.0943	.18	1.37
		.45	- .1006	.1002	.18	1.41

TABLE 5. (Continued)

1	2	3	4	5	6	7	8	9	10	11	12
Specimen No.	Notch	θ	w (in.)	h (in.)	R (in.)	h/w	R/w	$\frac{F_\sigma}{pw}$ (a)	$\frac{\sigma_{max}}{p}$ (Measured)	$\frac{\sigma_{max}}{p}$ (a) from Fig. 27	Percent Difference (b)
PS - 1	right	16°	2.50	0.70	0	.280	0	.080	1.85		
PS - 2	left	31°	2.52	1.08	0	.430	0	.200	4.00		
	right	31°	2.52	1.05	0	.420	0	.175	3.50		
PS - 3	right	30°	3.50	1.00	0.83	.285	.237	.151	2.35	1.60	- 32
PS - 4	left	30°	3.12	0.90	1.50	.288	.482	.151	1.85	1.42	- 23
	right	30°	3.00	0.90	1.05	.300	.350	.155	2.20	1.51	- 31
PS - 5	right	31°	3.10	1.00	2.30	.320	.740	.077	1.28	1.31	+ 2.3
PS - 6	right	40°	3.10	1.25	1.40	.404	.450	.161	1.48		

(a) - value of p based on nominal strain on same side as notch
(b) - percentage based on measured values.

TABLE 6. SUMMARY OF STRAIN GAGE MEASUREMENTS ON PROJECTING NOTCH SPECIMENS

1	2	3	4	5	6	7	8	9
θ	h	R	b (a)	$\frac{h+b}{b}$ (b)	$\frac{R}{2b}$ (c)	$\frac{\sigma_{max}}{p}$ (from Ref. 10)	$\frac{\sigma_{max}}{p}$ (from Ref. 30)	Percent Difference (d)
90^o	2	1	10	1.20	.050	2.25	2.0	- 11.1
	2	2	20	1.10	.050	1.96	1.79	- 8.7
60^o	2	1	10	1.20	.050	2.17 *	1.85	- 14.7
	2	2	12	1.17	.083	1.79 *	1.65	- 7.8
	2	4	14	1.14	.143	1.55 *	1.45	- 6.5
30^o	2	1	8	1.25	.063	1.76 *	1.72	- 2.3
	2	2	10	1.20	.100	1.60 *	1.57	- 1.9
	2	4	12	1.17	.167	1.45 *	1.39	- 4.1

(a) equal to half-width of projecting notch, "w", above which Fig. 30 gives an approximately constant value of σ_{max}/p

(b) equal to the parameter D/d in Fig. 57 of Ref. 10.

(c) equal to the parameter r/d in Fig. 57 of Ref. 10.

(d) percentage based on values in Col. 7.

* adjusted from $\theta = 90^o$ values, using Fig. 3 of Ref. 26.

TABLE 7. COMPARISON OF VALUES OBTAINED FROM FIGURES 25, 26, AND 27 FOR THE LIMITING CASE OF A BAR WITH SHOULDER FILLET, WITH VALUES FROM REFERENCE 10.

This page is intentionally blank.

This page is intentionally blank.

R/w clearly indicate that the stress parameter F_τ/pw is a function of the ratio R/w, as indeed it should be (F_τ/pw being theoretically infinite when R = 0). Although no values less than 0.30 are available for h/w, the F_τ/pw versus h/w curves of Figure 17 have been extended below this line since in this region the curves are reasonably well determined by the condition that when h/w = 0 (no notch), $F_\tau/pw = 0$, i.e., the curves must pass through the origin.

In order to extend the data obtained from the calculation to a wider range of values of the ratio R/w, an extrapolating curve was obtained graphically, i.e., by passing a smooth curve through points representing calculated values in the F_τ/pw versus h/w plot of Figure 17. This curve was then prolonged on both sides in what appear to be reasonable extensions. This extrapolation is shown in Figure 20. The F_τ/pw values used in preparing Figure 20 were those corresponding to h/w = 0.75. The ordinates to the curve in Figure 20 are expressed in terms of the ratio of the value of F_τ/pw for a particular R/w to the value of F_τ/pw for R/w = 0.40. In extending the curve of Figure 20 beyond the plotted points, the following limiting conditions were considered.

(1) As R/w approaches zero, the value of F_τ/pw becomes very large.

(2) As R/w becomes very large (limiting case: no notch), F_τ/pw approaches zero.

By assuming that the variation of F_τ/pw with R/w given by the above extrapolation curve applies for all values of h/w (an assumption which is reasonable in view of the approximately parallel directions which the calculated F_τ/pw versus h/w curves take for the different R/w values). F_τ/pw versus h/w curves for R/w = 0.05, 0.10, 0.20, 0.70, and 0.80 are shown in Figure 17.

Figure 17 clearly shows that for a given value of θ the shearing stress parameter F_τ/pw is a function of the parameters R/w and h/w. It is worth noting in connection with Figure 17 that for a given value of R/w, the stress parameter F_τ/pw increases very rapidly for small values of h/w, the rate of increase diminishing with increasing h/w. For h/w greater than about 0.60, the increase in F_τ/pw with h/w becomes very small, a trend which may be more clearly understood in terms of the diminishing efficiency* of the centerline section with increasing height of notch, i.e., as a greater portion of the section comes under compressive stress.

With the relationship between the stress parameter F_τ/pw and the geometrical parameters θ, h/w, and R/w known, the next step was to determine the relationship between c/w and R/w using Figure 9.

Table 5 clearly indicates that the ratio c/w is a function of R/w only and is independent of h/w and θ. This fact confirms the assumption made in this regard in connection with Neuber's notches. The procedure used in determining the relationship between c/w and R/w follows that used for Neuber's notches. A plot of the c/w versus R/w relationship is shown in Figure 21. In Figure 21 the tendency of the curve to flatten as R/w increases is due primarily to the fact that the triangular surface-shear load approximates the actual shearing stress distribution curve along the base section of the notch more closely for notches with large R/w values than for notches with small radii. This is apparent from a comparison of the shearing stress distribution curves corresponding to different values of R/w shown in Figure 15.

As in the case of Neuber's notches, the graph giving the stress concentration factor

*See page 8 for the special connotation attached to this term.

as a function of the geometrical parameters was obtained by superposing the relationships given in Figures 17 and 21 onto Figure 9. The composite plot for this case (θ = 90 degrees) is shown in Figure 22. In this figure a maximum value of 1.0 is shown for the ratio R/w. This value represents the limiting case above which the flank angle becomes less than 90 degrees.

The procedure to be followed in using Figure 22 is similar to that outlined for the analogous figure on Neuber's notches. Thus, for a notch of given dimensions, one proceeds as follows.

(1) From a point representing the given h/w value on the top scale, a vertical line is dropped until it intersects the curve marked A corresponding to the given value of R/w (estimating intermediate values, if necessary).

(2) One then moves from this point in a direction parallel to the curves marked B (again estimating intermediate values when necessary) to the given value of R/w as indicated on the bottom scale.

(3) A horizontal line drawn from this last point to the σ_{max}/p axis gives the stress concentration factor.

It is significant to note that the parameter R/w enters twice in the plot of Figure 22. The dependence of both stress parameters, F_τ/pw and c/w, on the radius of curvature of the notch profile clearly points to the marked influence of this parameter on the stress-raising action of the notch.

A more convenient form of the relationship given in Figure 22 is shown in Figure 25, which represents the final correlation for the case of notches with θ = 90 degrees. Figure 25 was prepared by first expanding and linearizing the R/w scale of Figure 22. This intermediate step is shown in Figure 22a, in which the final curve corresponding to h/w = 0.20 is presented as a dashed curve. (It will be noted that the expansion of the R/w scale of Figure 22 was carried out with respect only to the curves marked B, which are actually F_τ/pw curves; the curves marked A were superposed directly from Figure 17 after the h/w scale at the top of Figure 22a had been set.) Because the B curves of Figure 22 are not well defined for values of R/w less than 0.20, the corresponding curves in Figure 22a have been extended to cover this region. The shape of the extensions are indicated by the slope of the curves in the region R/w > 0.20 and by the fact that the curves tend to large values of σ_{max}/p as R/w approaches zero. However, the analysis has not been adequate in verifying the relationships in this low R/w region.

In Figure 25, the dashed line intersecting the h/w curves marks the boundary between notch profiles having R/w less than h/w and those having R/w greater than h/w. It will be noted that for the latter case the flank angle is actually less than 90 degrees, and is given in this case by the angle which the tangent to the circular arc at the top of the notch makes with the axis of the bar.

Notches with θ = 60 Degrees and θ = 30 Degrees

The same procedure as described above was used in analyzing notches with θ = 60 degrees and θ = 30 degrees. Stresses were calculated for values of h/w = 0.30, 0.45, 0.60, 0.75, and 0.90 in notches with θ = 60 degrees; and for h/w = 0.30 and 0.45 in notches with θ = 30 degrees.

The curves relating the stress parameter F_τ/pw and the geometrical parameters h/w and R/w for the above cases are shown in Figures 18 and 19. The F_τ/pw versus h/w curves in these figures were cut off at points

representing the maximum possible values of h/w associated with the respective R/w values. (The maximum value of the ratio h/w in each case corresponds to R = 0.) The extrapolation curves used to extend the range of the F_τ/pw versus h/w plots to other values of R/w, as well as the c/w versus R/w relationship for both of the above cases, are shown with the corresponding relationships for θ = 90 degrees (Figures 20 and 21, respectively). For notches with θ = 30 degrees the plotted points in Figure 20, representing calculated values, were based on F_τ/pw values for h/w = 0.45.

A comparison of the F_τ/pw versus h/w curves of Figures 17, 18, and 19 corresponding to the three values of θ under consideration shows that the curves associated with the larger values of R/w are almost coincident for notches with θ = 60 degrees and θ = 90 degrees, while the curves for θ = 30 degrees lie close to the corresponding curves for the above two values of θ. This indicates a diminishing effect of the flank angle on F_τ/pw as R/w increases. This decrease in the effect of θ with increasing R/w is also indicated in the c/w versus R/w relationships shown in Figure 21, where the single curve representing θ = 60 degrees and θ = 30 degrees joins the curve for θ = 90 degrees at the larger values of R/w. The above-noted tendency immediately becomes evident from a comparison of the calculated values of F_τ/pw and σ_{max}/p for the different cases given in Table 5.

The composite plots giving the stress concentration factor as a function of the geometrical parameters for notches with θ = 60 degrees and θ = 30 degrees are shown in Figures 23 and 24, respectively. As in Figure 22 (for θ = 90 degrees), a maximum value of 1.16 is shown for the ratio R/w in Figure 23, this value representing the limiting case above which the flank angle becomes less than 60 degrees. (The corresponding limiting value for notches with θ = 30 degrees is 1.99.)

Plots of Figures 23 and 24 in the same form as Figure 25 for θ = 90 degrees are given in Figures 26 and 27. The curves for the higher values of h/w in the latter figures were cut off at points corresponding to values of R/w for which they represent the maximum possible h/w values. As in the case of Figure 25, the dashed line cutting the h/w curves in Figure 26 (for notches with θ = 60 degrees) separates notch profiles with flank angles equal to 60 degrees from those in which the flank angle is less than 60 degrees, i.e., when R/w is greater than 0.50 h/w.

V. EXPERIMENTAL INVESTIGATION AND COMPARISONS WITH THEORETICAL ANALYSIS

A. EXPERIMENTAL INVESTIGATION

Even though small in number, the specimens tested in this study were intended to provide a basis for comparison with values obtainable from the theoretical analysis of the preceding chapter. Specifically, it was the author's intention to determine experimentally the maximum stresses and the total tensile force across the centerline section of the notch F_σ in each of the specimens.

As originally planned, the stresses were to be determined by means of strain gage as well as "Photostress" measurements. The latter method makes use of a sheet of birefringent plastic cut into the same shape and bonded onto the face of the specimen, and a reflection polariscope operating on essentially the same principle as the standard photoelastic apparatus. However, the strains at the centerline section of the notches were of such small magnitude that it was impossible to obtain accurate readings for the stresses along this section without loading the specimens to a point where the critical sections would have yielded. In view of this limitation, the Photostress measurements were abandoned and only strain gage readings were taken.

Test Specimens and Procedure

The six specimens tested were fabricated from 1/4-inch-thick plate conforming to American Society for Testing and Materials specifications for A7 steel. The general dimensions of the specimens are shown in Figure 28a, while the general shapes of the notch profiles are shown in Figure 28b. The measured values of the geometrical parameters defining the notch profiles are listed in Table 6, which also includes the results of the tests.

An average of ten metalfilm strain gages, having gage lengths of 1/16 of an inch and 1/32 of an inch, were used on each specimen. In two of the specimens, where slight variations in the measured values of the radii were observed, it was found advisable to install additional gages on the second notch. The 1/32-inch gages were used along a short length on the shaped edge of each specimen where the maximum strain was expected to occur; the 1/16-inch gages were used to measure the nominal strain and the strains along the centerline section of the notch.

The specimens were tested in a 120,000-pound Universal testing machine. Because some eccentricity in the loading was noted early in the tests (due to a slight curvature in the specimens as well as misalignment in the bolt holes), an effort was made to reduce the effect of this eccentricity by taking three series of readings with the gaged side of the specimen facing one direction and another three series of readings with the specimen turned 180 degrees. In order to minimize the effect of a non-uniform seating

of the bolts which fastened the specimen to the pullheads, the bolts were loosened at the end of each series of readings and retightened before the start of the next. Each series of readings was started from zero load, and then brought up to the maximum load in increments of 5000 and then 10,000 pounds. The maximum load was determined by estimating, on the basis of the small-load readings, the load which would just cause the material at the critical sections to yield. The maximum load for each case was then set slightly below this estimated value.

Test Results

Strain versus total-load plots for several of the gages on specimen PS-4 are shown in Figure 29. Similar plots were prepared for each of the gages used. It will be noted that in Figure 29 the lines tend to converge and form narrower bands as the load increases. The final strain-versus-total-load line for each gage was taken as a line connecting the origin with the point representing the average of the six measured strain values at the maximum load. The values of the stresses and their ratios to the calculated nominal stress were determined using the values of the strains obtained in this way. The total force across the centerline of the notch F_σ (which is equal to the total shearing force along one-half the base width of the notch F_τ) was determined graphically.

B. COMPARISON OF RESULTS OF THEORETICAL ANALYSIS WITH EXPERIMENTAL RESULTS

Column 11 of Table 6 lists the predicted stress concentration factors corresponding to the notches in Specimens PS-3, -4, and -5 as obtained from Figure 27. The per cent difference between the predicted values and the respective measured values are recorded in column 12. Except for the case of PS-5 which represents a notch with a relatively large radius of curvature, the values obtained from Figure 27 are considerably lower than the measured values.

In an effort to further check the values obtained by the finite-difference solution and the subsequent analysis, the case of projecting notches with low h/w or large w/h values was considered, i.e., notches approaching the case of a bar with shoulder fillets. For this purpose, Figure 30 was prepared showing the variation of the stress concentration factor with the ratio w/h for notches with θ = 90 degrees, 60 degrees, and 30 degrees, and R/h values of 0.50, 1.0, and 2.0. In this figure, the various curves were drawn as fine lines in regions where one or more of the defining parameters would no longer be realized. For instance, the entire curve for θ = 90 degrees and R/h = 2.0 was drawn as a fine line because θ is always less than 90 degrees for this value of R/h.

Figure 30 shows that for a particular value of θ and R/h, σ_{max}/p increases with increasing w/h until a value of the latter of about 5.0 is reached beyond which σ_{max}/p becomes approximately constant. This constant value of the stress concentration factor corresponds to the case of a projecting notch with relatively large width or a bar with a shoulder fillet and may, therefore, be compared with the corresponding empirically-based values given by Peterson[10] or Heywood.[11] Such a comparison is presented in Table 7.

Since Figures 25, 26, and 27 were based on a solution using a half-depth of bar b approximately equal to the half-width of the notch w, the value of b used in column 4 of Table 7 was made equal to the value of w corresponding to the w/h value at the point where the appropriate curve in Figure 30 becomes horizontal. The points marking these

w/h values are indicated by small crosses in Figure 30. The values of h and R used in Table 7 were chosen mainly to give the desired ratios of R/h = 0.50, 1.0, and 2.0. (The ratios of these quantities, rather than their absolute values, are the significant parameters.)

The values listed in column 7 of Table 7 were obtained from Figure 57 of Reference 10. Since the figure gives values corresponding to the case of θ = 90 degrees, the values taken from this figure were corrected for the cases where θ = 60 degrees and θ = 30 degrees by using the empirical relationship given in Figure B-3 of Reference 26. The last column in Table 7 gives the per cent difference between the stress concentration factors obtained from Reference 10 and those from Figure 30.

The values of the stress concentration factor as obtained from the analysis of the preceding chapter are found to be consistently lower than the corresponding values given by Peterson. The largest differences listed in column 9 of Table 7 occur for notches with small radii and flank angles of 60 degrees and 90 degrees. The values listed in columns 7 and 8 of Table 7, however, compare reasonably well. It is particularly worth noting the close agreement between the values for notches with θ = 30 degrees. This is in contrast to the large differences listed in Table 6 between the values from Figure 27 and the experimental results for specimens PS-3 and PS-4. This would seem to indicate that the measured values of σ_{max}/p listed in Table 6 for PS-3 and PS-4 are too high for the recorded R/w values and may have been caused by small irregularities at the critical sections of the profiles produced by grinding in the preparation of the specimens.

The above comparisons suggest that the values given by Figures 25, 26, and 27 may be slightly lower than what they should be. It may be noted here that had a further refinement of the grid spacing been possible in the previously-discussed finite-difference solution, slightly higher values of the stress concentration factor could have been obtained. (This could be expected on the basis of the observed increase in the calculated maximum stress accompanying each refinement of the grid spacing.)

• • •

VI. SUMMARY AND CONCLUSIONS

A. SUMMARY

The principal object of this study was the determination of the effects of the various geometrical parameters characterizing the profiles of projecting notches on the associated stress concentration factors. In particular, consideration was given to notches with circular transition curves (referred to here as idealized projecting notches) occurring symmetrically in a rectangular bar subjected to axial loading.

The method of analysis used here accomplished the object of the study indirectly by considering the effects of the different geometrical parameters on the magnitude and distribution of the shearing stresses along the base section of a projecting notch. As a preliminary step, the stresses along selected sections in a projecting notch in a half-plane were obtained using a solution given by H. Neuber. By combining these data with a solution by L. N. G. Filon for the stresses in a rectangular bar resulting from surface stress loads it was shown that the maximum longitudinal stress along the base section of a projecting notch is produced primarily by the shearing stress component along the base section. The effect of the normal stress component along the same section was shown to be negligible. This has led to the observation that the maximum stress in a projecting notch may be reasonably approximated by the longitudinal stress in a plain rectangular bar subjected to an axial load and a surface-shear stress loading of the proper magnitude and distribution.

The above observation was used as the basis for employing an equivalent surface-shear loading to approximate the stress-raising action of a projecting notch. As used in this study, the equivalent surface-shear load consists of a triangularly-distributed surface-shear loading having a total area under the distribution curve (from centerline to toe of notch) F_τ/p equal to that along the base section of the corresponding projecting notch; the apex of the triangular distribution curve (defined by the ratio c/w) is located such that the maximum longitudinal stress along the surface of a plain rectangular bar produced by such a loading -- acting together with an axial tensile load of intensity p at the ends of the bar -- is equal to the actual maximum stress occurring in the corresponding projecting notch.

Using the results of the equivalent surface-shear load method, a procedure was developed for establishing a correlation between the stress concentration factor and the geometrical parameters characterizing the profile of projecting notches. The procedure developed allows the extension of results of calculations for a relatively few cases to a wider range of values of the geometrical parameters. The resulting relationships, obtained for the case of Neuber's notches and also for idealized projecting notches (in which the stresses were obtained using a

finite-difference solution), provide a clear indication of the effects of the various parameters considered.

B. CONCLUSIONS

Although the values of the stress concentration factor obtained for the idealized projecting notch are approximate, owing to the approximations inherent in the finite-difference solution used, the following conclusions may be drawn validly from the above study.

(1) The stress-raising action of a projecting notch is a function of the magnitude and distribution of and may be reasonably well approximated by the effect of the shearing stress component along its base section. The effect of the normal stress component along the same section is negligible.

(2) The distribution of the shearing stress component along the base section of the notch is characterized principally by the stress parameters F_τ/pw and c/w (F_τ being the total shearing force along the half-width of the notch w, p being the nominal stress, and c being the distance from the peak of the shear stress intensity curve to the toe of the notch. The stress concentration factor increases with increasing values of F_τ/pw and decreasing c/w).

(3) The shearing stress parameter F_τ/pw is a function of the geometrical parameters R/w, h/w, and θ.

(a) The value of the stress parameter F_τ/pw increases with decreasing values of R/w, becoming theoretically infinite when R = 0. For a given value of h/w, the effect of R/w on F_τ/pw diminishes with decreasing values of the flank angle θ. (See Figures 17, 18, and 19.)

(b) For particular values of R/w and θ, F_τ/pw increases rapidly for small values of h/w, the rate of increase diminishing markedly and progressively becoming smaller as h/w exceeds a value of about 0.50. (See Figures 17, 18, and 19.)

(c) For given values of R/w and h/w, F_τ/pw decreases with decreasing values of the flank angle θ, the decrease being small for large values of R/w and increasing with decreasing values of R/w. (Compare Figures 17, 18, and 19.)

(4) The stress parameter c/w is a function only of the geometrical parameter R/w and is independent of h/w and θ. (See Table 5 and Figure 15.) It decreases with decreasing values of R/w.

(5) The stress concentration factor for idealized projecting notches is thus a function of all three geometrical parameters defining the notch profile, i.e., R/w, h/w, and θ, the most significant of these being R/w. The relative importance of each of these parameters varies with the values of the other parameters, as discussed above.

VII. REFERENCES

1. R. K. Sahgal and W. H. Munse, "Fatigue Behavior of Axially Loaded Weldments in HY-80 Steel," University of Illinois SRS 204, September, 1960.

2. A. J. Hartmann and W. H. Munse, "Fatigue Behavior of Welded Joints and Weldments in HY-80 Steel Subjected to Axial Loadings," University of Illinois SRS 250, July, 1962.

3. W. W. Sanders, Jr., A. T. Derecho, and W. H. Munse, "Effect of External Geometry on Fatigue Behavior of Welded Joints," Welding Journal, February, 1965.

4. H. Kihara, T. Yoshiaki, M. Watanabe, and Y. Ishii, "Effect of Flaws in Welds on Their Strength," Non-destructive Testing of Welds and Their Strength (The Society of Naval Architects of Japan [Tokyo, 1960]).

5. Newman and Gurney "Fatigue Tests in Plain Plate Specimens and Transverse Butt Welds," British Welding Journal, VI, No. 12 (December, 1959) 569-594.

6. J. E. Tomlinson and J. L. Wood, "Factors Affecting the Fatigue Behavior of Welded Aluminum," British Welding Journal, VII, No. 4 (April, 1960) 250-264.

7. W. O. Dinsdale, "Effect of Reinforcement Shape on Fatigue Behavior of Butt Welds in NP5/6," British Welding Journal, XI, No. 5 (May, 1964) 233-238.

8. H. Neuber, "Theory of Notch Stresses: Principles for Exact Stress Calculation," (English Translation by F. A. Raven, Translation 74, David Taylor Model Basin, Navy Department, Washington, D.C.).

9. M. M. Leven and A. J. Hartmann, "Factors of Stress Concentration for Flat Bars and Shafts with Centrally Enlarged Section," Proceedings SESA, IX, No. 1 (1951).

10. R. E. Peterson, Stress Concentration Design Factors, (John Wiley, New York, 1953).

11. R. B. Heywood, Designing by Photoelasticity, (Chapman & Hall, London, 1951).

12. T. A. McCreery, "A Computer Method for the Approximate Solution of Two-Dimensional Elastostatic Problems by Conformal Mapping," (University of Illinois Ph.D. Thesis, 1961).

13. Ernst Weinel, "Ueber die Spannungserhoehung in Kerbstaeben," (Proceedings of the Fifth International Congress for Applied Mechanics, Cambridge, Massachusetts, 1938) 51-53.

14. M. Hetenyi and T. D. Liu, "A Method for Calculating Stress Concentration Factors," Journal of Applied Mechanics, XXIII, No. 3 (September, 1956) 451-457.

15. A. Mathews, "Calculation of Stress Concentration Factors in Filleted Members by the Equivalent Surface-Shear Load Method," (University of Illinois Ph.D. Thesis, 1959).

16. M. M. Frocht, "Factors of Stress Concentration Photoelastically Determined," Transactions ASME, LVII (1935) A-67.

17. E. G. Coker and L. N. G. Filon, "A Treatise on Photoelasticity," (Cambridge University Press, 1931).

18. S. Timoshenko and Dietz, "Stress Concentration Produced by Holes and Fillets," Transactions ASME, XLVII (1925) 199-237.

19. L. N. G. Filon, "On an Approximate Solution for the Bending of a Beam of Rectangular Cross-Section Under Any System of Load, with Special Reference to Points of Concentrated of Discontinuous Loadings,"

Phil. Transactions of the Royal Society, CCI, Series A (London, 1902) 63-155.

20. D. Young, "Iterative Methods for Solving Partial Difference Equations of the Elliptic Type," Transactions American Mathematics Society, LXXVI (1954) 92-111.

21. F. G. Lehman, "Simultaneous Equations Solved by Over-Relaxation," (American Society of Civil Engineers Second Conference on Electronic Computation [September, 1960] 503-512.

22. S. Timoshenko and J. N. Goodier, Theory of Elasticity, (McGraw-Hill, New York, 1951).

23. M. Salvadori and M. Baron, Numerical Methods in Engineering, (Prentice-Hall, 1961).

24. S. H. Crandall, Engineering Analysis, (McGraw-Hill, 1956).

25. D. N. de G. Allen, Relaxation Methods in Engineering and Science, (McGraw-Hill, 1954).

26. K. R. Wichman, A. G. Hopper, and J. L. Mershon, "Local Stresses in Spherical and Cylindrical Shells Due to External Loadings," (Bulletin No. 107, Welding Research Council, August, 1965).

• • •

APPENDIX A. DEVELOPMENT OF NEUBER'S SOLUTION FOR A PROJECTING NOTCH IN A HALF-PLANE UNDER TENSILE LOADING[8]

A. GENERAL RELATIONSHIPS IN RECTANGULAR COORDINATES

The Three-dimensional Problem

Neuber approached the elasticity problem of satisfying the equilibrium equations in terms of displacements,

$$\left.\begin{aligned} (\lambda + G)\frac{\partial e}{\partial x} + G\nabla^2 u &= 0 \\ (\lambda + G)\frac{\partial e}{\partial y} + G\nabla^2 v &= 0 \\ (\lambda + G)\frac{\partial e}{\partial z} + G\nabla^2 w &= 0, \end{aligned}\right\} \qquad (A\text{-}1)$$

and the associated boundary conditions, by assuming displacement functions of the form

$$\left.\begin{aligned} 2Gu &= 2\eta\varphi_1 - \frac{\partial F}{\partial x} \\ 2Gv &= 2\eta\varphi_2 - \frac{\partial F}{\partial y} \\ 2Gw &= 2\eta\varphi_3 - \frac{\partial F}{\partial z} \end{aligned}\right\} \qquad (A\text{-}2)$$

where

$$F = \varphi_0 + x\varphi_1 + y\varphi_2 + z\varphi_3$$

and where u, v, w are the displacement components along the rectangular x,y,x axes, respectively, and

$$\left.\begin{aligned} e &= \frac{\partial u}{\partial x} + \frac{\partial v}{\partial y} + \frac{\partial w}{\partial z} \\ \lambda &= \frac{\nu E}{(1+\nu)(1-2\nu)} \end{aligned}\right\} \qquad (A\text{-}3)$$

$$\left.\begin{aligned} G &= \frac{E}{2(1+\nu)} \\ E &= \text{Young's modulus} \\ \nu &= \text{Poisson's ratio.} \end{aligned}\right\} \qquad (A\text{-}3)$$

When Equations (A-2) are substituted into Equations (A-1), it is seen that if the functions φ_0, φ_1, φ_2, and φ_3 are harmonic, i.e.,

$$\nabla^2\varphi_i \equiv \frac{\partial^2\varphi_i}{\partial x^2} + \frac{\partial^2\varphi_i}{\partial y^2} + \frac{\partial^2\varphi_i}{\partial z^2} = 0, \qquad (A\text{-}4)$$

$$i = 0,1,2,3,$$

the Equations (A-1) are satisfied provided the constant η has a value

$$\eta = 2(1-\nu). \qquad (A\text{-}5)$$

Generally, any one of the harmonic functions φ_i ($i = 0,1,2,3$) may be dropped without loss of generality. Thus, the problem is reduced to finding harmonic functions which satisfy the prescribed boundary conditions.

The Two-dimensional Problem

Similar relations hold for the two-dimensional case, where the stresses and deformations are functions of two coordinate variables (e.g., x and y in rectangular coordinates).

(a) Plane Strain. The equilibrium equations in terms of displacements are

$$\left.\begin{aligned}(\lambda + G)\frac{\partial e}{\partial x} + G\nabla^2 u &= 0\\ (\lambda + G)\frac{\partial e}{\partial y} + G\nabla^2 v &= 0\end{aligned}\right\} \qquad (A\text{-}6)$$

where

$$e = \frac{\partial u}{\partial x} + \frac{\partial v}{\partial y}\ .$$

Equations (A-6) are satisfied if the displacement functions are taken as

$$\begin{aligned}2Gu &= 2\eta\varphi_1 - \frac{\partial F}{\partial x}\\ 2Gv &= -\frac{\partial F}{\partial y}\end{aligned} \qquad (A\text{-}7)$$

where

$$F = \varphi_0 + x\varphi_1,$$

provided the functions φ_0 and φ_1 are harmonic, i.e.,

$$\nabla^2\varphi_i \equiv \frac{\partial^2\varphi_i}{\partial x^2} + \frac{\partial^2\varphi_i}{\partial y^2} = 0 \qquad i = 0,1 \qquad (A\text{-}8)$$

and

$$\eta = 2(1 - \nu). \qquad (A\text{-}9)$$

In establishing Equations (A-7), φ_2 in Equations (A-2) has been set equal to zero and φ_3 is necessarily equal to zero if the deformation is to be independent of z.

(b) Generalized Plane Stress. The equilibrium equations in terms of displacements for this case have a form similar to that of Equations (A-6),

$$\left.\begin{aligned}(\bar{\lambda} + G)\frac{\partial \bar{e}}{\partial x} + G\nabla^2 \bar{u} &= 0\\ (\bar{\lambda} + G)\frac{\partial \bar{e}}{\partial y} + G\nabla^2 \bar{v} &= 0\end{aligned}\right\} \qquad (A\text{-}10)$$

where

$$\bar{\lambda} = \frac{2\lambda G}{\lambda + 2G} = \frac{\nu E}{1 - \nu^2} \qquad (A\text{-}11)$$

and

$$\bar{e} = \frac{\partial \bar{u}}{\partial x} + \frac{\partial \bar{v}}{\partial y} = \int_{-t/2}^{t/2}\frac{\partial u}{\partial x}\,dz + \int_{-t/2}^{t/2}\frac{\partial v}{\partial y}\,dz, \qquad (A\text{-}11)$$

$\bar{e}$, $\bar{u}$, and $\bar{v}$ indicating mean values across the thickness t in the z direction.

If the displacement functions are again given by Equations (A-7), with u and v taken as mean values, Equations (A-10) are satisfied -- provided φ_0 and φ_1 are harmonic and

$$\eta = \frac{2}{1 + \nu}\ . \qquad (A\text{-}12)$$

B. THE PROBLEM IN CURVILINEAR COORDINATES

In the following, only orthogonal curvilinear coordinate systems are considered.

As stated earlier, assuming the displacement functions to be of the form given by either of Equations (A-2) or (A-7) with the constant η assigned the required value, the problem reduces to one of finding harmonic functions φ_1 satisfying the boundary conditions. When the boundary is other than straight, the boundary conditions are generally difficult to satisfy unless the boundary coincides with a coordinate line. Hence, the use of an appropriate curvilinear coordinate system simplifies this part of the problem considerably. However, the problem of finding harmonic functions, i.e., functions satisfying Laplace's equation, become comparatively complicated for the general case by the use of curvilinear coordinates. Thus, for an orthogonal curvilinear coordinate system defined by

$$x = x(\alpha, \beta, \gamma); \qquad y = y(\alpha, \beta, \gamma),$$

$$z = z(\alpha, \beta, \gamma),$$

the Laplacian (in three dimensions) is given by

$$\nabla^2 \equiv \frac{1}{h_\alpha h_\beta h_\gamma}\left[\frac{\partial}{\partial \alpha}\left(\frac{h_\beta h_\gamma}{h_\alpha}\frac{\partial}{\partial \alpha}\right) + \frac{\partial}{\partial\beta}\left(\frac{h_\alpha h_\gamma}{h_\beta}\frac{\partial}{\partial\beta}\right) + \frac{\partial}{\partial\gamma}\left(\frac{h_\alpha h_\beta}{h_\gamma}\frac{\partial}{\partial\gamma}\right)\right] \qquad \text{(A-13)}$$

where h_α, h_β, h_γ are the scale factors corresponding to the α, β, γ directions. For the two-dimensional case,

$$\nabla^2 \equiv \frac{1}{h_\alpha h_\beta}\left[\frac{\partial}{\partial\alpha}\left(\frac{h_\beta}{h_\alpha}\frac{\partial}{\partial\alpha}\right) + \frac{\partial}{\partial\beta}\left(\frac{h_\alpha}{h_\beta}\frac{\partial}{\partial\beta}\right)\right] . \qquad \text{(A-14)}$$

An important special case of orthogonal curvilinear coordinates is the isometric* (or conformal) system in which the scale factors are equal, i.e.,

$$h_\alpha = h_\beta = h,$$

and for which Equation (A-15) reduces to

$$\nabla^2 \equiv \frac{1}{h^2}\left(\frac{\partial^2}{\partial\alpha^2} + \frac{\partial^2}{\partial\beta^2}\right) . \qquad \text{(A-15)}$$

Thus, for an isometric system, the condition that the functions φ_0 and φ_1 be harmonic assumes the same simple form it takes in ractangular coordinates

$$\frac{\partial^2\varphi_i}{\partial\alpha^2} + \frac{\partial^2\varphi_i}{\partial\beta^2} = 0, \qquad i = 0, 1. \qquad \text{(A-16)}$$

Before going into the conditions which the displacement functions must satisfy along a free boundary, the expressions for the stresses in curvilinear coordinates will first be developed.

Expressions for Stresses in Curvilinear Coordinates

(a) The Three-dimensional Case. The displacement components along the α, β, γ axes, U, V, and W, respectively, may be obtained from the expressions for the displacement components in the x, y, z directions by noting that the cosines of the angles between the x axis and the α, β, γ axes are given by

$$\left.\begin{aligned} &\cos(x,\alpha) = \frac{1}{h_\alpha}\frac{\partial x}{\partial\alpha} \;;\; \cos(x,\beta) \\ &\qquad = \frac{1}{h_\beta}\frac{\partial x}{\partial\beta} \;;\; \cos(x,\gamma) = \frac{1}{h_\gamma}\frac{\partial x}{\partial\gamma} , \\ &\text{so that} \\ &\qquad h_\alpha^2 = \left(\frac{\partial x}{\partial\alpha}\right)^2 + \left(\frac{\partial y}{\partial\alpha}\right)^2 + \left(\frac{\partial z}{\partial\alpha}\right)^2 , \end{aligned}\right\} \qquad \text{(A-17)}$$

with similar expressions for the y and z axes. Using the above expressions, one obtains

$$\left.\begin{aligned} U &= \frac{1}{h_\alpha}\left(u\frac{\partial x}{\partial\alpha} + v\frac{\partial y}{\partial\alpha} + w\frac{\partial z}{\partial\alpha}\right) \\ V &= \frac{1}{h_\beta}\left(u\frac{\partial x}{\partial\beta} + v\frac{\partial y}{\partial\beta} + w\frac{\partial z}{\partial\beta}\right) \\ W &= \frac{1}{h_\gamma}\left(u\frac{\partial x}{\partial\gamma} + v\frac{\partial y}{\partial\gamma} + w\frac{\partial z}{\partial\gamma}\right) . \end{aligned}\right\} \qquad \text{(A-18)}$$

Substitution in the above equations of the expressions for u, v, and w from Equations (A-2) gives the displacement components along the curvilinear axes in terms of the harmonic functions φ_i,

$$\left.\begin{aligned} 2GU = \frac{1}{h_\alpha}\Bigg[&-\frac{\partial F}{\partial\alpha} + 2\eta\left(\varphi_1\frac{\partial x}{\partial\alpha}\right. \\ &\left.\left. + \varphi_2\frac{\partial y}{\partial\alpha} + \varphi_3\frac{\partial z}{\partial\alpha}\right)\right] \end{aligned}\right\} \qquad \text{(A-19)}$$

---

*For a curvilinear coordinate system defined by $x = f(\alpha, \beta)$; $y = g(\alpha, \beta)$ to be isometric, the following conditions must be satisfied:

$$\frac{\partial x}{\partial\alpha} = \pm\frac{\partial y}{\partial b}, \qquad \frac{\partial x}{\partial\beta} = \mp\frac{\partial y}{\partial\alpha} .$$

$$
\left.
\begin{aligned}
2GV &= \frac{1}{h_\beta}\left[-\frac{\partial F}{\partial \beta} + 2\eta\left(\varphi_1\frac{\partial x}{\partial \beta} + \varphi_2\frac{\partial y}{\partial \beta} + \varphi_3\frac{\partial z}{\partial \beta}\right)\right] \\
2GW &= \frac{1}{h_\gamma}\left[-\frac{\partial F}{\partial \gamma} + 2\eta\left(\varphi_1\frac{\partial x}{\partial \gamma} + \varphi_2\frac{\partial y}{\partial \gamma} + \varphi_3\frac{\partial z}{\partial \gamma}\right)\right] .
\end{aligned}
\right\} \quad \text{(A-19)}
$$

From geometrical considerations the following expressions are obtained for the strain components in the α, β, γ directions in terms of the displacement components

$$
\left.
\begin{aligned}
\epsilon_\alpha &= \frac{1}{h_\alpha}\left(\frac{\partial U}{\partial \alpha} + \frac{V}{h_\beta}\frac{\partial h_\alpha}{\partial \beta} + \frac{W}{h_\gamma}\frac{\partial h_\alpha}{\partial \gamma}\right) \\
\gamma_{\alpha_\beta} &= \frac{h_\alpha}{h_\beta}\frac{\partial}{\partial \beta}\left(\frac{U}{h_\alpha}\right) + \frac{h_\beta}{h_\alpha}\frac{\partial}{\partial \alpha}\left(\frac{V}{h_\beta}\right) .
\end{aligned}
\right\} \quad \text{(A-20)}
$$

similar relations being obtainable for ϵ_β, ϵ_γ, $\gamma_{\alpha\gamma}$, and $\gamma_{\beta\gamma}$. By substituting Equations (A-19) into the above equations, the following expressions are obtained for the strains in terms of the harmonic functions φ_i:

$$
\left.
\begin{aligned}
2G\epsilon_\alpha &= -\frac{\partial^2 F}{\partial n_\alpha^2} + \frac{2\eta}{h_\alpha}\left[\frac{\partial \varphi_1}{\partial \alpha}\frac{\partial x}{\partial \alpha} + \frac{\partial \varphi_2}{\partial \alpha}\frac{\partial y}{\partial \alpha} + \frac{\partial \varphi_3}{\partial \alpha}\frac{\partial z}{\partial \alpha}\right] \\
G\gamma_{\alpha\beta} &= -\frac{\partial^2 F}{\partial n_\alpha\, \partial n_\beta} + \frac{\eta}{h_\alpha h_\beta}\left[\frac{\partial \varphi_1}{\partial \beta}\frac{\partial x}{\partial \alpha} + \frac{\partial \varphi_1}{\partial \alpha}\frac{\partial x}{\partial \beta} + \frac{\partial \varphi_2}{\partial \beta}\frac{\partial y}{\partial \alpha} + \frac{\partial \varphi_2}{\partial \alpha}\frac{\partial y}{\partial \beta} + \frac{\partial \varphi_3}{\partial \beta}\frac{\partial z}{\partial \alpha} + \frac{\partial \varphi_3}{\partial \alpha}\frac{\partial x}{\partial \beta}\right] .
\end{aligned}
\right\} \quad \text{(A-21)}
$$

where

$$
\left.
\begin{aligned}
\frac{\partial^2}{\partial n_\alpha^2} &\equiv \frac{1}{h_\alpha}\frac{\partial}{\partial \alpha}\left(\frac{1}{h_\alpha}\frac{\partial}{\partial \alpha}\right) + \frac{1}{h_\alpha h_\beta^2}\frac{\partial h_\alpha}{\partial \beta}\frac{\partial}{\partial \beta} + \frac{1}{h_\alpha h_\gamma^2}\frac{\partial h_\alpha}{\partial \gamma}\frac{\partial}{\partial \gamma} \\
\frac{\partial^2}{\partial n_\alpha \partial n_\beta} &\equiv \frac{h_\alpha}{2h_\beta}\frac{\partial}{\partial \beta}\left(\frac{1}{h_\alpha^2}\frac{\partial}{\partial x}\right) + \frac{h_\beta}{2h_\alpha}\frac{\partial}{\partial \alpha}\left(\frac{1}{h_\beta^2}\frac{\partial}{\partial \beta}\right) ;
\end{aligned}
\right\} \quad \text{(A-22)}
$$

so that

$$
\nabla^2 \equiv \frac{\partial^2}{\partial n_\alpha^2} + \frac{\partial^2}{\partial n_\beta^2} + \frac{\partial^2}{\partial n_\gamma^2} .
$$

Similar expressions may be written for ϵ_β, ϵ_γ, $\gamma_{\alpha\gamma}$, and $\gamma_{\beta\gamma}$.

Substitution of the above expressions for strain into the stress-strain relationships,

$$
\left.
\begin{aligned}
\sigma_\alpha &= \lambda e + 2G\epsilon_\alpha \\
\sigma_\beta &= \lambda e + 2G\epsilon_\beta \\
\sigma_\gamma &= \lambda e + 2G\epsilon_\gamma ,
\end{aligned}
\right.
$$

where

$$
e = \epsilon_\alpha + \epsilon_\beta + \epsilon_\gamma
$$

and

$$
\left.
\begin{aligned}
\tau_{\alpha\beta} &= G\gamma_{\alpha\beta} \\
\tau_{\alpha\gamma} &= G\gamma_{\alpha\gamma} \\
\tau_{\beta\gamma} &= G\gamma_{\beta\gamma} ,
\end{aligned}
\right\} \quad \text{(A-23)}
$$

yields the following expressions for the stresses in terms of the harmonic functions:

$$\sigma_\alpha = -\frac{\partial^2 F}{\partial n_\alpha^2} + \frac{2\eta}{h_\alpha}\left[\frac{\partial \varphi_1}{\partial \alpha}\frac{\partial x}{\partial \alpha} + \frac{\partial \varphi_2}{\partial \alpha}\frac{\partial y}{\partial \alpha} + \frac{\partial \varphi_3}{\partial \alpha}\frac{\partial z}{\partial \alpha}\right] + \nu \nabla^2 F$$

$$\tau_{\alpha\beta} = -\frac{\partial^2 F}{\partial n_\alpha \partial n_\beta} + \frac{\eta}{h_\alpha h_\beta}\left[\frac{\partial \varphi_1}{\partial \beta}\frac{\partial x}{\partial \alpha} + \frac{\partial \varphi_1}{\partial \alpha}\frac{\partial x}{\partial \beta} + \frac{\partial \varphi_2}{\partial \beta}\frac{\partial y}{\partial \alpha} + \frac{\partial \varphi_2}{\partial \alpha}\frac{\partial y}{\partial \beta} + \frac{\partial \varphi_3}{\partial \beta}\frac{\partial z}{\partial \alpha} + \frac{\partial \varphi_3}{\partial \alpha}\frac{\partial z}{\partial \beta}\right], \quad \text{(A-24)}$$

etc.

(b) Stress Components for the Two-dimensional Case. Since for the two-dimensional case the stress distribution is independent of Poisson's ratio,* an arbitrary value may be assigned to this ratio without affecting the resulting expressions for the stresses. If a value of unity is assigned to Poisson's ratio, the constant η (see Equation A-5) becomes equal to zero so that the bracketed terms appearing in Equations (A-24) drop out. By noting that

$$\nabla^2 F \equiv \frac{\partial^2 F}{\partial n_\alpha^2} + \frac{\partial^2 F}{\partial n_\beta^2}$$

we obtain from Equations (A-24) the following expressions for the stresses:

$$\sigma_\alpha = \frac{\partial^2 F}{\partial n_\beta^2} \equiv \frac{1}{h_\alpha}\frac{\partial}{\partial \alpha}\left(\frac{1}{h_\alpha}\frac{\partial F}{\partial \alpha}\right) + \frac{1}{h_\alpha h_\beta^2}\frac{\partial h_\alpha}{\partial \beta}\frac{\partial F}{\partial \beta}$$

$$\sigma_\beta = \frac{\partial^2 F}{\partial n_\alpha^2} \equiv \frac{1}{h_\beta}\frac{\partial}{\partial \beta}\left(\frac{\partial}{h_\beta}\frac{\partial F}{\partial \beta}\right) + \frac{\partial}{h_\alpha^2 h_\beta}\frac{\partial h_\beta}{\partial \alpha}\frac{\partial F}{\partial \alpha}$$

$$\tau_{\alpha\beta} = -\frac{\partial^2 F}{\partial n_\alpha \partial n_\beta} \equiv \frac{h_\alpha}{2h_\beta}\frac{\partial}{\partial \beta}\left(\frac{1}{h_\alpha^2}\frac{\partial F}{\partial \alpha}\right) + \frac{h_\beta}{2h_\alpha}\frac{\partial}{\partial \alpha}\left(\frac{1}{h_\beta^2}\frac{\partial F}{\partial \beta}\right), \quad \text{(A-25)}$$

where F is given by Equations (A-7). It will be noted that the function F has the same character as Airy's stress function.

For an isometric system, Equations (A-25) reduce to

$$\sigma_x = \frac{1}{h}\frac{\partial}{\partial \beta}\left(\frac{1}{h}\frac{\partial F}{\partial \beta}\right) + \frac{1}{h^3}\frac{\partial h}{\partial \alpha}\frac{\partial F}{\partial \alpha}$$

$$\sigma_\beta = \frac{1}{h}\frac{\partial}{\partial \alpha}\left(\frac{1}{h}\frac{\partial F}{\partial \alpha}\right) + \frac{1}{h^3}\frac{\partial h}{\partial \beta}\frac{\partial F}{\partial \beta} \quad \text{(A-26)}$$

$$\tau_{\alpha\beta} = -\frac{1}{2}\frac{\partial}{\partial \alpha}\left(\frac{1}{h^2}\frac{\partial F}{\partial \beta}\right) - \frac{1}{2}\frac{\partial}{\partial \beta}\left(\frac{1}{h^2}\frac{\partial F}{\partial \alpha}\right);$$

or, performing the indicated differentiation,

$$\sigma_\alpha = \frac{1}{h^2}\frac{\partial^2 F}{\partial \beta^2} + \frac{1}{h^3}\left(\frac{\partial h}{\partial \alpha}\frac{\partial F}{\partial \alpha} - \frac{\partial h}{\partial \beta}\frac{\partial F}{\partial \beta}\right)$$

$$\sigma_\beta = \frac{1}{h^2}\frac{\partial^2 F}{\partial \alpha^2} + \frac{1}{h^3}\left(\frac{\partial h}{\partial \beta}\frac{\partial F}{\partial \beta} - \frac{\partial h}{\partial \alpha}\frac{\partial F}{\partial \alpha}\right) \quad \text{(A-26a)}$$

$$\tau_{\alpha\beta} = -\frac{1}{h^2}\frac{\partial^2 F}{\partial \alpha\, \partial \beta} + \frac{1}{h^3}\left(\frac{\partial h}{\partial \alpha}\frac{\partial F}{\partial \beta} + \frac{\partial h}{\partial \beta}\frac{\partial F}{\partial \alpha}\right).$$

Boundary Conditions Corresponding to a Free Boundary

The conditions on the function F corresponding to a free boundary for a two-dimensional curvilinear coordinate system will be derived by first considering the conditions for the case of rectangular coordinates.

*When body forces are neglected.

First, it should be noted that for the two-dimensional case, the function F appearing in the foregoing equations can be made to correspond to Airy's stress function. Thus if we consider F as given in Equations (A-7), i.e.,

$$F = \varphi_0 + x\varphi_1 ,$$

and take the displacement components in the x and y directions as

$$\left.\begin{aligned} 2Gu &= -\frac{\partial}{\partial x}(F - \eta\tilde{\varphi}_1) \\ 2Gv &= -\frac{\partial}{\partial y}(F + \eta\tilde{\varphi}_1) \end{aligned}\right\} \quad (A\text{-}27)^*$$

where

$$\tilde{\varphi}_1 = \int \varphi_1 \, dx ,$$

the equilibrium equations in terms of displacements are satisfied, provided the constant η is given by

$$\eta = 2(1 - \nu)$$

for the case of plane strain, and

$$\eta = \frac{2}{(1 + \nu)}$$

for the case of generalized plane stress.

With the displacement components assumed in the form of Equations (A-27), the stress components are given by

$$\sigma_x = \frac{\partial^2 F}{\partial y^2} , \quad \sigma_y = \frac{\partial^2 F}{\partial x^2} , \quad \tau_{xy} = -\frac{\partial^2 F}{\partial x \partial y} , \quad (A\text{-}28)$$

as in the case of Airy's stress function.

By next considering the equilibrium of an element located on a curved boundary S, bounded in the interior by sides parallel to the x and y axes (see Figure A-1), and denoting by X and Y the components of the external load per unit length of arc acting on the element, the following relationship is obtained:**

$$\left.\begin{aligned} X &= \frac{d}{ds}\left(\frac{\partial F}{\partial y}\right) \\ Y &= -\frac{d}{ds}\left(\frac{\partial F}{\partial x}\right) . \end{aligned}\right\} \quad (A\text{-}29)$$

If the boundary is free of external loads, then

$$\left.\begin{aligned} \left.\frac{\partial F}{\partial x}\right]_{\text{along boundary}} &= \text{constant, } c_1 \\ \left.\frac{\partial F}{\partial y}\right]_{\text{along boundary}} &= \text{constant, } c_2 \end{aligned}\right\} \quad (A\text{-}30)$$

The above conditions on F may be simplified for the case of a problem involving a single continuous boundary by introducing a new stress function,

$$\bar{F} = F - (c_1 x + c_2 y) \quad (A\text{-}31)$$

With the above form of the stress function, the expressions for the stresses given by Equations (A-28) remain unaffected, while the displacement components given by Equations (A-29) are each augmented by constant terms. For a problem involving only a single continuous boundary, these additional constants represent a rigid body displacement and hence do not alter the problem. (However, for a problem involving two disconnected boundaries, the constant terms appearing in the expressions for the displacement components of the boundaries represent a relative displacement of the boundaries with respect to each other.) If $\bar{F}$

---

*Obtained from Equations (A-7) by introducing the following transformations [the starred quantities refer to those appearing in Equations (A-7)]:

$$F^* = F + \eta\tilde{\varphi}_1$$

$$\varphi_1^* = \varphi_1$$

$$\varphi_0^* = \varphi_0 + \eta\tilde{\varphi}_1 .$$

**See, for example, pp. 100-101 of Reference 22.

is now substituted for F in Equations (A-30), one obtains

$$\left.\begin{aligned} \frac{\partial \bar{F}}{\partial x}\Big|_{\text{along boundary}} &= 0 \\ \frac{\partial \bar{F}}{\partial y}\Big|_{\text{along boundary}} &= 0 \end{aligned}\right\} \qquad \text{(A-32)}$$

Since one may write

$$\begin{aligned} \bar{F} &= F - c_1 x - c_2 y \\ &= \varphi_0 + x\varphi_1 - c_1 x - c_2 y \\ &= (\varphi_0 - c_2 y) + (\varphi_1 - c_1)x \\ \bar{F} &= \bar{\varphi}_0 + x\,\bar{\varphi}_1 \end{aligned}$$

where

$$\bar{\varphi}_0 = \varphi_0 - c_2 y,$$

$$\bar{\varphi}_1 = \varphi_1 - c_1,$$

and subject are new harmonic functions, the conditions corresponding to a single free boundary may be written as

$$\left.\begin{aligned} \frac{\partial F}{\partial x} &= 0 \\ \frac{\partial F}{\partial y} &= 0 \end{aligned}\right\} \quad \text{along the boundary.} \qquad \text{(A-33)}$$

Equations (A-33) may now be used to derive the corresponding conditions for a curvilinear coordinate system. This is done by writing $\partial F/\partial x$ and $\partial F/\partial y$ in terms of their respective components along the α and β axes. Thus,

$$\frac{\partial F}{\partial x} = \frac{1}{h_\alpha^2}\frac{\partial F}{\partial \alpha}\frac{\partial x}{\partial \alpha} + \frac{1}{h_\beta^2}\frac{\partial F}{\partial \beta}\frac{\partial x}{\partial \beta}$$

$$\frac{\partial F}{\partial y} = \frac{1}{h_\alpha^2}\frac{\partial F}{\partial \alpha}\frac{\partial y}{\partial \alpha} + \frac{1}{h_\beta^2}\frac{\partial F}{\partial \beta}\frac{\partial y}{\partial \beta}$$

Solving for $\partial F/\partial \alpha$ and $\partial F/\partial \beta$, one obtains

$$\left.\begin{aligned} \frac{\partial F}{\partial \alpha} &= \frac{1}{Dh_\beta^2}\left(\frac{\partial F}{\partial x}\frac{\partial y}{\partial \beta} - \frac{\partial F}{\partial y}\frac{\partial x}{\partial \beta}\right) \\ \frac{\partial F}{\partial \beta} &= \frac{1}{Dh_\alpha^2}\left(\frac{\partial F}{\partial y}\frac{\partial x}{\partial \alpha} - \frac{\partial F}{\partial x}\frac{\partial y}{\partial \alpha}\right) \end{aligned}\right\} \qquad \text{(A-34)}$$

where

$$D = \frac{1}{h_\alpha^2 h_\beta^2}\left(\frac{\partial x}{\partial \alpha}\frac{\partial y}{\partial \beta} - \frac{\partial x}{\partial \beta}\frac{\partial y}{\partial \alpha}\right).$$

Along a free boundary, $\partial F/\partial x = 0$ and $\partial F/\partial y = 0$. Hence, the conditions corresponding to a free boundary, for the case of a problem involving only a single continuous boundary, are given by

$$\left.\begin{aligned} \frac{\partial F}{\partial \alpha} &= 0 \\ \frac{\partial F}{\partial \beta} &= 0 \end{aligned}\right\} \quad \text{along the boundary.} \qquad \text{(A-35)}$$

(The above relations could have been deduced directly from Equations (A-33) by noting that the two components of the derivatives of F in two non-parallel directions -- in this case x and y -- are both equal to zero.)

Thus, the above solution of a problem in plane elasticity involving a single free boundary consists of finding harmonic functions φ_0 and φ_1 such that the function $F = \varphi_0 + x\varphi_1$ satisfies Equations (A-35) in addition to other prescribed boundary conditions (usually concerned with the type of loading). Once this is done, the stresses and displacements may be calculated from F using Equations (A-28) and (A-27), respectively.

C. SOLUTION FOR THE STRESSES IN A PROJECTING NOTCH IN A HALF-PLANE UNDER TENSILE LOADING

The projecting notch considered in the following is defined by the equations

$$x = \alpha + \frac{\alpha}{\alpha^2 + \beta^2} \quad \text{and} \quad y = \beta - \frac{\beta}{\alpha^2 + \beta^2} \tag{A-36}$$

with $\beta = \beta_o$ (a constant), and is assumed subjected to a uniform tensile stress directed parallel to the x axis. The profile of the notch, $\beta = \beta_o$, represents the lower boundary of a half-plane which extends indefinitely in both positive and negative x directions as well as in the positive y direction. Profiles corresponding to different values of the constant are shown in Figure 2. It will be noted from Equations (A-36) that α approaches x and β approaches y for large values of α and/or β.

The (α, β) coordinate system described by Equations (A-36) can be shown to be orthogonal,* and also isometric, i.e.,

$$h_\alpha^2 = h_\beta^2 = h^2 = 1 + \frac{2(\beta^2 - \alpha^2)+1}{(\alpha^2 + \beta^2)^2} . \tag{A-37}$$

For a loading consisting of a uniform tensile stress of intensity p directed parallel to the x axis and acting at infinity, the boundary conditions to be satisfied are:

$$\left.\begin{aligned} &\text{(a) at} \quad x = \alpha = \pm\infty: \\ &\qquad \sigma_x = \frac{\partial^2 F}{\partial y^2} = p. \\ &\text{(b) along} \quad \beta = \beta_o: \\ &\qquad \frac{\partial F}{\partial \alpha} = 0 \\ &\qquad \frac{\partial F}{\partial \beta} = 0. \end{aligned}\right\} \tag{A-38}$$

The solution is obtained by first considering a condition of uniform tensile stress in the x direction and then modifying it to account for the disturbance of the uniform stress field due to the presence of the notch. Thus, corresponding to the initial condition of a uniform tensile stress $\sigma_x = p$ throughout the region considered, one readily obtains

$$F = \frac{p}{2} y^2 . \tag{A-39}$$

The function F as given by Equation (A-39) may be obtained by taking the harmonic functions φ_0 and φ_1 as follows:

$$\left.\begin{aligned} \varphi_0 &= \frac{p}{2}(y^2 - x^2) \\ \varphi_1 &= \frac{p}{2} x . \end{aligned}\right\} \tag{A-40}$$

Then,

$$F = \varphi_0 + x\varphi_1 = \frac{p}{2} y^2 .$$

The next step is to transform F into curvilinear coordinates using Equations (A-36).

$$F = \frac{p}{2}\left[\beta^2 - \frac{2\beta^2}{\alpha^2+\beta^2} + \frac{\beta^2}{(\alpha^2+\beta^2)^2}\right]. \tag{A-41}$$

The corresponding expressions for the harmonic functions φ_0 and φ_1 are:

$$\begin{aligned} \varphi_0 &= \frac{p}{2}\left[\beta^2 - \alpha^2 - \frac{2(\alpha^2+\beta^2)}{\alpha^2+\beta^2} + \frac{\beta^2-\alpha^2}{(\alpha^2+\beta^2)^2}\right] \\ \varphi_1 &= \frac{p}{2}\left(\alpha + \frac{\alpha}{\alpha^2+\beta^2}\right) \end{aligned} \tag{A-42}$$

The expression for F given by Equation (A-41) now satisfies the first boundary condition. To satisfy the second boundary condition and to account for the disturbance of the uniform stress field due to the presence of the notch in the vicinity of $x = \alpha = 0$, additional terms must be appended to φ_0 and φ_1 as given by Equations (A-42). These auxiliary functions must be such that

---

*That is the relations defining the system, given by Equations (A-36), satisfy the orthogonality condition:

$$\frac{\partial x}{\partial \alpha}\frac{\partial x}{\partial \beta} + \frac{\partial y}{\partial \alpha}\frac{\partial y}{\partial \beta} = 0.$$

their effect vanishes for large values of x or α so that the satisfaction of the first boundary condition is unaffected by their addition. Since the final function F has to satisfy the boundary conditions along the surface of the notch, expressions having a form similar to the relations defining the notch profile become logical choices for these auxiliary terms. Among the harmonic functions in this category are:

$$\left.\begin{aligned} &\alpha, \quad \beta, \quad \frac{\alpha}{\alpha^2+\beta^2}, \quad \frac{\beta}{\alpha^2+\beta^2} \\ &\pm (\beta^2-\alpha^2), \quad \text{and} \quad \pm \frac{\alpha^2-\beta^2}{(\alpha^2\ \beta^2)^2} \end{aligned}\right\} \quad \text{(A-43)}$$

The functions φ_0 and φ_1 may now be written as

$$\left.\begin{aligned} \varphi_0 &= \frac{p}{2}\left[\beta^2-\alpha^2-2\left(\frac{\alpha^2+\beta^2}{\alpha^2+\beta^2}\right)\right. \\ &\quad + \frac{\beta^2-\alpha^2}{(\alpha^2+\beta^2)^2} + A\alpha \\ &\quad + B\beta + C(\beta^2-\alpha^2) + D\frac{\alpha}{\alpha^2+\beta^2} \\ &\quad \left. + E\frac{\beta}{\alpha^2+\beta^2} + G\frac{\beta^2-\alpha^2}{(\alpha^2+\beta^2)^2}\right] \\ \varphi_1 &= \frac{p}{2}\left[\alpha + \frac{\alpha}{\alpha^2+\beta^2} + H\frac{\alpha}{\alpha^2+\beta^2}\right] . \end{aligned}\right\} \quad \text{(A-44)}$$

The stress function F then becomes

$$\begin{aligned} F &= \varphi_0 + x\varphi_1 = \varphi_0 + (\alpha + \frac{\alpha}{\alpha^2+\beta^2}) \\ &= \frac{p}{2}\left\{\beta^2 - \frac{2\beta^2}{\alpha^2+\beta^2} + \frac{\beta^2}{(\alpha^2+\beta^2)^2}\right. \\ &\quad + A\alpha + B\beta + C(\beta^2-\alpha^2) + D\frac{\alpha}{\alpha^2+\beta^2} \\ &\quad + E\frac{\beta}{\alpha^2+\beta^2} + G\frac{\beta^2-\alpha^2}{(\alpha^2+\beta^2)^2} \\ &\quad \left. + H\left[\frac{\alpha^2}{\alpha^2+\beta^2} + \frac{\alpha^2}{(\alpha^2+\beta^2)^2}\right]\right\} . \end{aligned} \quad \text{(A-45)}$$

The constants appearing in Equation (A-45) are determined by making F satisfy the condition along the free boundary

$$\left.\frac{\partial F}{\partial \alpha}\right]_{\beta=\beta_o} = 0 \quad \text{and} \quad \left.\frac{\partial F}{\partial \beta}\right]_{\beta=\beta_o} = 0. \quad \text{(A-46)}$$

This gives the following:

$$\left.\begin{aligned} &A = C = D = 0 \\ &B = -2\beta_o \\ &E = \frac{2\beta_o}{2\beta_o^2+1} \\ &G = -\frac{3\beta_o^2+1}{2\beta_o^2+1} \quad \text{and} \quad H = -\frac{4\beta_o^2+1}{2\beta_o^2+1} \end{aligned}\right\} \quad \text{(A-47)}$$

Substituting the values of the above constants into Equation (A-45) gives

$$\begin{aligned} F = \frac{p}{2}\left[\beta^2 - 2\beta_o\beta\right. \\ \left. - \frac{(\beta-\beta_o)^2}{(2\beta_o^2+1)(\alpha^2+\beta^2)} - \frac{4\beta_o^2+1}{2\beta_o^2+1}\right] , \end{aligned} \quad \text{(A-48)}$$

which may be reduced to a simpler form by introducing a constant term (which does not affect the stresses)

$$\frac{p}{2}\left(\beta_o^2 + \frac{4\beta_o^2+1}{2\beta_o^2+1}\right) . \quad \text{(A-49)}$$

The final expression for the stress function then becomes

$$F = \frac{p}{2}(\beta-\beta_o)^2\left[1 - \frac{1}{(2\beta_o^2+1)(\alpha^2+\beta^2)}\right] \quad \text{(A-50)}$$

The above form of F makes it readily apparent that along the boundary $\beta = \beta_o$, F equals zero, so that the second boundary condition is indeed satisfied.

With the function F now known, the stress components σ_α, σ_β, and $\tau_{\alpha\beta}$ may be calculated using Equations (A-26a). The derivatives of h and F appearing in Equations (A-26a) have been calculated and are given below:

$$\left.\begin{aligned}
\frac{\partial h}{\partial \alpha} &= \frac{2\alpha(\alpha^2 - 3\beta^2 - 1)}{(\alpha^2+\beta^2)^2\left[(\alpha^2+\beta^2)^2+2\beta^2 - 2\alpha^2+1\right]^{1/2}} \\
\frac{\partial h}{\partial \beta} &= \frac{2\beta(3\alpha^2 - \beta - 1)}{(\alpha^2+\beta^2)^2\left[(\alpha^2+\beta^2)^2+2\beta^2 - 2\alpha^2+1\right]^{1/2}} \\
\frac{\partial F}{\partial \alpha} &= \left[\frac{\alpha(\beta-\beta_o)^2}{(2\beta_o^2+1)(\alpha^2+\beta^2)^2}\right] p \\
\frac{\partial F}{\partial \beta} &= (\beta-\beta_o)\left[1 - \frac{\alpha^2+\beta\beta_o}{(2\beta_o^2+1)(\alpha^2+\beta^2)^2}\right] p \\
\frac{\partial^2 F}{\partial \alpha^2} &= \left[\frac{(\beta-\beta_o)^2(\beta^2-3\alpha^2)}{(2\beta_o^2+1)(\alpha^2+\beta^2)^3}\right] p \\
\frac{\partial^2 F}{\partial \beta^2} &= \left[1 - \frac{\alpha^4+\alpha^2(6\beta\beta_o-\beta_o^2-3\beta^2)+\beta^2\beta_o(3\beta_o-2\beta)}{(2\beta_o^2+1)(\alpha^2+\beta^2)^3}\right] p \\
\frac{\partial^2 F}{\partial \alpha \partial \beta} &= \left[\frac{2\alpha(\beta-\beta_o)(\alpha^2+2\beta\beta_o-\beta^2)}{(2\beta_o^2+1)(\alpha^2+\beta^2)^3}\right] p \,.
\end{aligned}\right\} \quad (A\text{-}51)$$

As a check on the satisfaction of the first boundary condition, it will be noted that for large values of x and α, $h \to 1$,* $\sigma_\alpha \to \sigma_x$, and all of the terms entering into the expressions for the stress components, except $\partial^2 F/\partial\beta^2$ (which becomes equal to p), tend to zero. Thus, as $x \to \pm\infty$, $\sigma_x = p$, and $\sigma_y = \tau_{xy} = 0$. Also, for large values of β, $\sigma_x = p$ and $\sigma_y = \tau_{xy} = 0$, i.e., the stresses are finite as $y \to +\infty$.

*See Equation (A-37).

Along the surface of the notch, $\frac{\partial F}{\partial \alpha} = \frac{\partial F}{\partial \beta} = 0$, so that

$$\sigma_\alpha\Big|_{\beta=\beta_o} = \frac{1}{h^2}\frac{\partial^2 F}{\partial \beta^2}\Big|_{\beta=\beta_o} = \frac{\left[1 - \frac{1}{(2\beta_o^2+1)(\alpha^2+\beta_o^2)}\right]}{\left[1 + \frac{2\beta_o^2 - 2\alpha^2 + 1}{(\alpha^2+\beta_o^2)^2}\right]} p \,. \quad (A\text{-}52)$$

The maximum stress is obtained by differentiating the above expression for σ_α with respect of α and equating the result to zero. This gives

$$\alpha_{(\sigma_\alpha)_{max}} = \left[1 + \beta_o^2 \pm \sqrt{4\beta_o^2 + 4\beta_o^4}\right]^{1/2} \quad (A\text{-}53)$$

$$(\sigma_\alpha)_{max} = \left[1 + \frac{(1+4\beta_o^2)\left(\sqrt{1+\beta_o^2} - \beta_o\right)}{4\beta_o(1+2\beta_o^2)}\right] p \,. \quad (A\text{-}54)$$

The stress concentration factor is then given by the ratio $\frac{(\sigma_\alpha)_{max}}{p}$.

The curvature of the notch profile is given by

$$\kappa_{\beta_o} = \left(\frac{1}{\rho}\right)_{\beta_o} = \frac{2\beta_o(3\alpha^2 - \beta_o^2 - 1)}{\left[(\alpha^2+\beta_o^2)^2+2\beta_o^2 - 2\alpha^2+1\right]^{3/2}} \,, \quad (A\text{-}55)$$

Differentiation of the above expression for κ_{β_o}, to obtain the minimum radius of curvature of the notch profile, yields

$$\alpha_{R_{min}} = \sqrt{1+\beta_o^2}$$

and

$$R_{min} = 2\beta_o^2\sqrt{1+\beta_o^2} \,. \quad (A\text{-}56)$$

In transforming the stress components along the α and β directions to components parallel to the x and y directions, the angle between the α coordinate line (or β = constant line) and the x coordinate line at the point is required. This angle is given by the following:

$$\varphi = \tan^{-1}\left[\frac{2\,\alpha\,\beta}{(\alpha^2+\beta^2)^2+(\beta^2-\alpha^2)}\right]. \qquad \text{(A-57)}$$

APPENDIX B. DEVELOPMENT OF EXPRESSIONS FOR THE STRESSES IN A RECTANGULAR BAR DUE TO SURFACE STRESS LOADINGS*

In the following, consideration is given to a rectangular bar of length 2a, depth 2b, and thickness 2t, subjected to a uniform tensile stress p acting at its ends. In addition to the axial load p, a surface stress loading -- either shear or normal stress -- acting over a length 2w is imposed at the center on both top and bottom surfaces of the bar (see Figure B-1).

For the two-dimensional state of stress assumed here, the elasticity problem may be formulated in terms of Airy's stress function, F. When body forces are neglected this function is related to the stress components by the equations

$$\sigma_x = \frac{\partial^2 F}{\partial y^2}, \quad \sigma_y = \frac{\partial^2 F}{\partial x^2}, \quad \tau_{xy} = -\frac{\partial^2 F}{\partial x \partial y}. \tag{B-1}$$

The equations of equilibrium are identically satisfied by Equations (B-1), and in the absence of body forces the compatibility equation becomes the biharmonic equation in F,

$$\frac{\partial^4 F}{\partial x^4} + 2\frac{\partial^4 F}{\partial x^2 \partial y^2} + \frac{\partial^4 F}{\partial y^4} \equiv \nabla^4 F \nabla 0 . \tag{B-2}$$

For the particular case considered, the problem becomes one of finding a function F satisfying Equation (B-2) in the plane region considered as well as the following boundary conditions:

$$\left.\begin{aligned} \sigma_x &= \frac{\partial^2 F}{\partial y^2} = p \\ \sigma_y &= \tau_{xy} = 0 \end{aligned}\right\} \tag{B-3}$$

and

$$\left.\begin{aligned} \tau_{xy} &= -\frac{\partial^2 F}{\partial x \partial y} = f(x) \\ \sigma_y &= 0 \end{aligned}\right\} \text{along } y = \pm b \tag{B-4}$$

for the case of a surface-shear loading; or Equation (B-3) and

$$\left.\begin{aligned} \sigma_y &= \frac{\partial^2 F}{\partial x^2} = g(x) \\ \tau_{xy} &= 0 \end{aligned}\right\} \text{along } y = \pm b \tag{B-5}$$

for the case of a surface-normal stress loading. In the above equations, f(x) and g(x) are the distribution functions associated with the surface-shear and the surface-normal stress loadings, respectively.

For both of the above cases, the problem may be considered as divided into two parts. The first part, representing a condition of uniform stress $\sigma_x = p$ along the entire length of the bar due to the action of the uniform tensile stress p at its ends, corresponds to a stress function (as in Appendix A) of the form

$$F = \frac{1}{2} py^2, \tag{B-6}$$

which satisfies Equation (B-2) as well as the first boundary condition (B-3). The second part represents the stress condition arising

*See, for example, pages 46-52 of Reference 22.

from the action of the stress loading on the surface $y = \pm b$, the stress function for which must satisfy condition (B-4) in the case of a surface-shear loading or condition (B-5) in the case of a surface-normal stress loading. Moreover, the stress function for this second part must satisfy the condition

$$\sigma_x = \sigma_y = \tau_{xy} = 0 \qquad \text{at } x = \pm a. \tag{B-7}$$

The stress function for this second part corresponding to the two cases noted above will be considered separately.

A. SOLUTION FOR THE CASE OF A SURFACE-SHEAR LOADING DISTRIBUTED ANTI-SYMMETRICALLY ABOUT THE Y AXIS

For the case of the surface-shear loading shown in Figure B-1, the resulting state of stress in the bar will have a distribution which is symmetrical about the y axis (i.e., an even function of x). The solution to Equation (B-2) may then be taken as a series of the form*

$$F = \sum Y(y) \cos \alpha x \tag{B-8}$$

where $\alpha = \frac{n\pi}{a}$.

When Equation (B-8) is substituted into Equation (B-2) a fourth-order ordinary differential equation in Y(y) results which when solved, yields

$$Y(y) = C_1 \cosh \alpha y + C_2 \sinh \alpha y + C_3 y \cosh \alpha y + C_4 y \sinh \alpha y. \tag{B-9}$$

The stress function thus becomes

$$F = \sum_{n=0}^{\infty} (C_1 \cosh \alpha y + C_2 \sinh \alpha y + C_3 y \cosh \alpha y + C_4 y \sinh \alpha y) \cos \alpha x. \tag{B-10}$$

*See, for example, pages 46-50 of Reference 22.

From Equation (B-10),

$$\left.\begin{aligned}
\sigma_x &= \frac{\partial^2 F}{\partial y^2} \\
&= \sum_{n=1}^{\infty} \left[C_1\alpha^2 \cosh \alpha y + C_2\alpha^2 \sinh \alpha y \right. \\
&\qquad + C_3\alpha(2\sinh\alpha y + \alpha y \cosh \alpha y) \\
&\qquad \left. + C_4\alpha(2\cosh \alpha y + \alpha y \sinh \alpha y)\right] \cos \alpha x \\
\sigma_y &= \frac{\partial^2 F}{\partial x^2} \\
&= -\sum_{n=1}^{\infty} \left[C_1 \cosh\alpha y + C_2 \sinh \alpha y + C_3 y \cosh \alpha y \right. \\
&\qquad \left. + C_4 y \sinh \alpha y\right] \alpha^2 \cos \alpha x \\
\tau_{xy} &= -\frac{\partial^2 F}{\partial x \partial y} \\
&= \sum_{n=1}^{\infty} \left[C_1\alpha \sinh \alpha y + C_2\alpha \cosh \alpha y \right. \\
&\qquad + C_3(\cosh\alpha y + \alpha y \sinh \alpha y \\
&\qquad \left. + C_4(\sinh\alpha y + \alpha y \cosh \alpha y)\right] \alpha \sin\alpha x.
\end{aligned}\right\} \tag{B-11}$$

The constants C_1 to C_4 in Equations (B-11) are determined by using the boundary conditions of Equation (B-4). For this purpose, the function f(x) describing the distribution of the shearing stresses along $y = \pm b$ is expressed in terms of a Fourier sine series (the shearing stress distribution shown in Figure B-1 being anti-symmetrical about the y axis, i.e., an odd function of x). Thus

$$\left.\begin{aligned}
(\tau_{xy})_{y=+b} &= \sum_{n=1}^{\infty} A_n \sin \alpha x \\
(\tau_{xy})_{y=-b} &= \sum_{n=1}^{\infty} B_n \sin \alpha x \quad .
\end{aligned}\right\} \tag{B-12}$$

Substituting the above values into the third equation of Equations (B-11) and solving the resulting relationships together with the second of Equations (B-11) with $\sigma_y = 0$, one obtains

$$\left.\begin{aligned} C_1 &= -\left[\frac{b \sinh \alpha b}{\cosh \alpha b}\right] C_4 = \\ &\quad -\frac{(A_n - B_n)}{\alpha}\left[\frac{b \sinh \alpha b}{\sinh 2\alpha b + 2\alpha b}\right] \\ C_2 &= -\frac{b \cosh \alpha b}{\sinh \alpha b} C_4 = \\ &\quad -\frac{(A_n + B_n)}{\alpha}\left[\frac{b \cosh \alpha b}{\sinh 2\alpha b - 2\alpha b}\right] \end{aligned}\right\} \quad (B\text{-}13)$$

Noting that, by the usual sign convention for shearing stresses, $A_n = -B_n$, one immediately gets $C_2 = C_3 = 0$. Equations (B-11) now become

$$\left.\begin{aligned} \sigma_x &= \sum_{n=1}^{\infty} 2A_n \frac{2\cosh\alpha b - \alpha b \sinh\alpha b}{\sinh 2\alpha b + 2\alpha b} \cosh\alpha y \cos\alpha x \\ &\quad + \sum_{n=1}^{\infty} 2A_n \frac{\cosh\alpha b}{\sinh 2\alpha b + 2\alpha b} \alpha y \sinh\alpha y \cos\alpha x. \\ \sigma_y &= \sum_{n=1}^{\infty} 2A_n \frac{\alpha b \sinh\alpha b}{\sinh 2\alpha b + 2\alpha b} \cosh\alpha y \cos\alpha x \\ &\quad - \sum_{n=1}^{\infty} 2A_n \frac{\cosh\alpha b}{\sinh 2\alpha b + 2\alpha b} \alpha y \sinh\alpha y \cos\alpha x. \\ \tau_{xy} &= \sum_{n=1}^{\infty} 2A_n \frac{\cosh\alpha b \; \alpha b \sinh\alpha b}{\sinh 2\alpha b + 2\alpha b} \sinh\alpha y \sin\alpha x \\ &\quad + \sum_{n=1}^{\infty} 2A_n \frac{\cosh\alpha b}{\sinh 2\alpha b + 2\alpha b} \alpha y \cosh\alpha y \sin\alpha x. \end{aligned}\right\} \quad (B\text{-}14)$$

It will be noted that at the ends of the bar, $x = \pm a$, $\tau_{xy} = 0$; however, σ_x is not equal to zero and has a distribution other than uniform. Thus, it is difficult to satisfy fully the boundary condition specified by Equation (B-7). However, if the dimension a (i.e., the half-length of the bar) is made sufficiently large in comparison with b and w, instead of the stress distribution for σ_x given by the first of Equations (B-14), we may consider at $x = \pm a$, a statically equivalent uniform stress distribution without materially altering the stress condition in the immediate vicinity of the bar centerline, i.e., in the region of application of the surface-stress load. To do this, the total forces acting at the ends of the bar due to the stress σ_x must be calculated.

If the total tension at either end of the bar is denoted by T and the bending moment by M, then

$$(T)_{x=+a} = (T)_{x=-a} = \int_{-b}^{b} (\sigma_x)_{x=\pm a} \, dy,$$

or

$$\begin{aligned} (T)_{x=\pm a} &= \sum_{n=1}^{\infty} 2A_n \frac{2\cosh\alpha b - \alpha b \sinh\alpha b}{\sinh 2\alpha b + 2\alpha b} \cos\alpha a \int_{-b}^{b} \cos\alpha y dy \\ &\quad + \sum_{n=1}^{\infty} 2A_n \frac{\alpha \cosh\alpha b \cos\alpha a}{\sinh 2\alpha b + 2\alpha b} \int_{-b}^{b} y \sinh\alpha y dy \end{aligned}$$

$$(T)_{x=\pm a} = \sum_{n=1}^{\infty} 2A_n \frac{\cos\alpha a}{\alpha} . \quad (B\text{-}15)$$

By observing that $y \cosh\alpha y$ and $y^2 \sinh\alpha y$ are odd functions of y, it is found that

$$(M)_{x=\pm a} = -\int_{-b}^{b} y(\sigma_x)_{x=\pm a} \, dy = 0.$$

Thus, the condition of zero load at the ends of the bar can be satisfied -- insofar as the effects near the bar centerline are concerned --

by introducing uniform compressive stresses at the ends of the bar with a magnitude equal to the average stress corresponding to the total end force $(T)_{x=\pm a}$ given by Equation (B-15). This corrective stress loading, which is transmitted undiminished throughout the length of the bar, must be added to the expression for σ_x given by the first equation of Equations (B-14), which now becomes,

$$\overrightarrow{\sigma_x} = -\sum_{n=1}^{\infty} \frac{A_n}{b} \frac{\cos \alpha a}{\alpha} + \sum_{n=1}^{\infty} 2A_n \frac{2\cosh\alpha b - \alpha b \sinh\alpha b}{\sinh 2\alpha b + 2\alpha b} \cosh\alpha y \cos\alpha x + \sum_{n=1}^{\infty} 2A_n \frac{\cosh \alpha b}{\sinh 2\alpha b \quad 2\alpha b} \alpha y \sinh \alpha y \cos \alpha x. \tag{B-16}$$

The complete expression for the stress σ_x due to the action of the surface-shear loading shown in Figure B-1, together with a uniform longitudinal tensile stress p acting at the ends of the bar, will then be equal to $(p + \overrightarrow{\sigma_x})$. The expressions for σ_y and τ_{xy} as given by Equations (B-14) are unaffected by the corrective loading and the stress p at the ends of the bar.

Expression for the Fourier Coefficient A_n Corresponding to a Triangular Surface-Shear Loading

For the broken-line distribution of the surface-shear loading shown in Figure B-1, obtains

$$\left.\begin{aligned} \tau(x) &= -\frac{\tau_o}{w-c} x \quad \text{when } 0 \le x \le (w-c) \\ \tau(x) &= \frac{\tau_o}{c} (x-w) \quad \text{when } (w-c) \le x \le w \\ \tau(x) &= 0 \quad \text{when } x \ge w . \end{aligned}\right\} \tag{B-17}$$

The Fourier coefficient A_n in Equation (B-12) is then given by the following expression:

$$A_n = \frac{2}{ap} \int_o^a \tau(x) \sin \alpha x \, dx$$

$$= \frac{2}{ap} \left[-\frac{\tau_o}{w-c} \int_o^{(w-c)} x \sin \alpha x \, dx + \frac{\tau_o}{c} \int_{(w-c)}^{w} (x-w) \sin \alpha x \, dx \right]$$

or

$$A_n = \frac{2\tau_o}{ac\alpha^2 p} \left[\sin \alpha w - \frac{w}{w-c} \sin \alpha (w-c) \right]. \tag{B-18}$$

B. SOLUTION FOR THE CASE OF A SURFACE-NORMAL STRESS LOADING DISTRIBUTED SYMMETRICALLY ABOUT THE Y AXIS

When the loading on the surfaces of the bar $y = \pm b$ is purely normal and distributed as shown in Figure B-2, the stress function F in Equation (B-2) may again be taken in the form

$$F = \sum Y(y) \cos \alpha x.$$

As in the preceding section, the same expressions are obtained for the stress components in terms of the arbitrary constants C_1 to C_4 as given by Equations (B-11). The constants are similarly determined by applying the boundary conditions given by Equations (B-5), the normal stress loading now being expressed in terms of a Fourier cosine series,

$$\left.\begin{aligned} (\sigma_y)_{y=+b} &= \frac{C_o}{2} + \sum_{n=1}^{\infty} C_n \cos \alpha x \\ (\sigma_y)_{y=-b} &= \frac{D_o}{2} + \sum_{n=1}^{\infty} D_n \cos \alpha x \end{aligned}\right\} \tag{B-19}$$

For the loading distribution considered here, $C_o = D_o$. The terms $C_o/2$ and $D_o/2$ represent stress loadings of uniform intensity acting on the faces $y = +b$ and $y = -b$, respectively, over the entire length of the bar, and give rise to the stress components

$$\left.\begin{aligned} \sigma_y &= \frac{C_o}{2} = \frac{D_o}{2} \\ \sigma_x &= \tau_{xy} = 0 \end{aligned}\right\} \quad \text{(B-20)}$$

The effect of the first terms in Equations (B-19) having thus been accounted for, only the general term under the summation sign need be considered in connection with Equations (B-11). If the general terms in Equations (B-19) are now substituted into the second of Equations (B-11) and the resulting expressions solved simultaneously with the equations obtained by applying the boundary conditions,

$$(\tau_{xy})_{y=+b} = 0, \quad \text{and} \quad (\tau_{xy})_{y=-b} = 0$$

to the third of Equations (B-11), one obtains the following expressions for the constants C_1 to C_4:

$$\left.\begin{aligned} C_1 &= -\left(\frac{\sinh \alpha b + \alpha b \cosh \alpha b}{\alpha \sinh \alpha b}\right) \\ C_2 &= -\left(\frac{\cosh \alpha b + \alpha b \sinh \alpha b}{\alpha \cosh \alpha b}\right) \\ C_3 &= \left(\frac{C_n + D_n}{\alpha^2}\right)\left(\frac{\cosh \alpha b + \alpha b \sinh \alpha b}{\sinh 2\alpha b - 2\alpha b}\right) \\ C_4 &= \left(\frac{C_n + D_n}{\alpha^2}\right)\left(\frac{\sinh \alpha b + \alpha b \cosh \alpha b}{\sinh 2\alpha b + 2\alpha b}\right). \end{aligned}\right\} \quad \text{(B-21)}$$

For the loading shown in Figure B-2a, i.e., with a distribution symmetrical with respect to the x axis, $C_n = D_n$, so that $C_2 = C_3 = 0$. The stress components corresponding to the general terms in Equations (B-19) are thus given by

$$\left.\begin{aligned} \sigma_x &= \sum_{n=1}^{\infty} 2C_n \frac{\sinh\alpha b - \alpha b \cosh\alpha b}{\sinh 2\alpha b + 2\alpha b} \cosh\alpha y \cos\alpha x \\ &\quad + \sum_{n=1}^{\infty} 2C_n \frac{\sinh \alpha b}{\sinh 2\alpha b + 2\alpha b} \alpha y \sinh \alpha y \cos\alpha x. \\ \sigma_y &= \sum_{n=1}^{\infty} 2C_n \frac{\sinh\alpha b + \alpha b \cosh\alpha b}{\sinh 2\alpha b + 2\alpha b} \cosh\alpha y \cos\alpha x \\ &\quad - \sum_{n=1}^{\infty} 2C_n \frac{\sinh \alpha b}{\sinh 2\alpha b + 2\alpha b} \alpha y \sinh \alpha y \cos\alpha x. \\ \tau_{xy} &= -\sum_{n=1}^{\infty} 2C_n \frac{\alpha b \cosh \alpha b}{\sinh 2\alpha b + 2\alpha b} \sinh\alpha y \sin \alpha x \\ &\quad + \sum_{n=1}^{\infty} 2C_n \frac{\sinh \alpha b}{\sinh 2\alpha b + 2\alpha b} \alpha y \cosh\alpha y \sin\alpha x. \end{aligned}\right\} \quad \text{(B-22)}$$

A check of the resultant forces at the ends of the bar, $x = \pm a$, yields

$$(T)_{x=\pm a} = \int_{-b}^{b} (\sigma_x)_{x=\pm a} dy$$

$$= \sum_{n=1}^{\infty} 2C_n \frac{\sinh\alpha b - \alpha b \cosh\alpha b}{\sinh 2\alpha b + 2\alpha b} \cos\alpha a \int_{-b}^{b} \cosh\alpha y \, dy$$

$$+ \sum_{n=1}^{\infty} 2C_n \frac{\alpha \sinh \alpha b}{\sinh 2\alpha b + 2\alpha b} \cos\alpha a \int_{-b}^{b} y \sinh\alpha y dy = 0 \quad \text{(B-23)}$$

and (again by noting that $y \cosh \alpha y$ and $y^2 \sinh \alpha y$ are odd functions of y),

$$(M)_{x=\pm a} = \int_{-b}^{b} y(\sigma_x)_{x=\pm a} dy = 0.$$

Thus, in this case, there is no need to introduce corrective forces at the ends of the bar.

The final expressions for the stress components due to a surface-normal stress loading symmetrically distributed with respect to the y axis are then given by Equations (B-21), except that for σ_y the effect of the first term of the Fourier series expansion [given by Equations (B-20)] must be added. (However, it will be shown in the following section that for the distribution of normal stress loading considered here, $C_o = D_o = 0$.)

Expression for the Fourier Coefficient C_n Corresponding to a Linearly Varying Surface-Normal Stress Loading

For the distribution of the surface-normal stress loading shown in Figure B-2b, one obtains

$$\begin{aligned}
\sigma_n(x) &= -\sigma_n^{(-)} && \text{when } 0 \le x \le (s-t) \\
\sigma_n(x) &= \frac{\sigma_n^{(+)}}{w-s-g}(x-s) && \text{when } (s-t) \le x \le (w-g) \\
\sigma_n(x) &= \frac{\sigma_n^{(+)}}{g}(w-x) && \text{when } (w-g) \le x \le w \\
\sigma_n(x) &= 0 && \text{when } x > w\ .
\end{aligned} \tag{B-24}$$

In Figure B-2b, the quantities $\sigma_n^{(+)}$, w, s, and g are assumed to be given while the quantities $\sigma_n^{(-)}$ and r are to be calculated from the requirement that the sum of the negative (compressive) stresses must be equal to the sum of the positive (tensile) stresses. This condition occurs along the base section of a projecting notch. It can readily be verified that

$$r = \left(s - \sqrt{s^2 - (w-s-g)(w-s)}\right)$$

and

$$\sigma_n^{(-)} = \frac{r}{w-s-g}\,\sigma_n^{(+)}. \tag{B-25}$$

The Fourier coefficient C_n ($= D_n$) in Equations (B-19) is then given by

$$\begin{aligned}
C_n &= \frac{2}{ap}\int_o^a \sigma_n(x)\cos\alpha x\,dx \\
&= \frac{2}{ap}\left[-\sigma_n^{(-)}\int_o^{(s-r)}\cos\alpha x\,dx\right. \\
&\quad + \frac{\sigma_n^{(+)}}{w-s-g}\int_{s-r}^{w-c}(x-s)\cos\alpha x\,dx \\
&\quad \left. + \frac{\sigma_n^{(+)}}{g}\int_{w-c}^{w}(w-x)\cos\alpha x\,dx\right] \\
C_n &= \frac{2}{ap}\left[-\frac{\sigma_n^{(-)}}{\alpha}\sin\alpha(s-r)\right. \\
&\quad + \frac{\sigma_n^{(+)}}{\alpha(w-s-g)}\left\{r\sin\alpha(s-r)\right. \\
&\quad \left.\left. + \frac{1}{\alpha}\left[\cos\alpha(w-g) - \cos\alpha(s-r)\right]\right\}\right. \\
&\quad \left. - \frac{\sigma_n^{(+)}}{\alpha^2 g}\left[\cos\alpha w - \cos\alpha(w-g)\right]\right]
\end{aligned} \tag{B-26}$$

for n = 1, 2, 3,.... ∞. A separate calculation for the first term C_o gives

$$C_o = \frac{2}{ap}\int_o^a \sigma_n(x)\,dx = 0. \tag{B-27}$$

This result follows from the condition, stated earlier, that the algebraic sum of the surface-normal stresses on each of the surfaces $y = \pm b$ must be equal to zero.

APPENDIX C. BOUNDARY VALUES FOR THE STRESS FUNCTION USED IN THE FINITE DIFFERENCE SOLUTION

In the finite-differences method, the problem of finding a continuous function F that satisfies the compatibility equation as well as the associated boundary conditions is replaced by one requiring values of F at a discrete number of points, which also satisfy compatibility and the boundary conditions. Thus, the area under consideration is assumed to be subdivided by a grid (usually square) or lattice and the value of the stress function F is calculated at the intersections of the grid lines or node points (see Figure C-1). Corresponding to this discretization, the compatibility equation (B-2) is replaced by the finite-difference biharmonic equation shown diagramatically in Figure (C-2). The numbers within the circles in the bracketed biharmonic operator of Figure (C-2) represent the coefficients of the values of F at these node points.[23,24] To obtain the finite-difference approximations for the derivatives in terms of the values of the function at the node points, the usual procedure is to construct an interpolating polynomial (with degree equal to the order of the derivative) which takes on the given values of the function at the node points. The derivatives of the given function are then considered to be equal to the corresponding derivative of the interpolating polynomial.

For the particular case considered here, the stress function has to satisfy, in addition to the compatibility condition, the following boundary conditions (see Figure C-1):

$$\left.\begin{aligned} Y &= 0 \quad \text{everywhere} \quad (a) \\ X &= p \quad \text{on AB} \quad (b) \\ X &= 0 \quad \text{on BCDEF} \quad (c) \end{aligned}\right\} \quad (C\text{-}1)$$

where X and Y are the respective x and y components of the external stresses acting on the boundary of the area considered. Since Equations (C-1) are expressed in terms of stresses, it is necessary to transform them into the corresponding expressions in terms of the stress function F. This is done by using Equations (A-29) which relate X and Y with F, i.e.,

$$\left.\begin{aligned} X &= \frac{\partial}{\partial s}\left(\frac{\partial F}{\partial y}\right) \quad (a) \\ Y &= -\frac{\partial}{\partial s}\left(\frac{\partial F}{\partial s}\right) \quad (b). \end{aligned}\right\} \quad \begin{matrix}(A\text{-}29)\\(C\text{-}2)\end{matrix}$$

In applying the biharmonic operator to points near the boundary of the area considered, the value of the function F, as well as its derivatives, $\partial F/\partial x$ and $\partial F/\partial y$, are required. The latter are used in the interpolation and extrapolation formulas for determining the values of F at points adjacent to a boundary.

(a) Values of Derivatives $\partial F/\partial x$ and $\partial F/\partial y$ Along the Boundary. From Equations (C-1a) and (C-2b), one obtains

$$\frac{\partial F}{\partial x} = -\int_s Y\,ds = 0 + C_1.$$

Since F is known to be symmetrical about the vertical axis x = 0 (i.e., the line FG in

Figure C-1), its derivative $\partial F/\partial x$ must be anti-symmetrical about the same line. Hence,

$$\left.\frac{\partial F}{\partial x}\right|_{x=0} = 0, \quad \text{so that } C_1 = 0;$$

and

$$\frac{\partial F}{\partial x} = 0 \qquad \text{everywhere.} \qquad \text{(C-3)}$$

Along the vertical portion of the boundary AB, ds = dy. Using Equations (C-1b) and (C-2a)

$$\frac{\partial F}{\partial y} = \int_{AB} X\,ds = \int_{AB} p\,dy = py + C_2.$$

Again, since F is known to be symmetrical about the horizontal axis y = 0, $\partial F/\partial y$ must be anti-symmetrical about the same line, that is,

$$\left.\frac{\partial F}{\partial y}\right|_{y=0} = 0 \quad \text{hence} \quad C_2 = 0$$

and

$$\frac{\partial F}{\partial y} = py \qquad \text{on AB.} \qquad \text{(C-4)}$$

On the portion of the boundary BCDEF, X = 0, and

$$\frac{\partial F}{\partial y} = \int_{B-F} X\,ds = 0 + C_3.$$

The above equation indicates that $\partial F/\partial y$ has a constant value along BCDEF. From Equation (C-4), one obtains for point B,

$$\left.\frac{\partial F}{\partial y}\right|_{y=b} = \left.py\right|_{y=b} = bp.$$

Hence,

$$\frac{\partial F}{\partial y} = bp \qquad \text{on BCDEF} \qquad \text{(C-5)}$$

(b) Values of the Function F Along the Boundary. To calculate the values of the stress function F along the boundary, it is convenient to use the following expression for F:*

$$F = \int_s \left[\frac{\partial F}{\partial y}\cos(x,n) - \frac{\partial F}{\partial x}\sin(x,n)\right] ds \qquad \text{(C-6a)}$$

where

n = outward-directed normal to the boundary

(x,n) = angle between the positive x axis and the normal n.

Equation (C-6a) may be derived from the expression for the partial derivative of F with respect to s, i.e.,

$$\frac{\partial F}{\partial s} = \frac{\partial F}{\partial x}\frac{dx}{ds} + \frac{\partial F}{\partial y}\frac{dy}{ds}, \qquad \text{(C-6b)}$$

by noting that

$$\frac{dx}{ds} = -\sin(x,n) \quad \text{and} \quad \frac{dy}{ds} = \cos(x,n).$$

An alternative expression to Equation (C-6a) is obtained by integrating Equation (C-6b) by parts. This yields**

$$F = x\frac{\partial F}{\partial x} + y\frac{\partial F}{\partial y} - \int\left(x\frac{\partial^2 F}{\partial s \partial x} + y\frac{\partial^2 F}{\partial s \partial y}\right) ds \qquad \text{(C-6c)}$$

Proceeding now with the calculation of the values of the function F for the portion of the boundary AB (with ds = dy and (x,n) = 0), one obtains from Equations (C-6a), (C-3), and (C-4),

$$F = \int (py)\,dy = \frac{1}{2}py^2 + C_4.$$

---

*See, for example, page 109 of Reference 25.

**See, for example, page 484 of Reference 22.

Since the addition of an arbitrary constant to the values of F along AB does not affect the value of the prescribed stress $\sigma_x = \partial^2 F/\partial y^2 = p$ on AB, the constant C_4 may be chosen such that F = 0 at A. Hence,

$$F = \frac{1}{2} py^2 \quad \text{on AB.} \qquad \text{(C-7)}$$

On the portion of the boundary BC, ds = dx and the angle (x, n) = 90 degrees. Using Equations (C-3) and (C-6a), one obtains

$$F = \int (bp)\ (0)\ dx = 0 + C_5,$$

which indicates that F has a constant value along BC. From Equation (C-7),

$$F\Big]_B = \frac{1}{2} py^2\Big]_{y=b} = \frac{1}{2} b^2 p \quad \text{for point B.}$$

Thus,

$$F = \frac{1}{2} b^2 p \quad \text{on BC.} \qquad \text{(C-8)}$$

Along CDEF, Equations (C-3) and (C-5) give the following values of the derivatives of F:

$$\frac{\partial F}{\partial x} = 0 \qquad \frac{\partial F}{\partial y} = bp.$$

Using Equations (C-6a),

$$F = ybp - \int \left[y \frac{\partial}{\partial s}(bp) \right] ds = bpy + C_6.$$

It should be noted that the quantity (bp) appearing in the above integrand is a constant, so that the second term vanishes. For point C, with y = b, the above equation yields

$$F\Big]_C = b^2 p + C_6.$$

From Equation (C-8), also for point C,

$$F\Big]_C = \frac{1}{2} b^2 p.$$

The two preceding expressions for $F\Big]_C$ give

$$C_6 = -\frac{1}{2} b^2 p.$$

Thus,

$$F = bpy - \frac{1}{2} b^2 p \quad \text{on CDEF.} \qquad \text{(C-9)}$$

To summarize, the following boundary conditions in terms of the stress function F have been obtained:

(1) Derivatives Along the Boundary

$\frac{\partial F}{\partial x} = 0$ everywhere

$\frac{\partial F}{\partial y} = py$ on AB

$\frac{\partial F}{\partial y} = bp$ on BCDEF

(2) Function F Along the Boundary

$F = \frac{1}{2} py^2$ on AB

$F = bpy - \frac{1}{2} b^2 p$ on BCDEF.

With the values of the stress function and its derivatives along the boundary known, the values of the stress function at node points adjacent to the boundary may be obtained by interpolation and extrapolation. The finite-difference equations may then be written for the interior points using the biharmonic operator of Figure (C-2). This yields a system of simultaneous linear, algebraic equations in F which may be solved by either direct or iterative procedures.

(c) Interpolation Equations. When a curve forms part of the boundary of the area considered, not all the grid points generally can be made to coincide with the boundary. In

such a case, the regular finite-difference biharmonic operator of Figure (C-2) cannot be applied to interior grid points adjacent to the boundary. Moreover, in order to be able to apply the operator of Figure (C-2) to the second interior point in this case, it is necessary to use an external "fictitious" grid point. In this study, the value of the stress function at such points adjacent to the boundary have been calculated in terms of the values of the function at and near the boundary and of its derivatives at the boundary. The following interpolation and extrapolation equations, which are given by D. N. de G. Allen,[25] have been employed:

$$F_i = \frac{1+2\alpha}{(1+\alpha)^2} F_b + \frac{\alpha^2}{(1+\alpha)^2} F_a - \frac{\alpha \Delta}{1+\alpha} \left(\frac{\partial F}{\partial x}\right)_b \qquad \text{(C-10)}$$

$$F_e = \frac{4\alpha}{(1+\alpha)^2} F_b + \frac{(1-\alpha)^2}{(1+\alpha)^2} F_a + \frac{2(1-\alpha)\Delta}{1+\alpha} \left(\frac{\partial F}{\partial x}\right)_b ,$$

where (refer to Figure C-3)

F_i = value of the stress function F at the first interior grid point i

F_e = value of F at the first exterior ("fictitious") grid point e

F_b = value of F at the boundary point b (intersection of grid line with boundary)

F_a = value of F at the second interior point a

$\left(\frac{\partial F}{\partial x}\right)_b$ = value of the derivative of F at the boundary point b

Δ = length of regular mesh interval

α = ratio of the distance from the first interior point i to the boundary point b, to Δ

Equations (C-10) are derived from the equation of a second degree parabola obtained by specifying the values of the function at the second interior point a and the value of the function and its derivative at the boundary point b.

For the purpose of interpolating along grid lines in the y direction, only the last terms involving the derivatives need be changed in Equations (C-10).

• • •

This page is intentionally blank.

PUBLICATIONS OF THE COLLEGE OF ENGINEERING

Bulletins from the University of Illinois College of Engineering are detailed reports of research results, seminar proceedings, and literature searches. They are carefully reviewed before publication by authorities in the field to which the material pertains, and they are distributed to major engineering libraries throughout the world. They are available at a charge approximately equal to the cost of production.

The annual *Summary of Engineering Research* is available in the fall of each year. It contains a short report on every research project conducted in the College during the past fiscal year, including the names of the researchers and the publications that have resulted from their work. It is available for $5.00.

Engineering Outlook, the College's monthly newsletter, contains short articles about current happenings, new research results, recent technical publications, and educational practices in the College of Engineering. Free subscriptions are available upon request.

The Seminar and Discussion Calendar, which is published and distributed weekly, lists current meetings, lectures, and other events on the engineering campus that are open to the public. Free subscriptions are available upon request.

Requests for a catalog of available technical bulletins or for any of the above publications should be addressed to the Engineering Publications Office, College of Engineering, University of Illinois, Urbana, Illinois 61801.

OTHER PUBLICATIONS IN RELATED FIELDS BY THE ENGINEERING EXPERIMENT STATION

Bulletin 398. *A Critical Review of the Criteria for Notch-Sensitivity in Fatigue of Metals,"* by C. S. Yen and T. J. Dolan. 1952. *Fifty cents.*

Bulletin 384. *Fatigue Strength of Various Types of Butt Welds Connecting Steel Plates,"* by W. M. Wilson, W. H. Munse, and I. S. Snyder. 1950. *Fifty cents.*

Bulletin 344. *Fatigue Tests of Commercial Butt Welds in Structural Steel Plates,* by W. M. Wilson, W. H. Bruckner, T. H. McCrackin, Jr., and H. C. Beede. 1943. *Xerox copy only, Six dollars and ninety cents.*

Bulletin 276. *Stress Concentration at Fillets, Holes, and Keyways as Found by the Plaster-Model Method,* by F. B. Seely and T. J. Dolan. 1935. *Xerox copy only, One dollar and seventy cents.*

These publications are available from:
Engineering Publications Office
112 Engineering Hall
University of Illinois
Urbana, Illinois 61801